The PHILOSOPHICAL MAGAZINE

FIRST PUBLISHED IN 1798

. 1 Eighth Series No. 7 July 1956

A Journal of Theoretical Experimental and Applied Physics

PRICE £1 0s. 0d.
Annual Subscription £10 10s. 0d. payable in advance

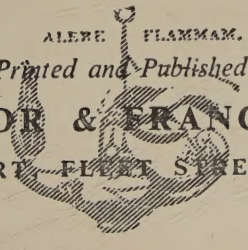

Printed and Published by
TAYLOR & FRANCIS LTD.
RED LION COURT, FLEET STREET, LONDON, E.C.4

CONTENTS OF No. 7.

**All communications for the Philosophical Magazine should be addressed, post-paid, to the Editors, c/o Messrs. TAYLOR AND FRANCIS, LTD., Red Lion Court, Fleet Street, London, England.

LXI. *The Levels of* ^{19}F *from Inelastic Neutron Scattering*

By Joan M. Freeman
Atomic Energy Research Establishment, Harwell†

[Received February 8, 1956]

Abstract

The gamma-rays following inelastic neutron scattering in ^{19}F have been studied as a function of neutron bombarding energy up to 2·2 Mev. The gamma-ray spectra in coincidence with radiation from the lowest excited levels, at 111 and 196 kev, have also been measured near the thresholds for excitation of the higher levels. The following gamma-rays have been found: 1·236±0·012 and 1·356±0·012 Mev, in coincidence with 111 kev radiation; 1·360±0·012 Mev, in coincidence with 196 kev radiation; 1·472±0·016 Mev corresponding to a ground-state transition. The results are interpreted in terms of ^{19}F levels at 1·557, 1·466 and 1·346 Mev. Branching ratios for the decay of each level to the ground, 111 kev and 196 kev states have been examined. No other levels up to 2·0 Mev have been found.

§ 1. Introduction

A considerable amount of work, both experimental and theoretical, has been carried out recently on the first few levels of ^{19}F. The relevant data available when this work was begun are summarized in the review by Ajzenberg and Lauritsen (1955); the levels found below 2 Mev excitation and the known gamma-ray transitions are shown in fig. 1. The first two excited states at 110 and 197 kev have been studied in a number of different reactions and the experiments of Peterson *et al.* (1954), Sherr and Christy (1954), Thirion *et al.* (1954) and Jones *et al.* (1954) strongly suggest the assignments $\frac{1}{2}^-$ to the 110 kev state and $\frac{5}{2}^+$ to the 197 kev state, the ground state being $\frac{1}{2}^+$. Evidence for the higher levels comes from studies of the inelastic scattering of protons by Arthur *et al.* (1952) (levels at 1·37 and 1·59 Mev), of neutron groups from the reaction ^{18}O (dn)^{19}F by Seale (1953) (levels at 0·9, 1·4 and 1·6 Mev,), and of the decay of ^{19}O by Jones *et al.* (1954) (level at 1·59 Mev). In the latter work it has been shown that the 1·59 Mev level decays predominantly to the 197 kev state and that it is most probably a $\frac{3}{2}^+$ level. Gamma-rays with energies 110, 197, 1234, 1349, 1460 and 1560 kev, arising from ^{19}F levels excited by the inelastic scattering of 2·5 Mev neutrons, have been reported by Day (1953), but no level assignments could be made from these measurements alone.

† Communicated by the Author.

Special interest is added to the study of the ^{19}F levels by the intermediate coupling calculations of Elliott and Flowers (1955), and Redlich (1955). Considering states formed by the configurational mixing of the 2s and 1d shells they predict, in the energy range up to 2 MeV, just two even-parity excited states, with spins $\frac{5}{2}$ and $\frac{3}{2}$ and with properties and energies in excellent agreement with those observed for the levels at 0·197 and 1·59 MeV respectively. An inference of this work is that other levels in this energy region should have odd parity. This has already been demonstrated for the 110 kev state. The positions and nature of other levels is therefore a matter of some interest.

Fig. 1

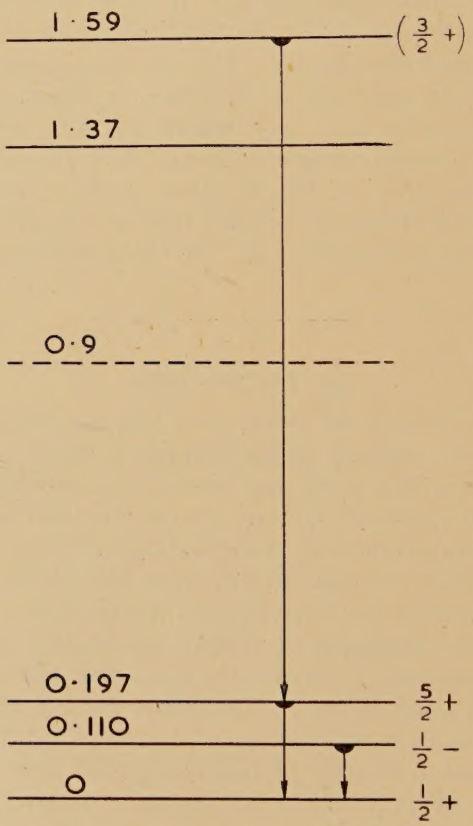

Energy levels of ^{19}F.

In the experiments to be described here the spectra of gamma-rays following inelastic neutron scattering in ^{19}F have been examined as a function of the neutron bombarding energy, and coincidences between the gamma-rays have also been observed. The ability to vary the incident neutron energy proved to be of considerable assistance in the deduction of the level scheme, since it allowed each level to be excited in turn as the neutron energy was increased. With bombarding energies going up to

2·2 MEV, gamma-rays of energies 0·111, 0·196, 1·236, 1·360 and 1·472 MEV were observed. The excitation functions and a preliminary interpretation of the threshold measurements have already been reported (Freeman 1955). The present results indicate three rather closely-spaced levels in ^{19}F, at 1·35, 1·47 and 1·56 MEV, in addition to the ground-state triplet ; the first decays by 1·24 MEV gamma-radiation to the 111 kev state, the second partly by 1·36 MEV gamma-rays to the 111 kev state and partly to the ground state, and the third, by radiation of very closely the same energy (1·36 MEV), to the 196 kev state. No evidence has been found for levels between 0·196 and 1·35 MEV. In particular no gamma-rays which could be attributed to the level suggested at about 0·9 MEV (Seale 1953) have been detected.

Very similar observations have been made recently by Toppel *et al.* (1956)†, who have invesitigated the gamma-rays following inelastic proton scattering in ^{19}F, obtaining evidence for a level scheme in satisfactory agreement with the results reported here.

§ 2. EXPERIMENTAL METHODS

2.1. *Ring Geometry Arrangement*

The first method used for examining the gamma-ray spectra from the ^{19}F(n, n′)^{19}F* reaction was similar to that previously described (Freeman *et al.* 1955). Neutrons having an energy spread of 30 to 40 kev were produced by the bombardment of a zirconium–tritide target with protons from the Harwell Van de Graaff machine. The mean energy of the neutrons was determined, from measurements of the T(p, n) threshold and some total cross section resonances, with an accuracy of about 10 kev. The fluorine scatterer consisted of a teflon (effectively CF_2) ring of outside diameter 10 cm, inside diameter 5·5 cm and thickness 2 cm placed with its axis in the direction of the proton beam and its centre 32 cm from the neutron source. Gamma-rays from the scatterer were detected by a sodium–iodide crystal, 3·8 cm in diameter and 2·5 cm thick, situated at the centre of the ring, and in optical contact with the photocathode of an EMI type 6260 photomultiplier. The crystal was shielded from the neutron source by a cone made up of 18 cm of polythene and 3 cm of lead. The neutron flux was monitored by means of a BF_3 long-counter set up in a direction making an angle of 45° with the proton beam direction.

The pulses from the detector were amplified and then recorded on a thirty-channel kicksorter. At each neutron bombarding energy a spectrum was obtained first with the teflon scatterer in position and secondly with a graphite scatterer of mass chosen to produce about the same amount of elastic scattering. The difference spectrum obtained by subtracting these two runs, after normalization to the same number of neutron monitor counts, then represented chiefly the gamma-rays due to inelastic neutron scattering in fluorine. The results of such experiments will be presented in § 3.

† I am grateful to Dr. D. H. Wilkinson for showing me these results in advance of publication.

2.2. *Coincidence Arrangement*

From a study of the gamma-ray spectra as a function of neutron bombarding energy by the method just described, it became evident that gamma-rays observed in the 1·3 Mev energy region must be the result of cascade transitions to the lower excited states of ^{19}F at 196 and 111 kev and that further information could be obtained by observing the harder gamma-ray spectra in coincidence with 196 and 111 kev radiation.

Fig. 2

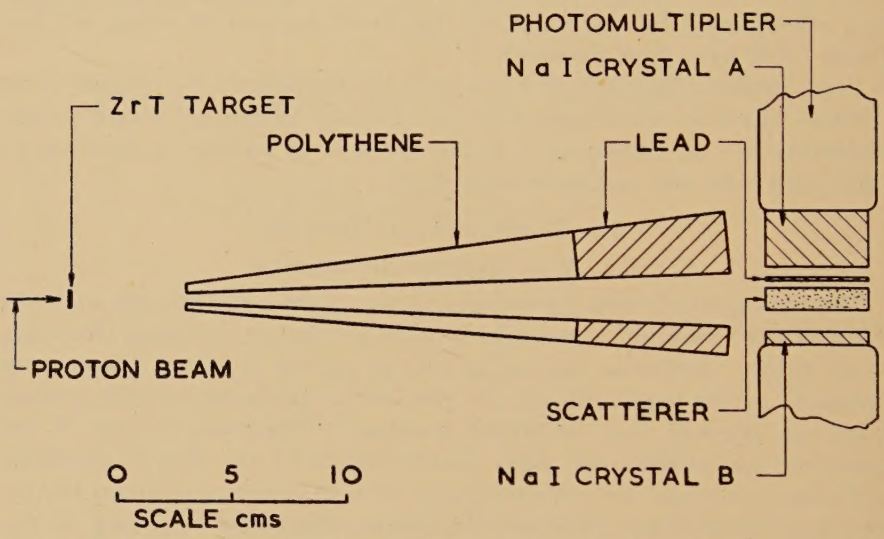

Experimental arrangement for coincidence measurements.

For such studies the arrangement shown in fig. 2 was used. Neutrons emitted in the forward direction from a ZrT target bombarded a teflon disc scatterer 4·5 cm in diameter and 1 cm thick situated 32 cm from the target. On one side of the disc a sodium–iodide crystal A, 3·8 cm in diameter and 2·5 cm thick, was used to detect the hard gamma-rays from the scatterer, and on the other side a crystal B of the same diameter and 0·6 cm thick detected the soft radiation. Each crystal was shielded from the neutron source by a cone comprising 18 cm of polythene and 7 cm of lead. Between crystal A and the scatterer a 2 mm-thick lead disc was inserted ; this was found to reduce considerably the effects caused by unwanted gamma-rays partly absorbed in crystal A with the production of secondary gamma-rays which could then reach crystal B and record a coincidence. The lead disc, while stopping many of these secondary gamma-rays, had little effect on the harder gamma-rays coming into crystal A from the fluorine scatterer.

The output pulses from the photomultiplier attached to crystal A were amplified and then fed simultaneously to a thirty-channel kicksorter and,

through a discriminator, to the first channel of a coincidence unit. The pulses from the photomultiplier attached to crystal B were fed, through separate discriminators, to the second and third channels of the coincidence unit ; the discriminator of channel two was set just below, and that of channel three just above, the pulse height corresponding to

Fig. 3

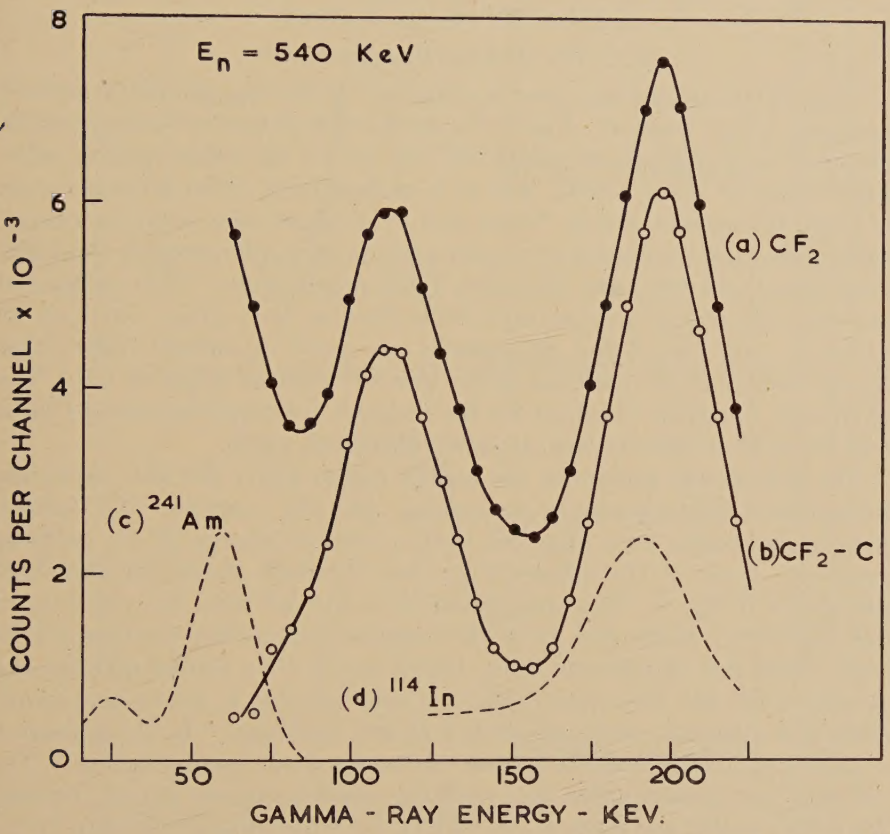

(*a*) Gamma-ray spectrum from a teflon ring ; (*b*) the same after subtraction of the spectrum from a carbon ring ; (*c*) and (*d*) calibration peaks due to ^{241}Am and ^{114}In respectively.

the photopeak due to the gamma-rays with which coincidences were required (196 or 111 kev). Coincidences between the pulses in channels one and two were then taken in anti-coincidence with the pulses in channel three. In this way an output pulse from the coincidence unit was obtained only when the incoming pulse from multiplier B had a height corresponding to the photopeak of the gamma-ray of interest and was in coincidence with a pulse from A. Each output pulse from the coincidence box was made to open a gate which allowed the thirty-channel kicksorter to record the pulse fed to it simultaneously from the multiplier A. The time constants were adjusted to allow a resolving time of $\frac{1}{2}$ microsecond

to be used. The background spectrum was obtained by replacing the teflon disc with an equivalent carbon disc and measuring the coincidence spectrum for the same neutron flux recorded in a suitably placed monitor. The random rates, measured by inserting a delay in channel one of the coincidence unit, were small compared with the real coincidence rates in the experiments to be described here.

§ 3. Experimental Results

3.1. *The Gamma-Rays from* $^{19}F^*$

Some of the gamma-ray spectra obtained by the ring-geometry method are given in figs. 3 and 4. Figure 3 is an example of the low-energy region, obtained with neutrons of energy 540 kev, (*a*) for the teflon ring, (*b*) after subtraction of the spectrum due to a carbon ring. The broken curves indicate the spectra due to ^{241}Am and ^{114}In which were used for energy calibrations and were assumed to give gamma-rays with energies 59·57 kev (Day 1955) and 191·5 kev (Mihelich 1952) respectively. The energies of the two low-energy gamma-rays from fluorine were thus found to be $111 \pm 1{\cdot}5$ and 196 ± 2 kev respectively, in good agreement with other measurements of the positions of the first two excited states of ^{19}F. The excitation functions obtained for the inelastic scattering process to these two levels have already been reported (Freeman 1955).

The gamma-ray spectra in the energy region above 200 kev were then investigated with gradually increasing neutron energies. No further gamma-ray peaks were observed until a neutron energy of 1·5 Mev was reached. Some of the difference spectra obtained above this threshold are shown in fig. 4. The energy scale was derived from the positions of the full-energy peaks due to a ^{60}Co source (gamma-ray energies 1·1723 and 1·3325 Mev (Lindström *et al.* 1953)) and a ^{22}Na source (gamma-ray energy 1·277 Mev (Alburger 1949)). Curve (*a*), fig. 4, shows the below-threshold spectrum obtained with 1·45 Mev neutrons. In (*b*) appears a 1·24 Mev gamma-ray resulting from 1·56 Mev neutron bombardment. The experimental points agree well with the single-spectrum shape obtained for a ^{22}Na source and given by the full curve, which was adjusted to fit the experimental points at the photopeak. With neutron bombarding energies above 1·6 Mev the gamma-ray spectrum became complex. The points shown in fig. 4 (*c*) were obtained with 1·72 Mev neutrons. The ^{22}Na spectrum shape has again been used to analyse this spectrum ; the full curve is the sum of the broken curves representing component gamma-rays of energies 1·24, 1·36 and 1·47 Mev. At a still higher neutron bombarding energy (2·03 Mev, curve (*d*)) the three components are again observed with greater intensity, for a given neutron flux, and in different proportions.

As a check on these observations an organic crystal (2·5 cm cube stilbene) was also used to observe the Compton spectra of the gamma-rays following neutron bombardment of the fluorine ring. Figure 5 shows some of the spectra obtained. The two end-points shown correspond to

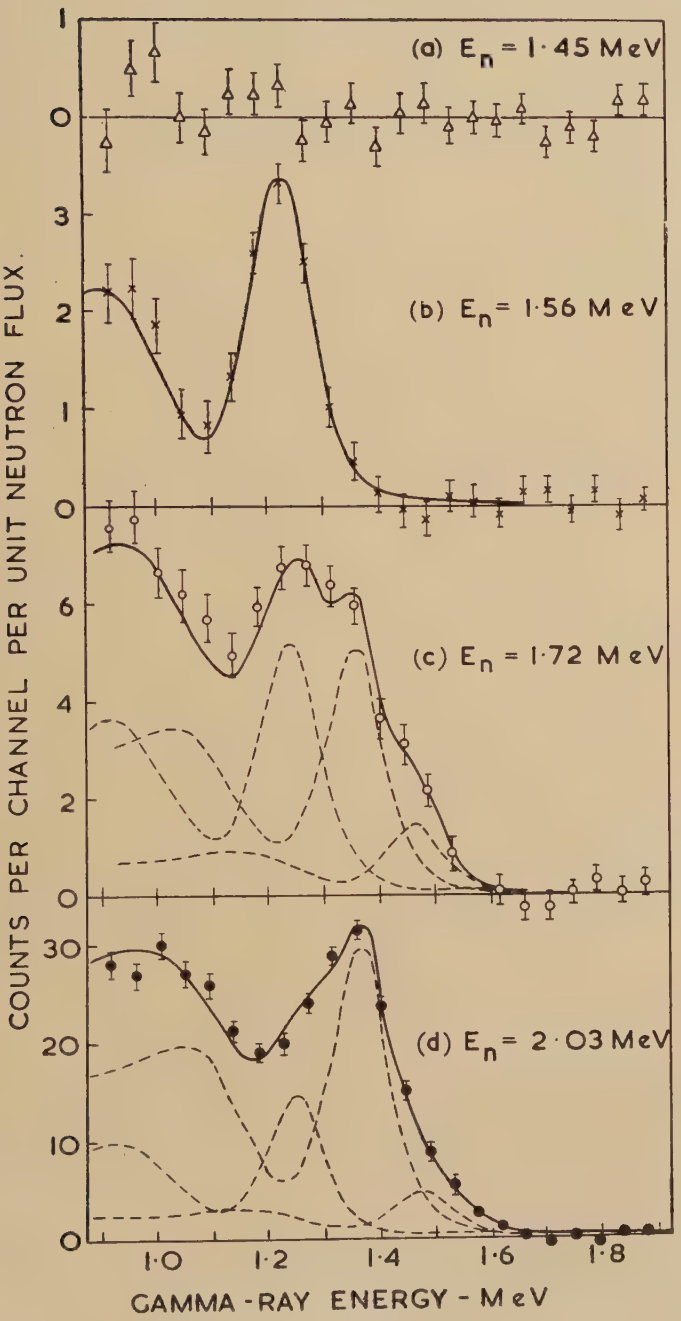

Fig. 4

Gamma-ray spectra due to inelastic scattering in fluorine for neutron energies of (*a*) 1·45 MEV, (*b*) 1·56 MEV, (*c*) 1·72 MEV and (*d*) 2·03 MEV. The broken curves, representing the shapes expected for single gamma-ray lines, were derived from a ^{23}Na spectrum; the full curves are the sums of the broken curves.

gamma-ray energies of 1·25 and 1·37 Mev and there is also some suggestion of a higher energy (~1·45 Mev) component at the higher neutron energies.

The apparent neutron energy thresholds observed for the excitation of the 1·24 and 1·36 Mev gamma-rays (for the excitation functions see Freeman 1955) suggest that these are not ground-state transitions, but arise rather from levels in ^{19}F which decay to either the 196 or 111 kev excited states. The most plausible explanation of the 1·36 Mev gamma-ray is that it comes from a 1·56 Mev level identified with the 1·59 Mev level

Fig. 5

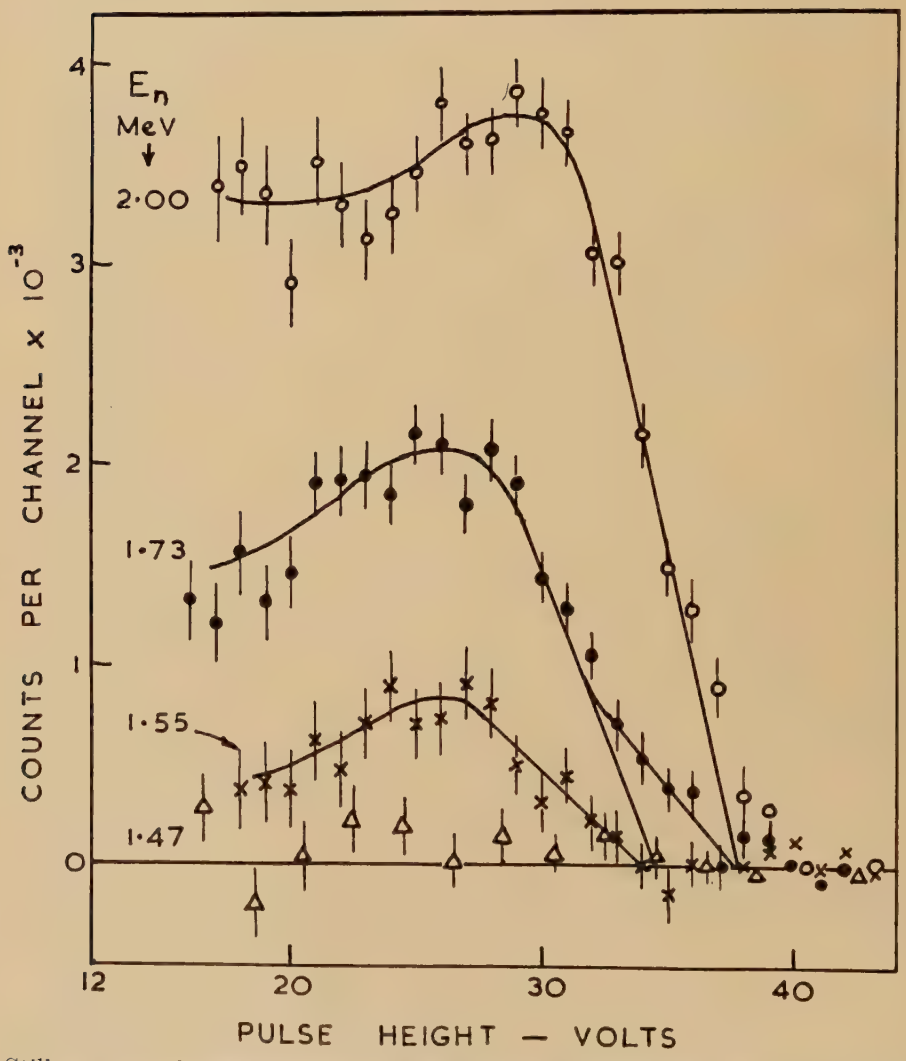

Stilbene crystal measurements of the Compton spectra due to gamma-rays from fluorine, for the neutron energies marked.

Fig. 6

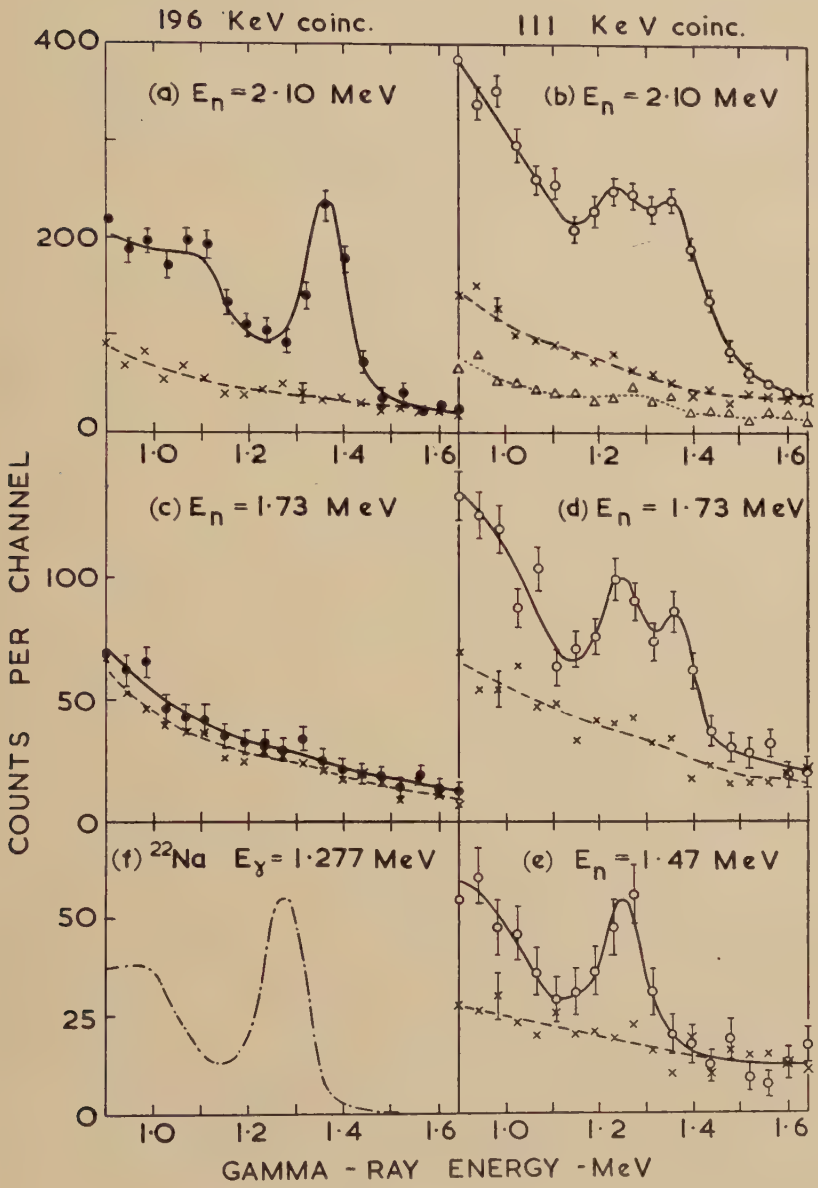

Gamma-ray spectra from fluorine in coincidence with 196 kev gamma-rays (full curves (*a*) and (*c*)), and with 111 kev gamma-rays (full curves (*b*), (*d*) and (*e*)) for the neutron energies indicated. Broken curves represent similar runs with a carbon scatterer. The dotted curve in (*b*) represents the random rate. Curve (*f*) shows a calibration spectrum from a ^{22}Na source.

previously observed in ^{19}O decay by Jones *et al.* (1954) and found to make transitions mainly to the 196 kev state ; the 1·24 Mev gamma-ray could be a transition either from a 1·44 Mev level to the 196 kev state or from a 1·35 Mev level to the 111 kev state ; the small component at about 1·47 Mev could then be interpreted as arising either from the 1·56 Mev level or possibly from the 1·44 Mev level. The coincidence experiments to be described below were undertaken in order to clarify these ambiguities. They have led to the conclusion that the level scheme is even more complicated than the above inferences would imply.

3.2. *Coincidence Measurements*

In figs. 6 (*a*) and (*b*) are shown the results obtained with a neutron bombarding energy of 2·10 Mev, sufficient to excite all the gamma-rays observed in the single-rate spectra discussed in § 3.1. The full curve (*a*) is the spectrum found to be in coincidence with 196 kev radiation ; the broken curve shows the corresponding spectrum obtained when the teflon scatterer was replaced by a carbon scatterer. The resultant spectrum due to fluorine shows a full energy peak and Compton edge corresponding to a single gamma-ray of energy 1·36 Mev. This result indicates the excitation of a level in ^{19}F at 1·56 Mev which decays by a transition to the 196 kev level, in confirmation of one of the suppositions made in § 3.1. The 1·24 Mev gamma-ray of the singles spectrum (fig. 4 (*d*)) does not appear in 6 (*a*) and we can therefore conclude that it is not in coincidence with 196 kev radiation as tentatively suggested by the threshold measurements.

Figure 6 (*b*) shows the corresponding spectrum and background when the coincidence arrangement was ' gated ' to allow coincidences with 111 kev radiation to be recorded. The 1·24 Mev gamma-ray is in evidence here, suggesting that it in fact arises from a 1·35 Mev level decaying via the 111 kev state. The surprising feature of this spectrum however is the appearance of a 1·36 Mev component, of energy indistinguishable from that in the 196 kev coincidence spectrum. Its appearance here cannot be accounted for by the random rate (the latter is shown by a dotted curve) nor can it be explained as being due to coincidences with pulses from the part of the tail of the 196 kev spectrum which happens to overlap the 111 kev ' gate '. The result therefore suggests the existence in ^{19}F of a third level in the same energy region, with an energy of 1·47 Mev, which decays to the 111 kev state. To test further this hypothesis the neutron bombarding energy was reduced to a value less than that required for excitation of the 1·56 Mev level. The results obtained at a neutron energy of 1·73 Mev are shown in fig. 6 (*c*) and (*d*). Figure 6 (*c*) shows the spectra with the fluorine scatterer (full curve) and a carbon scatterer (broken curve) in coincidence with 196 kev gamma-rays ; The 1·36 Mev gamma-ray has now disappeared, indicating that the 1·56 Mev level is not being appreciably excited. Figure 6 (*d*) is the spectrum in coincidence with 111 kev radiation and shows clearly that a 1·36 Mev

component, as well as the 1·24 MeV component, is still present. The neutron energy was then reduced to 1·62 MeV which is below the theoretical threshold for a 1·56 MeV level, and although the yield and therefore the statistical accuracy was somewhat lower, the evidence for a 1·36 MeV gamma-ray in coincidence with 111 kev radiation was still definite. Finally the neutron energy was decreased to a value below the threshold for excitation of a 1·47 MeV level but still above that for a 1·35 MeV level. The spectrum then obtained in concidence with 111 kev radiation, as well as the background spectrum, are shown in fig. 6 (*e*), for the case of 1·47 MeV neutrons. A peak due to 1·24 MeV gamma-rays is clearly evident, the 1·36 MeV component having now disappeared. These results can only be explained by postulating two levels in ^{19}F, at 1·47 and 1·35 MeV, decaying principally to the 111 kev state, in addition to the previously established level at 1·56 MeV which decays to the 196 kev state.

§ 4. The ^{19}F Decay Scheme

We have now to consider the 1·47 MeV gamma-rays which appeared in the single-rate spectra of fig. 4 (*c*) and (*d*). These could now be attributed to transitions either from the 1·47 MeV level to the ground state or from the 1·56 MeV level to the 111 kev state, or both. We note first that in the single-rate spectrum obtained at a neutron energy of 1·72 MeV (fig. 4 (*c*)) the 1·47 MeV gamma-ray appears, with an intensity of about 0·27 that of the 1·36 MeV component (the latter being about equal in intensity to the 1·24 MeV gamma-ray). Comparing now the coincidence measurements at almost the same neutron energy (figs. 6 (*c*) and (*d*)) it is evident from the 196 kev coincidence spectrum that the 1·56 MeV level is not being excited, and from the 111 kev coincidence spectrum that the intensities of the 1·36 and 1·24 MeV components are approximately equal. We can therefore infer that at this neutron energy all the 1·47 MeV gamma-rays must come from the 1·47 MeV level. Moreover, all or practically all the 1·36 MeV gamma-rays must also come from this level since (i) there is no measurable evidence for excitation of the higher level (ii) the ratios of the intensities of the 1·36 MeV and 1·24 MeV gamma-rays in the single rate spectrum (fig. 4 (*c*)) and the 111 kev coincidence rate spectrum (fig. 6 (*d*)) are both almost one and (iii) the single rate spectrum of fig. 4 (*b*), taken just below the threshold for the 1·47 MeV level, shows no evidence of 1·36 MeV gamma-rays coming from the 1·36 MeV state ($\leqslant 5\%$ of the 1·24 MeV transition). The 1·47 MeV state must therefore decay both to the 111 kev and the ground state with the relative probabilities 1 and 0·27($\pm$0·07).

At higher neutron energies there might be some 1·45 MeV gamma-radiation from the 1·56 MeV level. This would be in coincidence with 111 kev radiation. There is no definite evidence of a 1·45 MeV group in an analysis of the 111 kev coincidence curves (see, for example, fig. 6 (*b*)); an upper limit of 0·08 can be placed on the intensity of such a group relative to the 1·36 MeV component. The latter is about 1·1 times the

1·24 Mev component. In the corresponding single-rate spectra for neutron energies in the range 2·03 to 2·10 Mev the ratios of the intensities of the three gamma-rays (1·24, 1·36 and 1·47) are about 0·5 : 1 : 0·15. From these observations one obtains for the total 1·47 Mev radiation relative to the 1·36 Mev radiation from the 1·47 Mev level a ratio of 0·28, in agreement with the previous figure. The results are therefore consistent with the supposition that the 1·47 Mev gamma-rays are due entirely to the decay of the 1·47 Mev level, but do not exclude the possibility that up to about 25% of them could arise from the 1·56 Mev level.

Some further upper limits to branching ratios from the three relevant fluorine levels can be inferred from the measurements. In particular, the single-rate spectra (see fig. 4 (*b*)) obtained below the thresholds for the 1·47 and 1·56 Mev levels show that the 1·35 Mev level must decay almost exclusively to the 111 kev level. The results are summarized in

Fig. 7

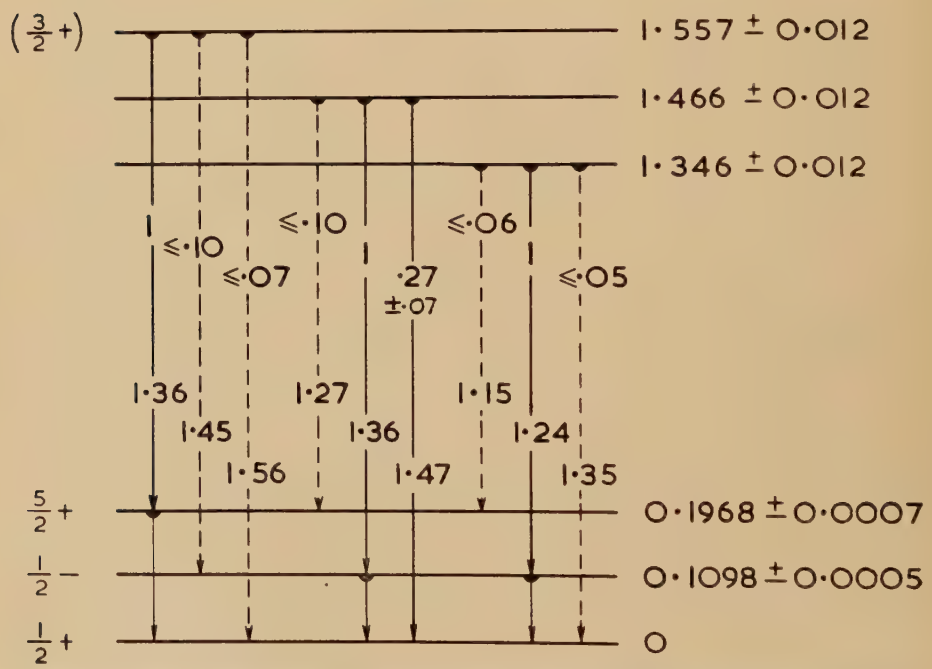

Levels in ^{19}F below 2 Mev. The level energies and the gamma-ray energies are given in Mev. Transition probabilities are given relative to the most prominent transition from each level.

fig. 7 where the branching ratios relative to the most probable transition for each level are given. For deriving the values given for the level positions we have used (i), for the low-lying levels, weighted means of published values (Ajzenberg and Lauritsen 1955, Barnes 1955) and those

of the present experiments, namely, 109·8±0·5 and 196·8±0·7 kev, (ii), for the hard gamma-rays, the means of all the energy measurements made in the present experiments, namely,

in coincidence with 110 kev radiation :
1·236±0·012 and 1·356±0·012 Mev
in coincidence with 197 kev radiation :
1·360±0·012 Mev ;
ground-state transition : 1·472±0·016 Mev.

The conclusions presented here are in good agreement with the deductions made by Toppel *et al.* (1956) ; they excited the fluorine levels by inelastic proton scattering, again using coincidence techniques to interpret the gamma-ray spectra. Being unable, because of the barrier factors for protons, to explore the regions near the level thresholds, as in the neutron work, they performed somewhat different experiments to arrive at the same conclusions. They were not able to investigate the branching ratios for the 1·35 Mev level as well as the neutron experiments allowed.

The data are insufficient to permit definite spin and parity assignments to the 1·47 and 1·35 Mev levels. Because of their preference for decay to the $J=\frac{1}{2}$ level, spin values greater than $\frac{5}{2}$ are improbable. At first sight one might postulate even parities for these states, assuming preferred E_1 transitions to the $\frac{1}{2}^-$ state. However it has been shown that reliable estimates of transition probabilities cannot be based on the single particle model, and in fact the $\frac{3}{2}^+$ level prefers to decay to the $\frac{5}{2}^+$ state, which has a similar configuration (Elliott and Flowers 1955). Similar arguments could therefore be invoked to suggest that the 1·47 and 1·35 Mev levels have configurations like that the $\frac{1}{2}^-$ level, with odd parity. For example, if the $\frac{1}{2}^-$ state is like a ^{20}Ne ground state nucleus with a ' hole ' in the $p\frac{1}{2}$ shell of its ^{16}O core (Christy and Fowler 1954), the two new levels may be like a ^{20}Ne nucleus in its first excited state, again with a hole in its core. A configuration of this type would be expected to give a $\frac{5}{2}^-$, $\frac{3}{2}^-$ doublet with an excitation energy about equal to or slightly less than that of the ^{20}Ne 2^+ state (1·63 Mev). Such an assignment would be consistent with the experimental observations, and also with the theoretical predictions concerning even parity states. Further investigations of these levels, and calculations of odd parity states are clearly desirable.

Note added in proof : We have recently extended the work on ^{19}F(n, n′) by using neutrons with energies up to 3·7 Mev. No further gamma-rays were observed until a neutron energy of almost 3·7 Mev was reached, when a 2·59±0·04 Mev gamma-ray appeared. This is attributed to a ^{19}F level at 2·79±0·04 Mev (cascading via the 197 kev state) which is identified with the level previously reported at 2·82 Mev (Ajzenberg and Lauritsen 1955). From the fact that the yield curve for this gamma-ray rises only very slowly from the threshold it is inferred that the level spin is $\geqslant 7/2$. Elliott and Flowers predict 9/2+ for this level.

Acknowledgments

I am very grateful to Dr. B. H. Flowers for his interest and advice in this work, to Drs. W. D. Allen, M. A. Grace, R. C. Hanna and J. O. Newton for helpful discussions, and to Mr. A. E. Pyrah for his efficient running of the Van de Graaff machine.

References

Ajzenberg, F., and Lauritsen, T., 1955, *Rev. Mod Phys.*, **27,** 77.
Alburger, D. E., 1949, *Phys. Rev.*, **76,** 435.
Arthur, J. C., Allen, A. J., Bender, R. S., Hausman, H. J., and McDole, C. J., 1952, *Phys. Rev.*, **88,** 1291.
Barnes, C. A., 1955 *Phys. Rev.*, **97,** 1226.
Christy, R. F., and Fowler, W. A., 1954, *Phys. Rev.*, **96,** 851.
Day, P. P., 1955, *Phys. Rev.*, **97,** 689.
Day, R. B., 1953, *Phys. Rev.*, **89,** 908.
Elliott, J. P., and Flowers, B. H., 1955, *Proc. Roy. Soc.* A, **229,** 536.
Freeman, J. M., 1955, *Phys. Rev.*, **99,** 1446.
Freeman, J. M., Lane, A. M., and Rose, B., 1955, *Phil. Mag.*, **46,** 17.
Jones, G. A., Phillips, W. R., Johnson, C. M. P., and Wilkinson, D. H., 1954, *Phys. Rev.*, **96,** 547.
Lindstrom, G., Hedgram, A., and Alburger, D. E., 1953, *Phys. Rev.*, **89,** 1303.
Mihelich, J. W., 1952, *Phys. Rev.*, **88,** 646.
Peterson, R. W., Barnes, C. A., Fowler, W. A., and Lauritsen, C. C., 1954, *Phys. Rev.*, **94,** 1075 ; **96,** 1250.
Redlich, M. G., 1955, *Phys. Rev.*, **99,** 1427.
Seale, R. L., 1953, *Phys. Rev.*, **92,** 389.
Sherr, R., Li, C. W., and Christy, R. F., 1954, *Phys. Rev.*, **96,** 1258.
Thirion, J., Barnes, C. A., and Lauritsen, C. C., 1954, *Phys. Rev.*, **94,** 1076.
Toppel, B. J., Wilkinson, D. H., and Alburger, D. E., 1956, *Phys. Rev.*, **101,** 1485.

LXII. *On the Nature of Particles Produced in Extremely Energetic Nuclear Collisions*

By F. A. Brisbout, C. Dahanayake†, A. Engler, Y. Fujimoto‡, and D. H. Perkins§

H. H. Wills Physical Laboratory, University of Bristol‖

[Received January 3, 1956]

Abstract

A detailed investigation into nuclear collisions of energy between 10^{12}–10^{13} ev is reported. The ratio of π^0-mesons to charged shower particles has been determined with high statistical accuracy yielding a value $R=0{\cdot}383+0{\cdot}044$. The central cores of the 'jets' have been carefully scanned to detect secondary interactions produced by the shower particles and the ratio, Q, of the number of interactions produced by neutral to the number produced by charged shower particles has been obtained. $Q=0{\cdot}25+0{\cdot}09$. If we assume that in nuclear collisions of very high energy, neutral and charged particles (other than π-mesons) are created in approximately equal numbers and that the interaction mean free path for such praticles does not differ appreciably from that of π-mesons, the values R and Q enable an estimate to be made of the fraction of shower particles which are not π-mesons. The results indicate that $\sim$25% of the shower particles must be heavy mesons, hyperons, nucleon–antinucleon pairs, and ejected nucleons.

In order to estimate the contribution to the above fraction from heavy mesons, a detailed analysis of the products of secondary disintegrations has been carried out. The results, although preliminary, are compared with those of Dahanayake *et al.* (1955) and are consistent with the assumption that most of these unidentified shower particles in the core are heavy unstable particles.

The lifetime of the π^0-meson has been determined by a method which does not involve the determination of the energy of the meson. The mean life obtained is $1{\cdot}8^{+3{\cdot}2}_{-1{\cdot}1}\times10^{-15}$ sec.

§ 1. Introduction

Since 1951, several investigations have been made (Daniel *et al.* 1952, Frier and Naugle 1953, Mulvey 1954, Kaplon *et al.* 1952, 1954, 1955, Lal *et al.*, 1954) into the nature of the particles produced in nuclear collisions in the energy interval 10^{12}–10^{13} ev. These events are commonly referred

† On leave of absence from the University of Ceylon.
‡ Now at the University of Kyoto, Japan.
§ Now on leave at the Radiation Laboratory, Berkeley.
‖ Communicated by Professor C. F. Powell, F.R.S.

to as ' jets ' for a large fraction of the secondary particles is projected forward in directions only narrowly inclined to that of the primary, as a consequence of the great velocity of the centre of mass of the collision-system (see Plate 21). The secondary charged particles emerging from the disintegration are made up of π-mesons and heavier particles which may be referred to as the ' shower ' particles. They must be distinguished from the *cascades* of electrons which do not originate directly in the disintegrations, but which eventually appear in great numbers in the region of the core due to the materialization of gamma rays. It is important to establish the nature of the ' shower ' particles, and, in particular the relative frequency of occurrence among them of π-mesons, K-mesons, nucleons and hyperons.

Nearly all previous experiments on ' jets ' have been carried out with nuclear emulsions, and the interpretation of the observations has had to meet two difficulties : Firstly, the events are rare ; and secondly, mass-measurements by conventional methods are commonly impossible owing to the great energy of the particles. Any conclusions reached hitherto have therefore been based on indirect methods of analysis.

In interpreting the results of the experiments, it has always been assumed hitherto that in the production of π-mesons the principle of charge-independence is valid (Van Hove *et al.* 1952). It was then possible to draw conclusions by comparing the observed number of ' electron pairs '—which result from the materialization of γ-rays arising through the decay of π^0-mesons—with the number of charged shower particles, n_s. The number of pairs due to γ-rays, led to an estimate of the number of π^0 particles, N_{π^0}, and thence to the number of charged π-mesons, $N_{\pi^\pm}$. The difference between the value, $N_{\pi^\pm}$, so determined and the number of shower particles, n_s, was assumed to represent the number $N_{\mathrm{K}^\pm}$, of heavy charged particles which are not $\pi^\pm$ mesons ; $N_{\mathrm{K}^\pm}=n_s-N_{\pi^\pm}$. The results reported hitherto do not differ significantly within the rather large statistical errors, but those obtained in this laboratory appear to correspond to a larger proportion of particles different from π-mesons than the values obtained by other workers.

In view of the fundamental importance of the problem, and since large blocks of stripped emulsions have recently become available for such investigations, a new attempt has been made to determine the ratio N_{π^0}/n_s by observations of greater statistical weight. Further, the correction for the finite time of flight of the π^0-mesons has been considered in detail and this has involved a determination of the mean lifetime of these particles by a new method.

In a large stack of stripped emulsions, it is possible to observe many of the secondary nuclear processes which follow from a single high-energy disintegration. By comparing the number of secondary nuclear interactions, in the ' core ' of the jet, which are produced by neutral and charged particles, respectively, the proportion of neutral shower particles which are not π^0-mesons can be determined. The essential point is that

the neutral π particles commonly decay before interacting, whereas the long-lived neutral particles have a large probability of interacting before they decay.

Finally, a method of analysis has been introduced which allows conclusions to be drawn with a minimum number of assumptions and which uses the latest information about the properties of the heavy unstable particles.

Recent experimental evidence (*Pisa Conference Report* 1955) indicates that, in interactions with nuclei, K and Y particles have the property of either colliding inelastically, or transforming one into the other. This property suggests that when K or Y particles collide with nuclei, a larger fraction of secondary particles of these types should emerge from the resulting disintegrations than from the nuclear collisions of nucleons or π-mesons of the same energy. If the K and Y particles form a substantial proportion of the secondary particles arising in the jets their presence might be established by studying the characteristics of their secondary nuclear interactions and thus proving that the proportions of tertiary K and Y particles is indeed exceptionally great. Although such an investigation is tedious, and this part of our work is still in its initial stages, it appears to be one of the most important aspects of the present experiments, for it could provide convincing evidence of the nature of the secondary particles produced in ' jets '.

§ 2. Experimental Procedure

The present evidence is based on a study of disintegrations produced by particles in the energy interval from 10^{12} to 10^{13} ev. The ' stars ' were found by scanning two large stacks of stripped emulsions, the details of which are given in table 1.

Table 1. Details of Stacks

Stack	Dimensions (cm)	No. of plates	Flight characteristics	
			Average altitude	Time of flight
G-stack	37×27	117	83000 ft.	6 h. above 80000 ft.
E-stack	20×15	80	105000 ft.	6 h. above 100000 ft.

Every high energy nuclear event is accompanied by a relatively narrow electromagnetic cascade, arising from the decay of π^0-mesons, which can be found relatively easily. The scanning procedure was therefore designed to detect these cascades and to trace them back to their origin. For

this purpose, several narrow areas parallel to those edges of the plates which were horizontal during the exposure of the stack were searched together with the corresponding vertical edges of each emulsion, using magnification of 300×. Table 2 lists the events found in this way, and table 3 gives a description of the ' jets '.

Table 2. Events found in the General Scan

Nature of Primary	Number of high energy events
Nucleonic (Jets)	
Proton	14
Alpha particle	5
Electromagnetic (Cascades)	
Single electron	3
Two single electrons and a photon	1
Single photon	19
Several photons	3

Table 3. Details of the Nuclear Events

Jet	Classification		Energy† in 10^{12} ev	Length per plate in mm	Length available for observations in cm
	N_h	n_s			
P–1	27	36	1	0·8	5·2
P–2	0	22	30	1·0	13·8
P–3	13	17	0·8	250·0	25·0
P–4	18	58	2	2·2	11·9
P–5	0	32	4	5·7	24·8
P–6	7	49	0·7	6·6	9·0
P–8	23	126	10	6·0	7·7
P–9	0	18	6	3·5	15·1
P–10	0	16	5	4·1	19·7
P–13	0	8	5	18	20·9
P–14	13	38	1	3·5	2·5
P–15	5	4	3	3·9	10·6
α–1	5	40	30 ×4	1·9	17·8
α–2	17	123	0·8×4	13·6	10·8
α–3	1	41	10 ×4	162·0	16·2
α–4	20	80	2 ×4	3·9	25·9
α–5	0	10	2 ×4	1·7	11·4

† The energy of the jets was estimated from the angular distribution of the shower particles. Two events which had bad geometry and hence were not studied are not included.

(*a*) *Ratio of Neutral π-mesons to Shower Particles*

It was first pointed out by Daniel *et al.* (1952) that, by determining the numbers of electron pairs associated with high-energy jets, the relative frequencies of $\pi^{\pm}$ mesons and other types of charged particles can be estimated. Thus, if $N_{\pi^{\pm}}$ and N_{π^0} denote the numbers of charged and neutral π-mesons, respectively and $N_{\mathrm{K}^{\pm}}$ that of charged shower particles of other types, then $n_s = N_{\mathrm{K}^{\pm}} + N_{\pi^{\pm}}$, and

$$R = \frac{N_{\pi^0}}{N_{\pi^{\pm}} + N_{\mathrm{K}^{\pm}}},$$

where R is the quantity experimentally determined.

The method employed in searching for electron pairs associated with jets was as follows : In the emulsion in which the jet originated, the track of the primary particle, and the central core of the ' jet ' were accurately aligned with one axis of the microscope stage. The ' core ' was then traced through successive emulsions, up to some convenient distance, L, from the origin. The total length of the track of each shower particle was measured within a rectangular strip of length L and width z, centred about the shower axis. The angular distribution of the particles was such that, on the average, for values of L between 10 and 45 mm and of z between 0·3 and 0·9 mm, half the shower tracks were completely contained within the strip. The number of electron pairs originating in the scanned volume was then determined. In three cases, the origin of an electron-pair could not be distinguished with certainty, as it was in the dense core of tracks close to the origin of the jet ; in each of them a close pair of tracks, each of minimum grain-density, g^0, or an apparently single track with $g = 2g^0$, narrowly inclined to the main axis of the core, was observed in the next emulsion of the stack. It was traced through successive emulsions until it was identified by bremsstrahlung and scattering of the electrons. Since, in this investigation, individual tracks were traced for a great distance through several emulsions, stray tracks could be easily eliminated, and the probability of missing electron pairs was very small.

Occasionally in traversing the scanned volume, a shower particle was observed to make a secondary interaction. In such a case, the potential path length of the particle through the strip was calculated by comparison with other shower particles, of similar dip and azimuthal angle with respect to the shower axis. The lengths in the scanned volume of the tracks of shower particles from the secondary star were measured and included in the total track length, together with corresponding measurements for any electron pairs. Since the value of R for the secondary stars may be different from that for the primary ' jets ', we have also determined its value from the observations in a scanned volume which extends only up to the first secondary interaction ; any such difference, if it exists, is less than the statistical errors.

In comparing the frequency of production of π^0-mesons with that of the charged shower particles, the following factors must be considered :

(i) Angular distributions of the photons relative to the shower particles :

(ii) differentiation between ' associated ' and ' bremsstrahlung ' pairs ;

(iii) the finite distance traversed by the π^0-mesons before decay ;

(iv) possible sources of γ-rays other than the decay of π^0-mesons. (This will be discussed in § 2.)

(i) We make the reasonable assumption that the angular distribution of the π^0-mesons, averaged over several jets, is identical with that of the shower particles. In the conditions of our experiment, the discrepancy between the potential path-length of a photon and that of its parent π^0-meson, in the scanned volume, is important only when the π^0-meson is emitted at nearly 90° in the C.M. System of the colliding nucleons. For such mesons, this discrepancy is less than $100/\bar{\gamma}^2\%$ where $\bar{\gamma}$ is the total energy (in rest units) of the meson in the C.M. System. Since in the jets examined $\bar{\gamma}$ is of the order of 10 for the π-mesons, the error introduced by assuming the angular distribution of the photons to be identical with that of the π^0-mesons, and presumably that of the shower particles, is less than 1%.

(ii) It is shown in the Appendix that the differentiation between ' associated ' pairs—that is those pairs produced by γ-rays resulting directly from the decay of π^0-mesons—and bremsstrahlung pairs, produced at points close to the star origin by secondary γ-rays from electrons, is straightforward and unambiguous, at least up to the distances of about one cascade unit from the star. The contribution to the pair frequency due to the process of direct decay of π^0-mesons into two electrons and a single photon has also been calculated and shown to be of the order of 1%

(iii) The mean distance traversed by the π^0-mesons before decaying is, for the jets considered, 0·87 mm. (See Appendix II.)

Let us assume tentatively that π^0-mesons constitute the sole source of γ-rays. If R is the ratio of π^0-mesons to shower particles, each of the latter corresponds to $2R$ photons. Let λ be the conversion length of high energy photons in the emulsion (3·75 cm)†, and ρ the mean distance traversed by the π^0-mesons before decay. We assume, for the moment, that all π^0-mesons have the same energy. Then, if λ is the length of a particular shower track in the scanned volume, this will correspond to

$$2Rf(l)=2R\left\{(1-e^{-l/\lambda})-\frac{\rho}{\lambda-\rho}(e^{-l/\lambda}-e^{-l/\varrho})\right\}$$

electron pairs. The total number of associated electron pairs expected in the scanned volume is therefore $2R\sum_{i=1}^{n} f(l\gamma)$ summed over the n shower tracks in the scan.

† Recently an upper limit of $4{\cdot}5\pm1$ cm for the conversion length in emulsion has been obtained in this laboratory by K. Pinkau.

The search for electron pairs was carried out for 11 of the jets. These events were such that the mean track-length per emulsion was greater than 2 mm and they were selected from the total of 19 only for this reason. The observed number of associated pairs was 77, and the numbers calculated for various assumed values of ρ are given in table 4.

Table 4. Variation of R with $\bar{\rho}$

Mean energy of π^0 (Bev)	Mean distance travelled $\bar{\rho}$ (mm)	Number of pairs expected	R
	0·00	210·0 R	0·367 ± ·042
75	0·43	205·2 R	0·375 ± ·043
150	0·87	201·0 R	0·383 ± ·044
300	1·75	194·4 R	0·396 ± ·045

$\bar{\rho}$ is the mean distance travelled by the π^0-meson before decay. The number of pairs observed is 77 and the estimated $\bar{\rho}$, 0·87 mm.

The above formula is valid only for π^0-mesons of the same energy. However, in the conditions of our experiment, $\rho \ll \lambda, l$, so that the last term is negligible and f (l) varies linearly with ρ. Thus if the energy spectrum of the π^0-mesons is not too extended the above formula will still be valid if the mean value of ρ, $\bar{\rho}$, is used. As mentioned above, the measured value of $\bar{\rho}$ is 0·87 mm giving $R = 0{\cdot}383 \pm 0{\cdot}044$. If the estimate of $\bar{\rho}$ is incorrect by a factor two, in either direction, then it is seen from table 4 that R assumes values which are still within the statistical errors associated with the number of pairs observed.

(*b*) *Ratio of Secondary Stars Produced by Neutral and Charged Shower Particles*

As mentioned in the introduction, the proportion of neutral particles which are not π^0-mesons can be determined under reasonable assumptions by comparing the number of interactions induced by neutral and charged secondary particles.

The search for secondary stars was made by the following method :

The core of the shower was aligned with the axis of the microscope stage and a strip, of width 720 μ and length equal to the maximum length of shower tracks in the plate, was carefully examined for all stars. This procedure was repeated from plate to plate until a distance from the original star of the order of 10 cm was reached. At this distance, only a few mesons and other heavy particles remain within the scanned area, most of the tracks being due to the electrons of the accompanying cascade.

As a further limitation, only those secondary stars in the core of the jet were accepted for which $n_s \geqslant 4$.

Whilst a secondary disintegration due to a charged particle of the jet can be identified without ambiguity whatever its energy those due to neutral particles can give rise to difficulties of interpretation. By confining attention to secondary stars of high energy, the direction of the neutral primary can be inferred, at least approximately, and the observed characteristics shown to be consistent with the assumption that it originated in the primary disintegration.

Altogether 9 stars with neutral primaries (see Plate 22) and 36 with charged primaries were found.

If we denote by Q the ratio of the numbers of stars produced by neutral and by charged particles respectively then from the above data we obtain

$$Q=0{\cdot}25\pm0{\cdot}09.$$

Provided the mean free path for interactions of the different types of particles is the same, Q is a true measure of the ratio of the flux of neutral to that of charged shower particles in the core. Therefore we may write $Q=N_0/(N_{K^\pm}+N_{\pi^\pm})$ where N_0 is the number of neutral particles (other than π^0-mesons) in the inner core, and $N_{K^\pm}$ is defined as before.

From the known density of background stars with $n_s \geqslant 4$, and by considering the geometrical features of the observations we estimate that the probability that one of the nine ' stars ' produced by neutral particles is due to a chance coincidence is $\sim$6% or less.

Since the effective track-length of shower particles arising from the secondary interactions is small compared with that from the primary, the number of tertiary interactions among our ' stars ' must be small. Further, since the statistical errors in Q are rather large, we believe that the possible inclusion of a small number of tertiary interactions will not seriously alter our results, provided that the difference in the value of Q for secondary stars and the primary interaction is not large.

Since the mean distance traversed by the π^0-mesons before they decay is small, and since the distances from the origin at which our neutral secondary interactions were observed to occur were, with one exception (i.e. 7 mm), greater than 1·5 cm we conclude that the probability that π^0-mesons have contributed to the secondary nuclear interactions is very small.

(c) *Examination of Secondary Stars*

Our present knowledge of K-mesons leads us to expect the following reactions to occur in their collisions with nuclei (*Pisa Conference* 1955) :—

$$(1)\ K^+ + N \rightarrow \begin{cases} (a)\ \theta^0 + N + \ldots \pi \\ (b)\ K^+ + N + \ldots \pi \end{cases}$$

$$(2)\ K^- + N \rightarrow \begin{cases} (a)\ \bar{\theta}^0 + N + \ldots \pi \\ (b)\ K^- + N + \ldots \pi \\ (c)\ \Sigma + \pi + \ldots \pi \\ (d)\ \Lambda^0 + \pi + \ldots \pi \end{cases}$$

If these reactions take place in complex nuclei, the velocity of the heavy secondary particles may be appreciably reduced by collisions with nucleons. Daniel *et al.* (1952) have studied the variation of star size as a function of primary energy. Applying their results to the interactions produced by the shower particles in the outer core of our jets (i.e., those lying outside the median angle) we deduce that their average energy is $\sim$5 Bev. If therefore an appreciable fraction of these particles were K mesons, some should lose sufficient energy in nuclear collisions to be subsequently identified.

In following the tracks of shower particles for 17·02 metres we observed 51 interactions with two or more outgoing tracks. The corresponding value of the interaction length is $33{\cdot}4\pm4{\cdot}7$ cm. In addition 4 large angle single scatters ($\geqslant10°$) have been observed. If these are included in the number of interactions the mean free path becomes $31{\cdot}0\pm4{\cdot}2$ cm. (The geometrical mean free path in emulsion, assuming $R_A=1{\cdot}38\times10^{-13}\times A^{1/3}$, is 27 cm (Lal *et al.* 1954).)

From the secondary stars produced by shower particles in the outer core, all tracks with ionization $g\geqslant1{\cdot}5g_0$ and projected length $\geqslant1$ mm per plate were followed either to the end of their range, or to their point of exit from the stack. Thirty-two stars have been examined thus far. Two heavy unstable particles with $g>2g_0$ were found, one a χ meson which decayed at rest, the other a hyperon decaying in flight.†

To estimate the number of heavy unstable particles in the secondary stars which could have been produced by the reaction

$$\pi+N\rightarrow\mathrm{Y}+\mathrm{K}$$

we have compared our results with those of Dahanayake *et al.* (1955). In a similar number of stars, and for the same selection criteria as employed in this experiment, Dahanayake *et al.* observed only $0{\cdot}16\pm{\cdot}05$ heavy unstable particles.

§ 3. Discussion

The observed ratio $N\pi^0/n_s$ gives the fraction of charged shower particles which are not π-mesons if it is assumed (*a*), that the γ-rays originate only from the decay of π^0-mesons ; and (*b*), that π-mesons are produced in a charge independent way ; i.e. $N_{\pi^\pm}=2N_{\pi^0}$.

Assumption (*a*) might fail if, in high energy collisions, particles of high spin are produced which could contribute γ-rays by 'Abstrahlung' (Schiff 1949, Oehme 1951) ; or if the hypothetical hyperon Σ^0, which decays according to the reaction $\Sigma^0\rightarrow\Lambda^0+\gamma$ with lifetime $\geqslant10^{-18}$ sec., is produced with appreciable frequency . At present there is no evidence for particles with spin >1 and the evidence for the existence of the Σ^0 is uncertain. It is therefore reasonable to assume tentatively that the π^0-mesons are indeed the only source of γ-rays. Further, the assumed validity of 'charge independence' in the production of π-mesons is

† Another hyperon emitted from a primary interaction, and having $g=1{\cdot}5\ g_0$ was observed to decay in flight.

supported by experiments at energies up to 50 Bev (Carlson *et al.* 1950, Salvini and Kim 1952). We may therefore write

$$f = \frac{N_{K\pm}}{N_{\pi\pm}} = \frac{0{\cdot}5}{R} - 1 = 0{\cdot}30 \pm 0{\cdot}14.$$

With the exception of the result of Mulvey (1954) which was based on a single event, the values of R reported by the various laboratories do not differ widely, indicating $R \simeq 0{\cdot}4$. For this value an error of 10% in R would lead to an error of $\sim 30\%$ in f.

It appears that it would be very difficult to increase greatly the accuracy of the determination of R because of the rarity of high energy events and possible sources of systematic error. It follows that the significance of information to be obtained from the determination of R is very limited. From the ratio of the numbers of stars produced by neutral and charged secondaries respectively, the fraction of shower particles which are not π-mesons can be deduced if the following assumptions are made :

(*a*) These particles are nucleons and/or heavy mesons (K^+, K^-, θ^0, $\overline{\theta}^0$), with isotopic spin $\tau = \frac{1}{2}$, which are also produced in a charge independent way (Gell-Mann 1953, Gell-Mann and Pais 1954, Nakano and Nishijima, 1953, Nishijima 1954). In this case, in contrast with π-mesons, the numbers of charged and neutral particles are equal.†

(*b*) The mean free path for interaction at high energies is the same for the different types of particles.

Then since
$$Q = \frac{N_0/N_{\pi\pm}}{N_0/N_{\pi\pm}+1},$$

we obtain
$$f = \frac{N_K{}^{\pm}}{N_{\pi\pm}} = \frac{N_0}{N_{\pi\pm}} = 0{\cdot}33 \pm 0{\cdot}16$$

in agreement with the value of f obtained from R. On the above assumptions we would also expect

$$2R + Q = 1.$$

In fact we obtain

$$2R + Q = 1{\cdot}02 \pm 0{\cdot}13.$$

From the ratios R and Q we can obtain in addition a quantity which is dependent on assumption (*b*) only :

$$\frac{N_0}{N_{\pi^\circ}} = \frac{Q}{R} = 0{\cdot}65 \pm 0{\cdot}25.$$

It should be pointed out that because of the present statistical errors in R and Q, it cannot be inferred from the above results that the interaction

† Dr. R. H. Dalitz has pointed out to us that, in general $N_K{}^{\pm} \neq N_{\theta^0, \bar{\theta}^0}$. However at very high energies, where the number of particles created is large, the assumption $N_K{}^{\pm} \simeq N_{\bar{\theta}^0, \theta^0}$ seems reasonable.

lengths for the various types of particles is really the same. It may be shown that the value for the interaction mean free path of the neutral particles obtained from that of the charged particles and the ratios R and Q is extremely sensitive to these ratios.

From the evidence presented hitherto it is difficult to estimate the number of heavy mesons among the unidentified shower particles. In view of the fact that the fraction of particles different from π-mesons is appreciable, then if these particles were only nucleons, one would have to assume a very large number of secondary collisions in the target nucleus. Moreover, it appears from the work of Camerini *et al.* (1951) that at low energies the proportion of protons among the shower particles is $\leqslant 10\%$; at the extremely high energies with which we are dealing one might expect this fraction to be smaller in view of the larger multiplicities involved. To test this hypothesis it would be necessary to increase the statistics of our observations. One could then subdivide the jets into two classes according as $N_h=0$ and $N_h>0$ (N_h is the number of grey and black prongs). Since a large fraction of the stars of the first type, $N_h=0$, would represent collisions with hydrogen, light nuclei or glancing collisions with heavy nuclei, the ratios R and Q should be different for these stars as compared to the stars of the type $N_h>0$, if a large proportion of the unidentified shower particles were actually nucleons ejected from the target nucleus.

From the foregoing considerations the necessity for the investigation of secondary stars becomes obvious. The evidence from various experiments accumulated hitherto indicates that a large proportion of the shower particles in high energy nuclear interactions are mainly produced through a multiple production mechanism. This would imply that most of the particles in the outer core of our jets are those moving backwards in the C.M. system but are otherwise identical in their composition with the particles in the inner core.

From the ratios R and Q it appears that $\sim 25\%$ of the charged shower particles are not π mesons. On the other hand the results of § 2(*c*) are consistent with the presence of an appreciable proportion of heavy mesons among the shower particles in the outer core, and if so most of the unidentified particles in the inner core of jets would also be heavy mesons.

It is interesting to note that a fraction of the unidentified particles could be accounted for by the creation of nucleon- anti-nucleon pairs. However, since our statistics are poor we cannot draw any far reaching conclusions until further evidence from the study of secondary interactions is available.

Acknowledgments

We are deeply indebted to Professor C. F. Powell for extending to us the hospitality of his laboratory and for his constant encouragement and criticism.

We wish to thank Dr. R. H. Dalitz and many of our colleagues in the laboratory for many fruitful discussions ; and Miss S. Bult, Mrs. M. Davies and Mrs. M. Herman for scanning the plates.

C.D. wishes to thank the Government of Ceylon and Y.F. the British Council for Maintenance Grants.

APPENDIX

Differentiation between Associated, Direct and Bremsstrahlung Pairs

Pairs originating at points distant from the star can be of two types, which we term ' associated ' or ' bremsstrahlung ' pairs. Associated pairs are due to external conversion of γ-rays resulting directly from the decay of π^0-mesons. Bremsstrahlung pairs result from conversion of γ-rays of secondary origin, i.e. those radiated by ' bremsstrahlung ' of electrons closer to the star origin.

Fig. 1

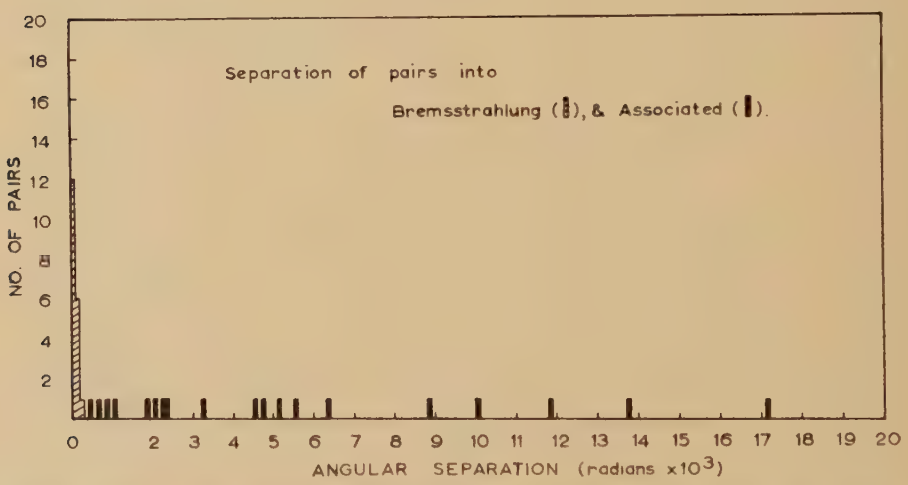

Distribution of the angular separation of electron pairs, from the nearest electron track, measured with respect to the origin.

Let u be the lateral distance between the origin of a pair and the nearest parallel electron track, produced earlier in the cascade (or shower), and let x be the distance of the pair origin from the star. Thus u/x measures the angular separation, relative to the star origin, of the pair from the electron track nearest to it. The distribution in u/x for a sample of pairs in the jets examined is shown in fig. 1. These pairs will of course exclude the first pair, nearest to the star. It is clear from this graph that the pairs are of two types. Bremsstrahlung pairs occur at angles less than

3×10^{-4} radians and associated pairs are limited to angles greater than 5×10^{-4} radians. Thus at least for values of x less than one radiation length, differentiation between the pairs of the two types is unambiguous.

Differentiation between associated and direct pairs is not possible, but the contribution of the direct pairs can be calculated and shown to be small. A fraction $p=1/70$ of the π^0-mesons undergo the alternative mode of decay into two electrons and a single γ-ray. Then if n_0 is the number of π^0-mesons which undergo direct decay and produce pairs which are counted as associated, the error introduced in R can be shown to be $100(n_0/n_p-p/2)\%$ where n_p is the total number of pairs observed.

Altogether, there were 370 shower particles or $(370R)$ π^0-mesons in the jets examined. Of these, 370 $R\times p$ or $\simeq 5R$ would undergo direct decay. About half of the direct electron pairs would make relatively large angles with the central core of the jet, and since they would be of low energy, would appear to originate within a few microns of the star and be easily distinguishable. Since $R\simeq 0{\cdot}4$ we therefore estimate that only one direct pair occurring in the dense forward core of the jets would be wrongly counted as an associated pair. Since the total number of associated pairs observed was 77 the error arising from the contribution of direct pairs is about $0{\cdot}6\%$.

APPENDIX II

Observations to determine ρ, the distance traversed by π^0-Mesons before Decay

From table 4 it is seen that the value of R is dependent upon the assumed value of ρ. We have attempted to find the appropriate value of ρ by the following method :

Fig. 2

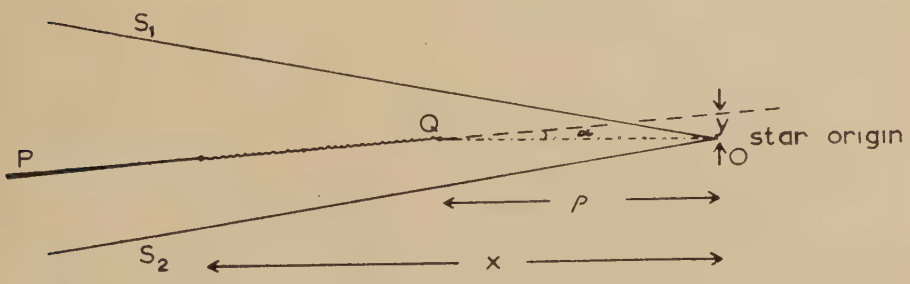

Measurement of the distance, y.

Suppose a π^0-meson, emitted from a star O, decays at the point Q, one of the γ-rays being emitted at an angle α and converting into a pair P (fig. 2). If the γ-ray is of very high energy, the electrons form a single

track. If S_1 and S_2 are the tracks of two shower particles, measurement of the separation between P, S_1 and S_2 at known distances from the star, will determine the intercept $y=\rho \tan \alpha$. In the diagram, y will be positive for S_2 and negative for S_1. It must be assumed that the scattering along the tracks P, S_2 and S_1 as well as their relative distortion over the length measured is negligible. Such conditions can often be achieved in practice in the central cores of jets where multiple Coulomb scattering of the particles is very small and where the track density is such that shower particles with dip very close to that of the pair can usually be found. Another necessary condition for accurate measurement of ρ is that the distance traversed by the pair before separating into two distinguishable minimum tracks must be comparable with the distance x of the pair origin from the star. These factors in practice limit measurements to high energy pairs in the central core, converting at distances x less than $\sim$1 cm from the star.

If θ represents the direction of emission of the γ-ray in the rest system of π^0

$$\gamma \tan \alpha = \sin \theta/(1+\cos \theta).$$

Now, $\rho=\gamma ct$, where t is the lifetime of a particular π^0-meson in its own rest system, and γ the total energy of the π^0-meson in terms of its rest-energy. Thus $y=\rho \tan \alpha = ct\gamma \tan \alpha$. Assuming an exponential distribution in the proper time t, the distribution in the projected value of the intercept, $y_p=y \cos \phi$, in the plane of the emulsion is

$$N(\geqslant y_p)=\int_{\varphi=0}^{\varphi=(\pi/2)} \frac{2}{\pi} d\phi \int_{\tau=0}^{\tau=\infty} \frac{\tau^2 e^{-\tau} d\tau}{[\tau^2+y_p^2/\cos^2 \phi]}$$

and can be computed numerically. This distribution has a mean value $y_p=0{\cdot}763\, c\tau$ where τ is the mean π^0-lifetime. Thus measurement of y_p yields the lifetime directly, independent of the energy of the particular π_0-mesons selected. It will be seen that the principle of the method is similar to that of Carlson, Hooper and King (1950), but is capable of much higher accuracy.

In fig. 3 are shown (*a*) the distribution of the projected intercept y_p between a single electron pair and nearby shower tracks, and (*b*) the corresponding distribution of the intercept y'_p, say, between the shower tracks themselves. In the absence of errors of measurement, scattering and distortion, y'_p would be zero, so that the distribution obtained represents the combined effect of these errors. The difference between the two distributions appears significant, and must correspond to a finite time of flight of the π^0-meson of the order of 10^{-15} sec. In this particular case, conditions of measurement were very favourable, as relative measurements could be made with four shower tracks, over a distance of 7 mm. The pair originated at a distance of 3·5 mm from the star.

Fig. 3

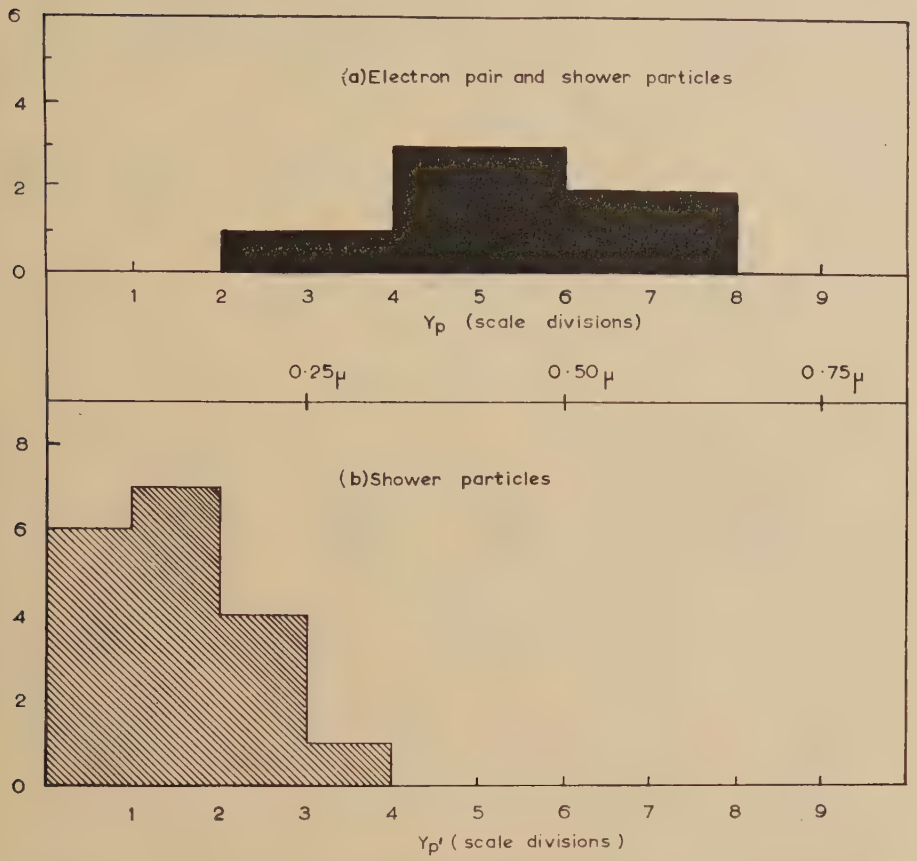

Distribution of separation at origin between (*a*) a single electron pair and shower particles, and (*b*) shower particles only.

So far, suitable conditions of measurements have been found on only ten high energy pairs, and the results are shown in fig. 4. Each square of the histograms represents the mean of several independent measurements of y_p and y'_p (figs. (*a*) and (*b*) respectively) relating to a single electron pair. For every pair examined, it was found that, if y_p was positive for a shower particle on one side of the pair, it was negative for a shower particle on the other side, and vice versa, thus confirming that the quantity y_p represents a real effect and does not consist merely of errors of measurement. From fig. 4 (*b*) it will be seen that the r.m.s. deviation amounts to about $0{\cdot}2\,\mu$. Their distribution will not be necessarily Gaussian, since the effects of distortion for each event will not be random. On account of these errors the mean value of y_p obtained from fig. 4 (*a*) will only yield an upper limit for the lifetime. This limit is $(2{\cdot}6 \pm 1{\cdot}2)\ 10^{-15}$ sec. A more reliable estimate can be found by considering only those three pairs for

which y_p exceeds $0{\cdot}8\,\mu$, i.e. more than three times the error of measurement. We then find that the lifetime lies with a 90% probability within the limits $1{\cdot}8^{+3{\cdot}2}_{-1{\cdot}1} \times 10^{-15}$ sec. This estimate will be greatly improved when more statistics become available. It will, however, be noted that the above value is in good agreement with that obtained by a completely independent method by Anand (1953).

In order to determine ρ from the above measurement of lifetime, the energy of the π^0-mesons must be known. This can be accomplished by

Fig. 4

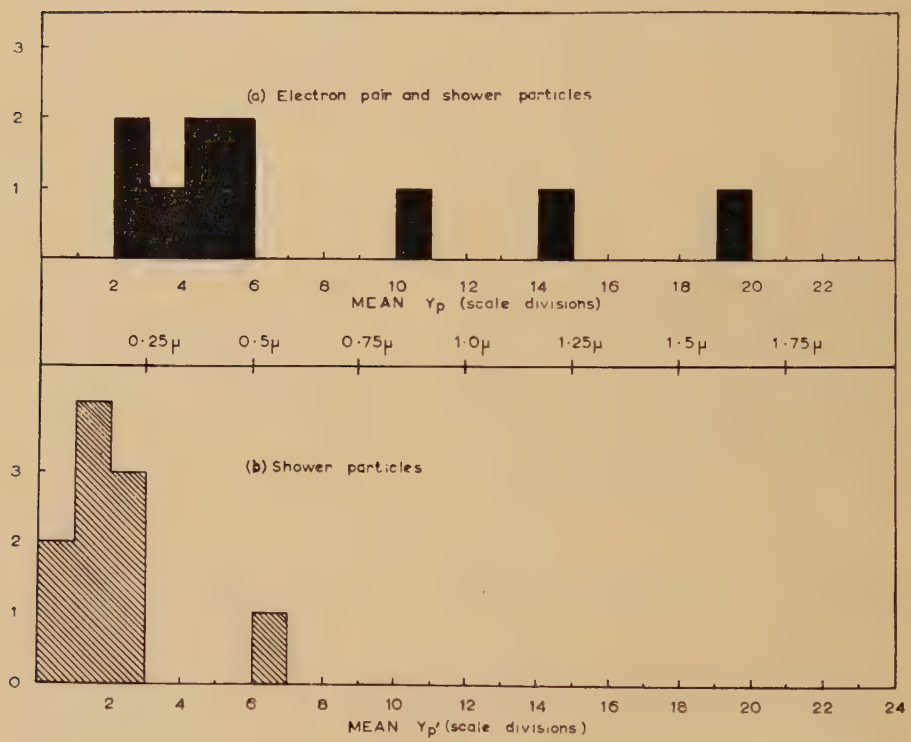

Distribution of the mean projected separation at origin between (*a*) the electron pairs and shower particles, and (*b*) between the shower particles only.

measurement of the relative Coulomb scattering between electrons of the pairs. For a given γ-ray of energy E the distribution of the relative scattering along a given length of the electron tracks can be calculated from the known disparity distribution (Bethe and Heitler), account also being taken of the gradual decrease of energy of the electrons by radiation loss. The distribution in the mean scattering angle is very wide, and thus the value obtained from any one pair is subject to large statistical fluctuations. We have therefore found the mean pair energy ($\bar{E}$) (75 Bev)

and hence the mean π^0-energy $2(\bar{E})$ (150 BEV), by averaging over a large number of pairs occurring in the central cores of the jets examined. This leads to a value of $\bar{\rho}=0{\cdot}87$ mm.

REFERENCES

ANAND, B. M., 1953, *Proc. Roy. Soc.*, **220,** 183.

CAMERINI, U., DAVIES, J. H., FRANZINETTI, C., LOCK, W. O., PERKINS, D. H., and YEKUTIELI, G., 1951, *Phil. Mag.*, **42,** 1261.

CARLSON, A. G., HOOPER, J. E., and KING, D. T., 1950, *Phil. Mag.*, **41,** 701.

DAHANAYAKE, C., FRANCOIS, P. E., FUJIMOTO, Y., IREDALE, P., WADDINGTON, C. J., and YASIN, M., 1955, *Nuovo Cim.*, V, 888.

DANIEL, R. R., DAVIES, J. H., MULVEY, J. H., and PERKINS, D. H., 1952, *Phil. Mag.*, **43,** 753.

FREIER, P., and NAUGLE, J., 1953, *Phys. Rev.*, **92,** 1086.

GELL-MANN, M., 1953, *Phys. Rev.*, **92,** 833.

GELL-MANN, M., and PAIS A., 1954, *Proc. of the Glasgow Conf. on Nuclear and Meson Physics*, 342.

KAPLON, M. F., and RITSON, D. M., 1952, *Phys. Rev.*, **88,** 386.

KAPLON, M. F., WALKER, W. D., and KOSHIBA, M., 1954, *Phys. Rev.*, **93,** 1424.

KOSHIBA, M., and KAPLON, M. F., 1955, *Phys. Rev.*, **97,** 193.

LAL, D., YASH PAL and RAMA, 1954, *Suppl. Nuovo Cim.* 12.

MULVEY, J. H., *Proc. Roy. Soc.*, 1954, **221,** 367.

NAKANO and NISHIJIMA, K., 1953, *Prog. Theor. Phys.*, **10,** 581.

NISHIJIMA, K., 1954, *Prog. Theor. Phys.*, **12,** 107.

OEHME, R., 1951, *Zeits. f. Phys.*, **129,** 573.

Report of the Pisa Conference 1955.

SALVINI, G., and KIM, Y., 1952, *Phys. Rev.*, **85,** 921 ; **88,** 40.

SCHIFF, L., 1949, *Phys. Rev.*, **76,** 89.

VAN HOVE, L., MARSHAK, R. E., and PAIS, A., 1952, *Phys. Rev.*, **88,** 1211.

LXIII. *The Measurement of the Distance of Radio Sources by Interstellar Neutral Hydrogen Absorption*

By D. R. W. Williams and R. D. Davies

Jodrell Bank Experimental Station, University of Manchester †

[Received December 2, 1955]

Abstract

The distance of a radio source can be determined from its absorption spectrum produced by interstellar neutral hydrogen. Three methods have been used to obtain a distance from these data. It can be decided where any source lies within the Galaxy or whether it is extragalactic. A method is also described for obtaining the kinetic temperature of interstellar neutral hydrogen from absorption and emission spectra.

The Cygnus source was found to be extragalactic, the Cassiopeia source appears to lie at a distance of between 2·5 and 5·5 kiloparsecs; while the Sagittarius source is about 3 kiloparsecs from the sun in the direction of the galactic centre.

§ 1. Introduction

Early attempts by Ryle (1950), Smith (1951) and Mills (1951) to measure distances of radio sources by the method of parallax served to place the major radio sources outside the solar system at a distance greater than $\frac{1}{2}$ parsec. This paper describes a new technique of distance measurement. It involves the measurement of the absorption spectrum of the source produced by interstellar neutral hydrogen at a wavelength of 21 cm. Three different methods have been used to obtain a distance from the absorption spectrum.

(i) The existence of absorption at the frequency of emission from a spiral arm in the direction of a source places it in relation to that arm.

(ii) The distance can be determined from the amount of hydrogen between the sun and the source if the distribution of hydrogen in the direction of the source is known.

(iii) The absorption linewidth of a source enables its distance to be determined in a way analogous to that used in optical astronomy. The last two methods are useful in the galactic centre and anticentre regions where the neutral hydrogen has only a small Doppler displacement relative to the sun. Accordingly, the position of a source within the Galaxy can be determined and moreover it can be established whether any source is

† Communicated by Professor A. C. B. Lovell, F.R.S.

extragalactic. The technique has been applied to the four intense sources in Cassiopeia (23N 5A), Cygnus (19N 4A), Taurus (05N 2A) and Sagittarius (17S 2A).

§ 2. Equipment

The receiver, which is a radio spectrometer, is used in conjunction with a 30 ft focal plane paraboloid illuminated by a dipole feed with reflector. The beamwidth to half-power points is 1·45° in the H-plane and 1·65° in the E-plane. The aerial mounting is alt-azimuth, and in order to follow a source to within a quarter of a beamwidth a tracking mechanism is included in the altitude and azimuth driving circuits.

The receiver employs the comparison technique in order to obtain the required stability. It is switched at 30 c/s between the line frequency and a comparison band 1 Mc/s on one side of the line. By use of a new technique which involves having a second pair of receiving bands, one on the line frequency and a comparison band on the other side of the line, it is possible to observe the line continuously. This ' double comparison technique ' gives an improvement in sensitivity of 1·5 db over the single comparison method. The line profile is obtained by varying the frequency of the first local oscillator. The noise factor of the receiver measured with an argon noise source was 8·5 db, and this value was checked by comparing the receiver noise temperature with the aerial temperature of the sun. The receiver bandwidth was 40 kc/s and the observing time constant was 30 seconds which gave peak to peak fluctuations of 7°K on the recorder output.

A total power receiver is required to measure the intensity of the continuum radiation from the radio sources. A rotating capacity switch having a switching ratio of 20 db enabled the temperature of the aerial and a dummy load to be compared at 30 c/s and this gave the desired stability. The continuum measurements were made using the broadband (1·1 Mc/s) section of the receiver. The absolute aerial temperatures of the sources were obtained by comparing the source emission with the neutral hydrogen emission at $l=50°$ and $b=0°$ (taken as 100°K) using a bandwidth of 40 Kc/s.

§ 3. Observational Methods of Establishing the Distances of Radio Sources

3.1. *The Distance of a Radio Source Obtained from its Absorption Spectrum*

This method enables a radio source to be placed in relation to the galactic spiral arms whose existence is now well established (van de Hulst *et al.* 1954). The following simple picture is used to describe the method and to explain the observed absorption results. Let a source lie between two spiral arms A and B as in fig. 1. Figure 1 (*a*) represents the spectrum observed very close to the source, and it is assumed to be the spectrum in that direction if the source were absent. The first peak is

due to emission from the nearer spiral arm A and the second peak is due to arm B. Figure 1 (*b*) is the absorption spectrum of the source due to its continuous emission traversing spiral arm A and being absorbed at the frequency of that arm. Then the observed spectrum in the direction of the source will be the sum of (*a*) and (*b*) and is shown in fig. 1 (*c*).

Fig. 1

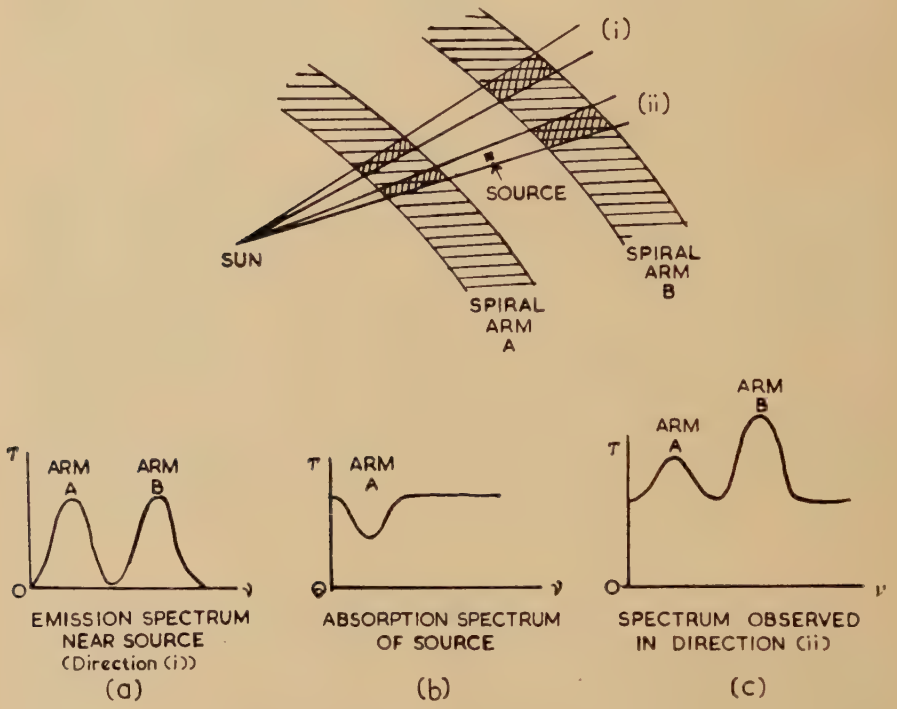

A diagram to show the formation of the spectrum in the direction of a radio source. The spectrum, (*a*) is taken in direction (i) near the source and shows emission peaks due to the spiral arms A and B. The absorption spectrum, (*b*) of the source is added to (*a*) to give the spectrum, (*c*) observed in the direction of the source.

Alternatively, the absorption spectrum of the source, which contains all the required information, can be obtained by subtracting spectrum (*c*) from spectrum (*a*). In this model it is assumed that the source itself blocks out only a negligible amount of neutral hydrogen from behind it (i.e. either its diameter is small compared with the aerial beamwidth or it is optically thin, or both).

If a source lies beyond or within a spiral arm it will exhibit absorption at the frequency characteristic of that arm. Thus if an absorption spectrum is obtained for a source and it shows a peak at the frequency characteristic of a spiral arm in that direction, then the source must lie

beyond that arm. If, in addition, there is no absorption at the frequency of the next most distant spiral arm, the source lies between the two spiral arms. The exact position of these spiral arms depends upon an accurate knowledge of the rotational velocity in all regions of the Galaxy. In the present study the circularly symmetrical Oort model is used in conjunction with the hydrogen-line profiles to establish the distance of the arms in the direction of the sources. Moreover, the above method can be used to indicate whether any source is extragalactic since hydrogen is found in all directions in space and will produce absorption in the spectrum of the source.

However, this method is not applicable to sources inside the galaxy where there is little or no differential motion since a source cannot be placed relative to spiral arms which are not distinguishable by their frequencies of emission. Two ways of treating such cases are described in § 3.1 and § 3.3 below.

3.2. *The Distance of a Source Obtained from the Spatial Distribution of Hydrogen*

The observed absorption spectrum of a source allows an estimate to be made of the number of neutral hydrogen atoms, N_H (source), per unit cross section in the line of sight to the source. (van de Hulst *et al.* 1954.)

$$N_H\,(\text{source}) = 1{\cdot}84 \times 10^{13}\, T_K \int_0^\infty \tau(\nu)\, d\nu. \quad . \quad . \quad . \quad . \quad . \quad (1)$$

where T_K is the kinetic temperature of the gas which is assumed to be 125°K and $\tau(\nu)$ is the optical depth of the hydrogen at frequency ν in the absorption spectrum. Then, if $n_H(x)$, the distribution of hydrogen with distance, x, is determined by some means, the distance of the source, X, can be found such that

$$N_H\,(\text{source}) = \int_0^X n_H(x)\, dx. \quad . \quad . \quad . \quad . \quad . \quad . \quad . \quad (2)$$

For sources lying in the direction of the galactic centre, such as the Sagittarius source, a useful estimate of the distribution can be made by studying the emission spectra of neutral hydrogen from the inner parts of the Galaxy. These spectra show a sharp cut-off at the low-frequency end due to emission from hydrogen at the tangent point of galactic rotation in the line of sight. A circular rotation model is assumed and the observed brightness temperature at the cut-off frequency is taken as a measure of the density of neutral hydrogen at that point. The locus of these tangent points is a circle centred half-way between the sun and the galactic centre. The density at each of these points can be obtained from the observed brightness temperature if we know the velocity distribution (η) of the clouds and the depth of emission at that distance. The values of (η) given by Kwee *et al.* (1954) were used but the depth of emission at each point is difficult to assess and, to a first order, may be taken as the depth of hydrogen which has an emission bandwidth equal to the observing

bandwidth. The density at each value of R (the distance from the galactic centre) along this semicircular locus is then taken to be the density at the same value of R along the line of sight from the sun to the centre. The absolute density distribution is obtained by making the total number of atoms in this distribution equal to the total number derived from the emission spectrum in this direction.

3.3. *The Distance of a Source Obtained from its Equivalent Width*

In optical astronomy the intensities of interstellar absorption lines are known to give a statistical measure of the distance of stars. In a recent study Beals and Oke (1953) compared the measured distance of a large number of stars up to 2·5 kiloparsecs with the equivalent width of their absorption lines and found a linear relationship. The distance of individual stars could be measured to an accuracy of 25% using the derived linear relation. The error was largely due to non-uniform distribution of absorbing dust in the direction of the star.

This method can now be used to measure the distance of a radio star by calculating the equivalent width, H, of its neutral hydrogen absorption line. It is defined as follows :

$$H=\int_{-\infty}^{+\infty}\frac{I_0-I_v}{I_0}\,dv \text{ km/sec} \quad . \quad . \quad . \quad . \quad . \quad . \quad (3)$$

where I_0 is the intensity of the unabsorbed continuum from the source and I_v is the intensity of absorbed radiation at a velocity v km/sec. It follows from this definition that H is independent of the receiver bandwidth. A calibration curve relating H and distance is required to give the distance of a radio source whose equivalent width has been found. Such a curve is obtained by plotting the distances determined for the Cassiopeia, Cygnus and Taurus sources against their equivalent widths.

The method of obtaining the distance of a source from its equivalent width requires further justification. The hydrogen-line equivalent width relation (see § 4.3)

$$r=220 \text{ H parsecs} \quad . \quad . \quad . \quad . \quad . \quad . \quad . \quad (4)$$

may be compared with the optical result for the interstellar calcium K line (Beals and Oke 1953),

$$r=34{\cdot}8 \text{ K parsecs} \quad . \quad . \quad . \quad . \quad . \quad . \quad . \quad (5)$$

which held at least to a distance of 2·5 kiloparsecs. The hydrogen absorbing line is then six times weaker than the calcium line and the linear relationship for hydrogen may be expected to hold to 15 kiloparsecs before saturation effects come into play. Moreover, this calibration curve becomes increasingly accurate for more distant sources although it is liable to some error for the nearer sources because of the known non-uniform distribution of neutral hydrogen.

At first sight it is unexpected that the equivalent width of a line should increase linearly with distance since it has been shown theoretically (Oort 1953) that clouds are likely to have optical depths of the order of

unity and therefore, where there are a number of clouds in the line of sight, saturation effects may be present. However, this argument fails to account for the fact that each cloud has its peculiar random velocity which spreads the absorption spectrum and making the total equivalent width nearly equal to the sum of the individual equivalent widths. The above explanation was derived from Wilson and Merrill (1937) who clarified a similar anomaly in the optical case. It is assumed in this method that the distribution of neutral hydrogen is uniform on a large scale (of the order of a kiloparsec). Moreover, the method is applicable in the optical case using interstellar sodium and since the constituents of the interstellar medium are believed to be similarly distributed (Spitzer 1948), it should apply with equal accuracy (about 25%) in the radio case. The observed linear relation between distance and equivalent width in fig. 5 also justifies the basic assumption.

§ 4. Results

4.1. *The Absorption Spectrum of the Sources*

The initial experiments (Williams and Davies 1954) were designed to detect whether interstellar neutral hydrogen absorbed the continuous radiation of the sources. The maximum absorption was expected at the peaks of the hydrogen-line profiles in the direction of the sources. Accordingly, the sources in Cassiopeia and Cygnus were allowed to drift through the aerial pattern with the receiver turned to the peak frequencies in each spectrum. The observation was then repeated at frequencies placed $\frac{1}{2}$ Mc/s either side of the peaks, and about twenty such sets of observations were obtained and averaged. The Cygnus source was found to show absorption at both peak frequencies. The Cassiopeia source was clearly absorbed at the frequency of the inner peak but the absorption at the outer peak was near the limits of error.

These preliminary results showed that a more sensitive equipment was necessary in order to measure the absorption in the Cassiopeia and Cygnus sources more accurately and to allow observations on weaker sources. With improved equipment it became possible to track the radio source and obtain a spectrum so obtaining the absorption spectrum in any direction. In addition, the position of the aerial was accurately calibrated for all parts of the sky by observing the sources on total power and broad-band using the rotating switch.

The changing spectrum of the hydrogen near the source must be accounted for in obtaining the real emission spectrum in the precise position of the source. Accordingly it was necessary to observe the spectrum not only in the direction of the source itself but also in directions adjacent to the source. Spectra were taken on a grid of 8 points displaced 2° either side of the source in right ascension and declination and at the 4 diagonal points. Sets of 3 spectra were taken across the source and were repeated 3 times. Two such spectra, one obtained near the Cassiopeia source and one on it, are shown in fig. 2. Two idealized spectra are then derived for each source ; one is the average of all points surrounding the source and represents the emission spectrum of the hydrogen if the source

were not present, and the other is the average of the spectra taken on the source. The absorption spectrum for a source is obtained by subtracting these two spectra and it may be converted into a fractional absorption spectrum by dividing by the aerial temperature of the source. (A 10% correction is required to the observed aerial temperature of the source to allow for partial reception at the image frequency.) The two idealized spectra and the fractional absorption spectrum for each of the sources in Cassiopeia, Cygnus, Taurus and Sagittarius are given in fig. 3.

Fig. 2

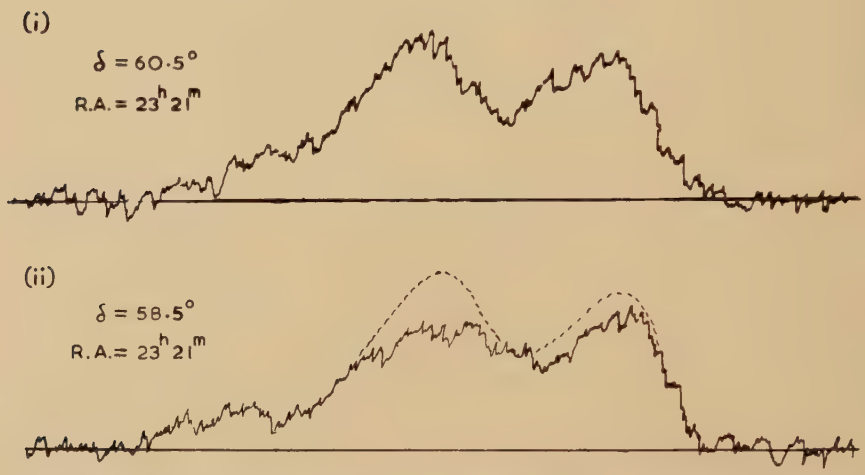

Two recordings of spectra obtained in Cassiopeia. (i) is a spectrum taken near the source and (ii) is taken in the direction of the source. The smoothed upper spectrum is repeated as a dotted line on the lower tracing.

The spectrum in the Cygnus region has two peaks due to neutral hydrogen concentrated in spiral arms at 4 and 8 kiloparsecs. Since the spectrum of the Cygnus source shows absorption at the frequency of both spiral arms, it must be extragalactic. In the Cassiopeia region the emission spectrum has three peaks which are due to spiral arms at 0·5, 3·0 and 5·5 kiloparsecs. The Cassiopeia source shows absorption in the inner two arms but not in the outer one ; this places it at a distance of between 3·0 and 5·5 kiloparsecs. In the vicinity of the Taurus and Sagittarius sources there is insufficient Doppler displacement to assign distances to the emitting neutral hydrogen and consequently the above method is not applicable to these sources.

4.2. *The Distribution of Neutral Hydrogen Towards the Galactic Centre*

The distribution of neutral hydrogen in the direction of the Sagittarius source can be obtained from the emission spectra of the inner parts of the Galaxy between $l=350°$ and $l=35°$. In a preliminary survey, a number of spectra were taken with a 18 kc/s bandwidth at galactic latitude $-1·5°$. The narrow bandwidth was necessary in order to delineate more

clearly the arm structure shown in the profiles obtained by Kwee *et al.* (1954). At the low frequency end of the prolfies there is a sharp rise in temperature when the line of sight is tangent to a spiral arm. In other directions there is a tail to the spectrum showing the existence of inter-arm hydrogen which is emitting at the frequency expected on the Oort rotation model. The temperature is then read off the spectrum at the frequency expected at the tangent point in the line of sight. In the interarm regions the effect of the adjacent spiral arm at a slightly higher

Fig. 3

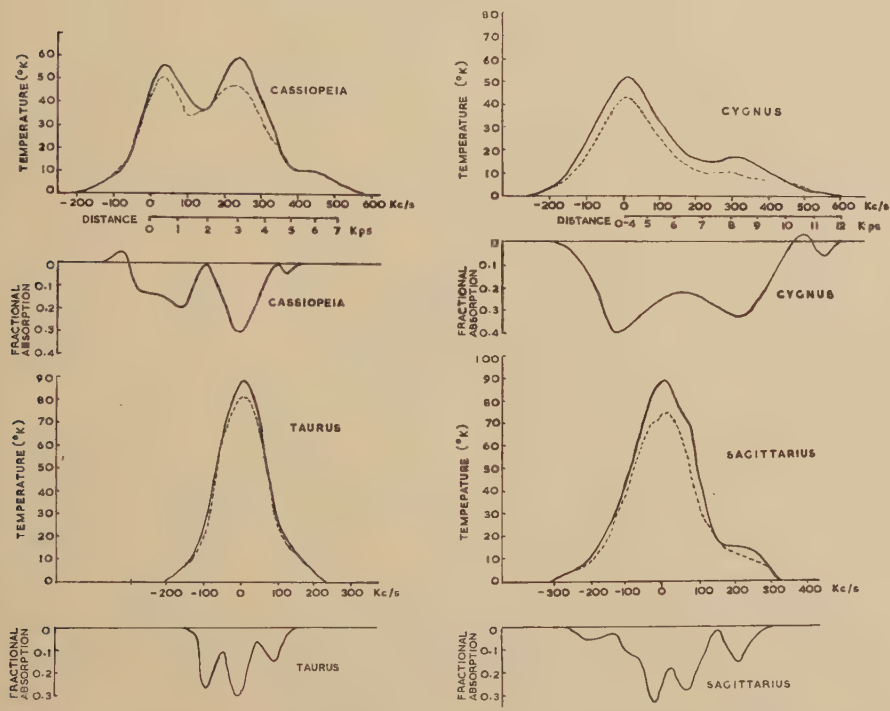

Spectra of the sources in Cygnus, Cassiopeia, Taurus and Sagittarius. The upper spectra in each case are the idealized emission spectra for each source ; the full line is the average of spectra near the source and the dotted line is the spectrum observed in the direction of the source. The lower spectrum for each source is the fractional absorption spectrum.

frequency is removed before the temperature can be estimated. The distribution of brightness temperature with distance from the galactic centre shows maxima at $R=4{\cdot}0$, $5{\cdot}8$ and $8{\cdot}8$ kiloparsecs. Temperatures are then converted into optical depths and the distribution of hydrogen with distance from the galactic centre is derived as described in § 3.2. The result is shown in fig. 4. The number of hydrogen atoms between the Sagittarius source and the sun was computed from the absorption spectrum of the source to be $1{\cdot}9\times10^{21}$ per cm^2 (compared with $6{\cdot}5\times10^{21}$ per cm^2 in the line of sight to the centre of the Galaxy). The result

places the source at a distance of 2·2 kiloparsecs from the sun. This estimate of distance is believed to be reliable within 1 kiloparsec for the following reasons. The calculated number of neutral hydrogen atoms between the sun and the source is 0·3 of the total number toward the galactic centre; thus placing the source in the centre of the second spiral arm in this direction. An error of 70% in the estimate of the number

Fig. 4

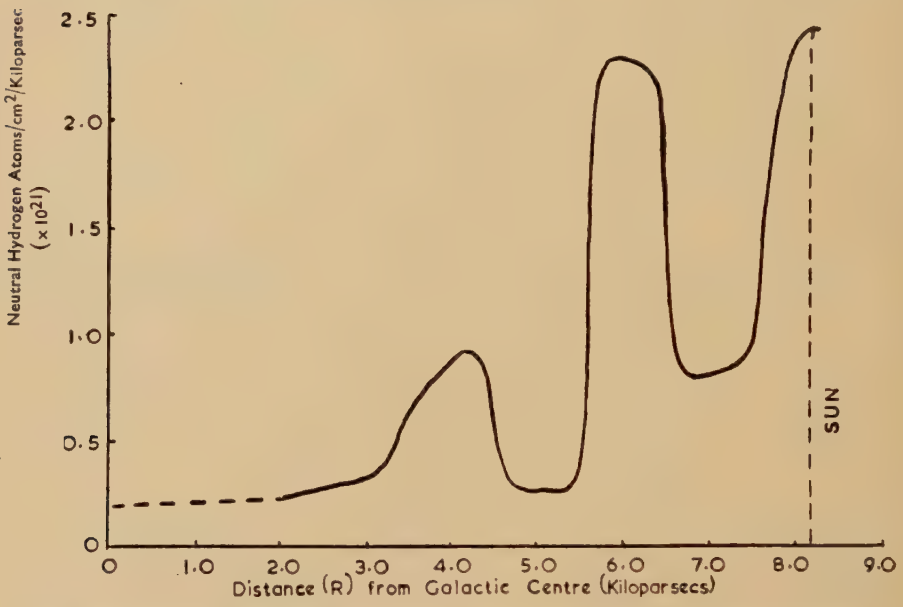

The distribution of neutral hydrogen in the direction of the galactic centre.

of atoms between the sun and the source would be required to shift the source into the regions of low density either side of the arm. Such an error could arise if the kinetic temperature of a large part of the neutral hydrogen in this direction was appreciably different from 100°K. This appears to be unlikely because the inner spiral arms, when observed obliquely (i.e. when their optical depth is greater than unity) all show brightness temperatures of this order.

4.3. *The Equivalent Widths of the Sources*

The equivalent width of the neutral hydrogen absorption line was determined from the absorption spectrum of each source by measuring the area under the absorption curve with a planimeter; the results are given in table 1. An error due to the noise fluctuations on the original records is given for each value of equivalent width. Also included in the table are the source distances, which are assigned as follows. The Cassiopeia source is placed as near to the optical position as is consistent with the interpretation of § 3.1. This is discussed more fully in § 5.2. The distance given in the case of Cygnus is the distance to the outer arm

Fig. 5

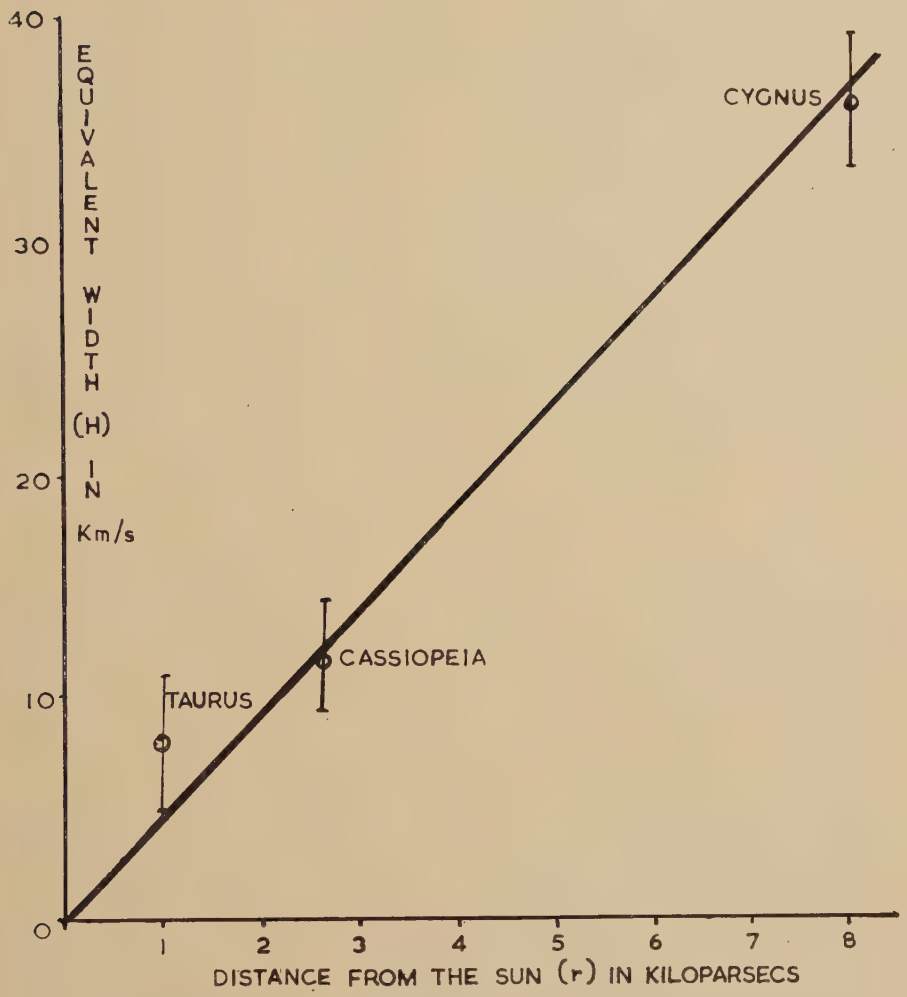

A plot of the equivalent width against the distance for the sources in Cygnus Cassiopeia and Taurus. $\overset{\top}{\underset{\perp}{\circ}}$ represents the error in each observation.

of the Galaxy in that direction ; this is the path length to the source lying in neutral hydrogen. Taurus is known to be at a distance of 1·1 kiloparsecs (Greenstein and Minkowski 1953). The data in table 1 enable a linear linewidth against distance calibration curve to be drawn through the origin as in fig. 5. The corresponding linear relation may be written

$$r = 220\,H \text{ parsecs} \quad . \quad . \quad . \quad . \quad . \quad . \quad . \quad . \quad (4)$$

where r is the distance from the sun and H the equivalent width of the neutral hydrogen absorption line in km/sec. From this relation, an equivalent width of 14 km/s for the Sagittarius source corresponds to a distance of 2·9 kiloparsecs. At the present time, since there are only

Table 1

Source	I.A.U. designation	Distance (parsecs)	equivalent width (km/s)
Cassiopeia	23N 5A	2 500	13±2
Cygnus	19N 4A	8 000	36±3
Taurus	05N 2A	1 100	8±3
Sagittarius	17S 2A	?	14±3

a few sources whose distances are known optically, the calibration curve in fig. 5 cannot be considered reliable. Also this method is not completely independent of method (i) which was used to determine the distance of the Cassiopeia source. However, it has been used to illustrate the principle of the method in the case of the Sagittarius source.

§ 5. Interpretation and Discussion

5.1. *The Cygnus Source.* (19N 4A)

The Cygnus source shows absorption at the frequency of both the spiral arms which its radiation traverses and consequently it is outside the spiral structure of the Galaxy. This result is consistent with the identification made by Baade and Minkowski (1954) with a system of colliding galaxies at 64 megaparsecs from the sun on the new distance scale.

5.2. *The Cassiopeia Source.* (23N 5A)

The present investigation shows that the radiation from the Cassiopeia source is absorbed at the frequency characteristic of the emission from the two inner spiral arms but not the outer one, thus suggesting that it lies between 3·0 and 5·5 kiloparsecs (the distances of the outer two spiral arms). This result is at variance with the distance of 500 parsecs found by Baade and Minkowski (1954) for a nebulosity in this direction. One uncertainty in the radio method (i) for determining distances is the relation between galactic rotation and distance which must be assumed in order to determine the distances of the spiral arms. However, the model gives an apparently reliable distance (3·0 kiloparsecs) for the second spiral arm because it agrees well with the distance of four O-associations between $l=80°$ and $105°$ observed by Morgan *et al.* (1953) at an average distance of 2·4 kiloparsecs. The nearest this source could be placed is at the inner side of the second spiral arm at, say, 2·5 kiloparsecs.

It is possible that some neutral hydrogen clouds which belong to the nearest spiral arm may have a high random velocity and produce absorption at frequencies characteristic of the second spiral arm. However, since a line profile, when expressed in terms of optical depth, may be considered as the probability distribution of cloud velocities within the arms, a cloud can only belong to the spiral arm within whose velocity limits it lies. As the profile in the direction of Cassiopeia falls almost to zero

between the arms when observed with a 18 kc/s bandwidth it is very unlikely that a cloud with a velocity characteristic of one arm should belong to another.

Hagen *et al.* (1954) have studied the Cassiopeia source with a bandwidth of 8 kc/s and have found fine structure within the two absorption peaks, one line within the first peak and two within the second. These narrow absorption features may be due to groups of unresolved clouds or individual clouds. The first possibility is likely because the density of clouds in the line of sight is about 10 per kiloparsec within a spiral arm (Oort 1953). In this case the groups of clouds must belong to different spiral arms. On the other hand, if the second possibility obtains, the probability of the two high velocity clouds belonging to the inner arm may be calculated assuming the line profile is of the Gaussian form. The probability is 1 in 10^4 and suggests that this contention is unlikely. Thus it would seem that the results of Hagen *et al.* confirm the result of the present investigation that the Cassiopeia source lies at a distance greater than the second spiral arm, namely, 2·5 kiloparsecs.

5.3. *The Sagittarius Source* (17S 2A)

Two separate estimates of the distance of the source in Sagittarius have been made. They are derived from two sets of observations which are largely independent (the one method involved a measurement of the equivalent line width of the source and an estimate of the average density of neutral hydrogen in the galactic plane, while the other method involves a different analysis of the absorption spectrum and an attempt to obtain the precise density distribution in the direction of the source). The two results suggest strongly that the source is not at the galactic centre at 8 kiloparsecs, but is much nearer, at about 2 to 3 kiloparsecs.

Further information is available to clarify the nature of the Sagittarius source. Its diameter at 21 cm can be obtained from a comparison between the intensity observed with the present equipment using a beamwidth of 1·6° and the intensity observed by Hagen *et al.* (1954) using a beamwidth of 0·9°. From an examination of the Jodrell Bank records it was evident that the size of the source was less than the beamwidth because no appreciable broadening of the beam pattern was observed. The reduced ratio of intensity of the Sagittarius to the Cassiopeia source on the N.R.L. survey could be explained if the Sagittarius source has a diameter between 0·8° and 1·0°. This result is similar to that obtained at the lower frequencies (Mills 1952) and corresponds to a region about 50 parsecs across at 3 kiloparsecs.

The spectrum already published (Davies and Williams 1955) has now been extended to 3·15 cm by Haddock and McCullough (1955) who confirm that it is due to emission from an optically thin body.

The above evidence regarding the size, distance, position and spectrum of the source led Davies and Williams to suggest that the Sagittarius source may be associated with a group of 38 O and B type stars and

emission nebulae observed by Hiltner (1954) and Sharpless (1953) to lie in this direction at a distance of 3 kiloparsecs. Such an identification has since been tentatively proposed by Haddock and McCullough.

5.4. *The Taurus Source.* (05N 2A)

The absorption measurements on the Taurus source allow an estimate to be made of the number of neutral hydrogen atoms per cm^2 between the sun and source. In addition, the emission spectrum near the source gives the total number of atoms per cm^2 in a line of sight in this direction (the kinetic temperature of the gas was taken as 125°K). These calculations show that 30% of the neutral hydrogen atoms in this direction lies in front of the source. The Taurus source has been identified with the Crab Nebula which is known to be 1·1 kiloparsecs (Greenstein and Minkowski 1953). This information is of some value because in this part of the Galazy ($l=153°$, $b=1{\cdot}5°$) there is very little Doppler displacement in this line of sight to enable the distribution of hydrogen to be obtained by the conventional method (van de Hulst *et al.* 1954). The published survey of the Galaxy (van de Hulst *et al.* 1954) gives the hydrogen distribution only up to $l=135°$ and beyond $l=160°$. These density contours were extrapolated across this region and the percentage of hydrogen up to, and beyond, a distance of 1·1 kiloparsecs was found to be precisely that obtained in the present work. This suggests that there may be some justification in extrapolating the distribution given by van de Hulst *et al.* across the region $l=135°$ to 160°.

5.5. *The Kinetic Temperature of Interstellar Neutral Hydrogen*

When the continuous emission from a source completely traverses a spiral arm whose emission profile is known, the kinetic temperature of the neutral hydrogen within the arm may be determined as follows. If $I\nu$ is the measured intensity of the source at frequency ν and I_0 is the unabsorbed intensity then

$$I\nu = I_0 \exp\left[-\tau(\nu)\right] \quad . \quad . \quad . \quad . \quad . \quad . \quad . \quad . \quad (6)$$

where $\tau(\nu)$ is the optical depth of the absorbing neutral hydrogen at frequency ν. The total number of absorbing atoms will then be

$$N_H = 1{\cdot}84 \times 10^{13}\, T_K \int_{\nu_1}^{\nu_2} \tau(\nu)\, d\nu \quad . \quad . \quad . \quad . \quad . \quad . \quad . \quad (7)$$

where ν_1 and ν_2 define the limits of the spiral arm, T_K is the kinetic temperature of the gas, and $\tau(\nu)$ is obtained from eqn. (6). From the emission profile of the arm another estimate may be made of the number of hydrogen atoms within the arm. The relation

$$T(\nu) = T_K\{1 - \exp\left[-\tau'(\nu)\right]\} \quad . \quad . \quad . \quad . \quad . \quad . \quad . \quad (8)$$

where $T(\nu)$ is the brightness temperature of the hydrogen at frequency ν, enables the optical depth to be obtained for the emitting hydrogen. Then the number of emitting atoms is

$$N'_H = 1{\cdot}84 \times 10^{13}\, T_K \int_{\nu_1}^{\nu_2} \tau'(\nu) d\nu. \quad . \quad . \quad . \quad . \quad . \quad . \quad . \quad (9)$$

If the same neutral hydrogen is responsible for the emission and absorption profiles, a value of T_K can be obtained which satisfies the relation

$$\int_{\nu_1}^{\nu_2} \tau(\nu) d\nu = \int_{\nu_1}^{\nu_2} \tau'(\nu) d\nu. \quad . \quad . \quad . \quad . \quad . \quad . \quad . \quad . \quad . \quad (10)$$

There are three spiral arms, two in Cygnus and one in Cassiopeia for which these calculations can be made. The results are shown in table 2.

Table 2

Spiral arm	$T°$K
Cygnus (inner)	130
Cygnus (outer)	60
Cassiopeia (inner)	250

The above calculations are only rigorous when the same neutral hydrogen is responsible for emission and absorption thereby making the emission and absorption spectra the same shape. The present 40 kc/s bandwidth spectra do not give sufficient resolution to decide whether the above condition holds. However, if there are more than 2 or 3 clouds in the line of sight the average value of H_H will be close to that responsible for the observed emission spectrum and the results should carry some weight in the Cygnus results, for example.

Acknowledgments

The authors wish to acknowledge the interest and encouragement of Professor A. C. B. Lovell the Director of this Station and to thank Mr. R. Hanbury Brown for his assistance and helpful criticism during the course of this investigation.

References

Baade, W., and Minkowski, R., 1954, *Astrophy. J.*, **119**, 206.
Beals, C. S., and Oke, J. B., 1953, *M.N.R.A.S.*, **113**, 530.
Davies, R. D., and Williams, D. R. W., 1955, *Nature, Lond.*, **175**, 1079.
Greenstein, J. L., and Minkowski, R., 1953, *Astrophy. J.*, **118**, 1.
Haddock, F. T., and McCullough, T. P., 1955, *Astron. J.*, **60**, 161.
Hagen, J. F., Lilley, A. E., and McClain, E. F., 1955, N.R.L. Report, **4448**.
Hiltner, W. A., 1954, *Astrophy, J.*, **120**, 41.
Kwee, K., Muller, C. A., and Westerhout, G., 1954, *B.A.N.*, **12**, 211.
Mills, B. Y., 1952, *Aust. J. Sci. Res.*, **A5**, 266.
Mills, B. Y., and Thomas, A. B., 1951, *Aust. J. Sci. Res.*, **A4**, 158.
Morgan, W. W., Whitford, A. E., and Code, A. D., 1953, *Astrophy. J.*, **118**, 318.

Oort, J. H., 1955, *Symposium of Dynamics of Cosmic Clouds* (Amsterdam : North Holland Publ. Co.).
Ryle, M., 1950, *Rep. Prog. Phys.*, **13,** 218.
Sharpless, S., 1953, *Astrophys. J.*, **118,** 362.
Smith, F. G., 1951, *Nature, Lond.*, **168,** 962.
Spitzer, L., 1948, *Astrophy. J.*, **108,** 276.
van de Hulst, H. C. Muller, C. A., and Oort, J. H., 1954, *B.A.N.*, **12,** 117.
Williams, D. R. W., and Davies, R. D., 1954, *Nature, Lond.*, **173,** 1182.
Wilson, O. C., and Merrill, P. W., 1937, *Astrophy. J.*, **86,** 44.

LXIV. *The Energy Distribution of Cosmic Ray Particles over Northern Italy*

By P. H. Fowler and C. J. Waddington
H. H. Wills Physical Laboratory, Bristol †

[Received June 1, 1956]

Abstract

The energies of 200 multiply-charged particles of the primary cosmic radiation have been determined from measurements of the multiple Coulomb scattering. These particles were found in a stack of emulsions exposed over Northern Italy. The energy determinations have been shown to be reliable up to an energy of at least 3·0 Bev per nucleon. From these measurements the cut-off energy has been shown to be $1{\cdot}55\pm0{\cdot}06$ Bev per nucleon, instead of the 1·05 Bev per nucleon predicted by geomagnetic theory. The integral energy spectrum between 1·8 and 3·0 Bev per nucleon has been shown to be given by $N\ (>E)=370/(m_0c^2+E)^{1\cdot50}$, and between the above cut-off energy and 800 Bev per nucleon—from a consideration of α-particle produced 'jets'—to have an exponent of 1·49. A value for the α-particle flux at the top of the atmosphere has been found of 93 ± 8 α-particle/m²/ster/sec.

§ 1. Introduction

It was realized at the 1955 Mexico Conference (Simpson *et al.*, Waddington), that previously accepted geomagnetic theory was unable to give the true cut-off energies of cosmic-ray particles. As a result it is desirable to make experimental determinations of these energies at different geographic localities. Using nuclear emulsions such determinations are best made on the multiply charged components of the cosmic radiation, but are limited by the experimental difficulty of measuring energies above a certain value. For energy determinations from multiple Coulomb scattering this limiting energy will depend on the geometrical conditions of the tracks of the particles in the emulsions, and has been set as low as 0·30 Bev per nucleon by Biswas *et al.* (1955). On the other hand the results of Brisbout *et al.* (1956 a) suggest that the limit may often be appreciably higher than this; as do the results of a previous cut-off energy determination of one of us, Waddington (1956).

We have therefore used nuclear emulsion techniques to determine the experimental cut-off energy over Northern Italy, $\lambda=46°$N. The internal evidence of these measurements indicates that the energy values cannot have been seriously affected by systematic errors of the type that can occur in work with emulsions.

† Communicated by the Authors.

In the course of this investigation we have also obtained the primary energy spectrum between the cut-off energy and an energy of 3·0 Bev per nucleon. This energy spectrum is compared with one deduced from the flux of α-particles found in the present experiment and that of α-particles having an energy greater than 800 Bev per nucleon—primaries of ' jets '.

In addition, the previously reported flux value of α-particles at this geographic position, Waddington (1956), has been redetermined with greater statistical weight, thus enabling the cut-off energy to be deduced at other geographical positions having a similar α-particle flux.

§ 2. The Alpha Particle Flux Determination

The α-particle flux value reported previously for this geographic position (Waddington 1956), was obtained in the same stack of emulsions as that used in the present experiment. The value at the top of the atmosphere determined previously was

$$88 \pm 13 \text{ α-particles/m}^2\text{/ster/sec.}$$

The statistical weight has been increased and a new value obtained of

$$93 \pm 8 \text{ α-particles/m}^2\text{/ster/sec.}$$

An analysis of the experimental data to determine the efficiency of detection in this experiment is given in an Appendix, and closely follows those analyses given previously. From this Appendix it can be seen that any effects of inefficient detection are almost certainly less than the quoted statistical error.

§ 3. Experimental Details

(*a*) *Stack and Exposure Details*

We have used a stack of 80, 20 cm × 15 cm Ilford G5 600 μ stripped emulsions exposed for 5 hours 40 minutes at a mean altitude of 105 000 feet. This exposure was made in Northern Italy at a mean geomagnetic latitude of 46° N (geographic coordinates 8° E, 45·5° N) and was at no time more than 0·25° from this latitude. At such a latitude geomagnetic theory, using the centred dipole approximation, suggests that the cut-off energy should be 1·05 Bev per nucleon. The use of the eccentric dipole approximation should not alter this value appreciably.

(*b*) *Particle Selection Criteria*

In order to determine the multiple Coulomb scattering, and thus the energies of the multiply charged particles, it was necessary to impose stringent geometrical conditions on the tracks of the particles. These conditions were designed to ensure that there should be an appreciable number of independent cells available for measurements, in spite of the large cell sizes that must be used at high energies. Each track selected had a length in each emulsion of more than 2 cm, and a total length on

which measurements could be made of greater than 4 cm. All this track length had to be in emulsion which was not within 1 cm of a processed edge.

The majority of the emulsions have had a scan made near the top edge for particles of charge greater than three. In these scans 52 particles were found whose geometrical conditions satisfied the above requirements. In addition, non-systematic scans were made in many of the emulsions for the tracks of α-particles of similar geometrical quality. Altogether 148 suitable α-particle tracks were found. All the particles used were traced back to their point of entry into the stack in order to reduce the possibility of their being of secondary origin.

(*c*) *Energy Determination*

On each track the multiple scattering was measured by the coordinate method, Fowler (1950), using a basic cell size c, of $1000\,\mu$. From this basic cell, c_1, overlapping cells were constructed of $2\,c_1$ (c_2) and $3c_1$ (c_3); and the influence of signals not due to multiple Coulomb scattering, eliminated between these various cell sizes by using relation (1) for the scattering parameter, $\bar{\alpha}$:

$$\bar{\alpha}_{21}=\frac{1\cdot 8}{\pi}\left\{\left[\bar{D}_2{}^2-\left(\frac{c_2}{c_1}\right)^{2x}\bar{D}_1{}^2\right]\Big/\left[c_2{}^3-\left(\frac{c_2}{c_1}\right)^{2x}c_1{}^3\right]\right\}^{1/2} \quad . \quad . \quad (1)$$

where $\bar{\alpha}_{21}$ is the measure of the multiple coulomb scattering in degrees per 100 micron cell-size, $\bar{D}_2$ and $\bar{D}_1$ are the mean second differences in microns corresponding to c_2 and c_1 respectively; c_2 and c_1 are measured in units of 100, microns, and x was the index of the variation of non-Coulomb signal with cell size. A similar relation, with $\bar{D}_2$ and c_2 replaced by $\bar{D}_3$ and c_3, applied for elimination between c_3 and c_1, giving $\bar{\alpha}_{31}$.

In determining the experimental value of the scattering parameter the weighted mean of $\bar{\alpha}_{21}$ and $\bar{\alpha}_{31}$ was taken.

All the measurements of scattering in this experiment were made on two Cooke M 4000 microscopes, and on very straight tracks gave values of x of about 0·5. These measurements, although made on tracks selected for their low scattering parameters, did not give values of x which depended only on the assumed constant parameters of the measurements—stage noise, reading errors, etc.—but also depended on the characteristics of the emulsions. As a result, although a value of x equal to 0·5 was used to calculate the scattering parameters, it was considered to be a provisional value. (See § 3 (*d*).)

Relation (1) can give rise to physically significant values of the scattering parameters only when $\bar{D}_2$ or $\bar{D}_3$ contains an appreciable proportion of multiple Coulomb scattering. Various criteria of significance have been proposed, but in the conditions of this experiment calculated values of the scattering parameter have been regarded as significant only when

$$\frac{\bar{D}_2}{\bar{D}_1}\geqslant 2, \text{ or } \frac{\bar{D}_3}{\bar{D}_1}\geqslant 3. \quad . \quad . \quad . \quad . \quad . \quad . \quad . \quad . \quad . \quad (2)$$

This condition is purely empirical, but has the advantage of being easy to apply to the experimental data. While its use does not exclude the possibility of ' spurious ' scattering of the type proposed by Biswas *et al.* (1955) giving rise to apparently significant but actually high scattering parameters, it will be shown later that such ' spurious ' scattering is unlikely to have introduced serious errors at the energies being considered in this experiment.

For those tracks for which eqn. (2) was only satisfied by $\bar{\alpha}_{31}$, this value of the scattering parameter was taken as being the best value, although of reduced statistical weight. For those tracks for which neither of the scattering parameters satisfied this condition the value calculated from

$$\bar{\alpha}_3 = \frac{1{\cdot}8}{\pi}\{\bar{D}_3^2/2c_3^3\}^{1/2} \quad . \quad . \quad . \quad . \quad . \quad . \quad . \quad . \quad . \quad (3)$$

was taken as a plausible value to the upper limit of the true value of the scattering parameter.

In all the measurements the influence of large angle deflections was eliminated by replacing values of second differences greater than four times the mean value, $4\bar{D}$, by $4\bar{D}$. Using this method of single scatter elimination, and for cell sizes of the magnitude used, the scattering constant for multiply-charged particles has been taken as 32·0. This value was obtained when due allowance was made for the charge of the particles being considered.

The energy of each particle in the emulsion was calculated from the experimentally determined scattering parameters. Assuming that each particle observed was of primary origin, these energies were then extrapolated to the top of the atmosphere, using the range–energy relation of the Rome group. Except at the lowest energies and highest charges, the magnitude of this correction was less than the statistical uncertainties on the individual energy determinations. Thus in general the effect of an incorrect assumption of primary origin was not serious, although cases where the change of charge was great and the change occurred deep in the atmosphere could result in a considerable under-estimate of the true energy. However, at these depths in the atmosphere ($\sim$14 g/cm^2) only about 10% of the α-particles, and 20% of the heavy particles, can have been of secondary origin.

(*d*) *Systematic Errors in the Energy Determinations*

It has been shown by Biswas *et al.* (1955) that the energies of particles determined from measurements of multiple scattering in emulsions may be systematically under-estimated due to the influence of previously unsuspected distortions of the emulsions. It is therefore necessary to prove that the results obtained in this experiment have not been affected in this manner.

(i) In order to show that if there are any systematic errors introduced by local distortions these distortions are comparatively uniformly

distributed throughout the stack of emulsions, we have divided the stack into eight parts and examined the relative number of different energy values obtained in each. The results are shown in table 1. In this table there is shown for each group of ten emulsions the total number of $\bar{D}$ measurements made in the emulsions of that group,† the number from particles having apparent energies less than 2·0 Bev per nucleon, and the number from particles having apparent energies greater than 4·0 Bev per nucleon. Also shown are the numbers expected in each of these two classes, calculated from the overall numbers in the stack.

Table 1

Plate Nos.	Total (all E)	$E<2{\cdot}0$ Bev/n	No. exp.	$E>4{\cdot}0$ Bev/n	No. exp.
1–10	55	15	13	16	16
11–20	37	11	8·5	6	11
21–30	56	17	13	13	16
31–40	64	13	15	23	19
41–50	65	12	15	17	19
51–60	38	0	9	17	11
61–70	32	9	7	4	9·5
71–80	71	17	16	24	21

It can be seen from this table that in none of the groups of plates is there evidence for a significant lack of apparently high energy particles, or a significant excess of apparently low energy particles. We conclude, therefore, that any systematic tendencies that may affect the energy determinations are uniform throughout the stack.

(ii) The above conclusion is supported by the $\bar{D}$ values obtained on individual tracks in different emulsions. We have examined those tracks which were measured in two separate emulsions and which gave apparent energies between 2·0 and 3·0 Bev per nucleon. The distribution of the ratios of the $\bar{D}_3$ values obtained in the two emulsions is quite consistent with the assumption that there are no significant differences between apparent energy values obtained in different emulsions.

(iii) Having shown that the entire stack may be regarded as a homogeneous unit, we can now find the magnitude of the distortion which is presumably present to affect the energy determinations. It has been shown by Brisbout *et al.* (1956 a), see also Lohrmann and Teucher (1956) and Fay (1955), that the variation with cell size of the signal due to distortions of the type suggested by Biswas *et al.* is less rapid than that of the signal due to multiple Coulomb scattering. Thus we can assume that all forms of signal other than that due to multiple Coulomb scattering can

† Two separate $\bar{D}$ measurements were made on each track.

be considered together and that they will vary with cell size as c^x, where $x<1{\cdot}5$. We establish the following simultaneous equations :

$$\bar{D}_1^2=s_1^2+n_1^2 \quad . \quad . \quad . \quad . \quad . \quad . \quad . \quad . \quad . \quad . \quad . \quad . \quad . \quad . \quad 4a$$

$$\bar{D}_2^2=\left(\frac{c_2}{c_1}\right)^3 s_1^2+\left(\frac{c_2}{c_1}\right)^{2x} n_1^2=8s_1^2+2^{2x}n_1^2 \quad . \quad . \quad . \quad . \quad b$$

$$\bar{D}_3^2=\left(\frac{c_3}{c_1}\right)^3 s_1^2+\left(\frac{c_3}{c_1}\right)^{2x} n_1^2=27s_1^2+3^{2x}n_1^2 \quad . \quad . \quad . \quad . \quad c$$

where s_1 and n_1 represent the signals due to multiple Coulomb scattering and other causes respectively.

Experimentally, x has the value $0{\cdot}60\pm0{\cdot}10$ when all the data of the present experiment are used. Since over 8000 independent cells were measured it can be seen that, due to the small ratio of n_1/s_1, the above method of determining x cannot be used in experiments of this type except on samples of large statistical weight.

(iv) From eqns. 4(a) and (c) we have calculated the value of n_1 :

$$n_1=\{[27\bar{D}_1^2-\bar{D}_3^2]/[27-3^{2x}]\}^{1/2}. \quad . \quad . \quad . \quad . \quad . \quad (5)$$

This expression is not sensitive to the precise value of x used when it is less than one. Using $x=0{\cdot}6$, we have calculated n_1 for three groups of particles, selected on the basis of their apparent energies, and the results are shown in table 2.

Table 2

BEV/n	0–2·5	2·5–4·0	4·0–∞
$27\bar{D}_1^2-\bar{D}_3^2$	3·13±12%	3·05±6%	3·33±3%
n_1 (μ)	0·37± 6%	0·36±3%	0·38±1·5%

Also shown is the numerator of eqn. (5) (expressed in microns^2), since this is independent of the assumed value of x.

It is clear from this table that n_1 does not vary for the different groups of tracks, thus showing that low apparent energies are not due to anomalously high values of n.

It appears, therefore, that a better value of the scattering parameter may be obtained from eqn. (1) by using the above value of x instead of 0·5. The energy difference introduced is small, but has been shown in plotting the energy spectrum. See fig. 2.

The procedure given here will remove only those forms of extraneous signal which vary more slowly with cell size than does multiple Coulomb scattering. However, the results of Brisbout *et al.* (1956 a) who, in this stack, compared energy estimates obtained from measurements of relative scattering with those obtained from ordinary measurements of scattering, show that any effects of this sort must be small.

§ 4. Experimental Results

The energy values at the top of the atmosphere of the 200 particles considered are shown in fig. 1. Of the 139 particles with apparent energies less than 4 Bev per nucleon, 100 satisfied eqn. (2) both for $\bar{\alpha}_{21}$ and $\bar{\alpha}_{31}$, while 27 satisfied it for $\bar{\alpha}_{31}$ only. The remaining 12 values, the lowest of which was 2·9 Bev per nucleon, represented only lower limits to the true energy as defined by eqn. (3). In constructing the energy spectrum these 12 values have been distributed between 2·9 and 4·0 Bev per nucleon, and greater than 4·0 Bev per nucleon, in proportion to the number of other particles in each of these energy ranges.

Fig. 1

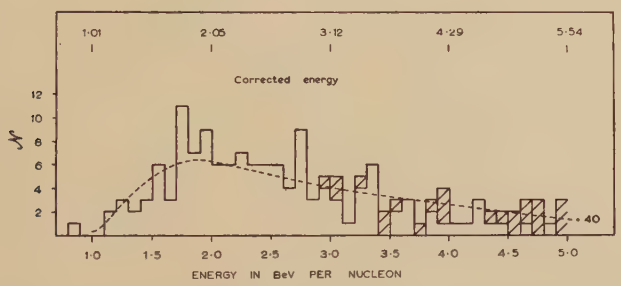

The distribution of the energies at the top of the atmosphere of 200 multiply-charged particles. Those energy values for which it was possible to obtain only an upper limit, as defined by eqn. (3), are shown shaded. The correction introduced by changing x from 0·5 to 0·6 is shown (§ 3(*d*)). Also shown by the dashed line is the distribution that would be expected if there was a sharp cut-off energy at 1·55 Bev per nucleon, but each energy determination had a statistical error of ~19%.

The mean number of independent cells measured on each individual track was 20, thus the average statistical error of those results for which both scattering parameters were significant was ~19%. For those results where only $\bar{\alpha}_{31}$ was significant the mean error was ~28%.

(i) The Energy Spectrum

(*a*) *From Direct Measurement*

In order to construct an energy spectrum from the data given in fig. 1 it has been assumed that all the multiply-charged components of the cosmic radiation have spectra whose slopes do not vary appreciably with charge. It has recently been suggested, Singer (1956), that this approximation is not valid, but that the slopes of the spectra become increasingly steep as the charge of the particle increases. However, we cannot find any statistically significant difference between the observed energy distributions of the α-particles and the other particles, and have therefore combined all our results.

The integral energy spectrum, representing all the particles as α-particles, and using the flux value of § 2, is shown in fig. 2, together with those

spectra obtained previously, in rather similar experiments, by Waddington (1956) over Southern England and Minnesota, U.S.A. This energy spectrum can be represented by :

$$N(>E)=\frac{C}{(m_0c^2+E)^m} \quad . \quad . \quad . \quad . \quad . \quad . \quad . \quad (6)$$

Fig. 2

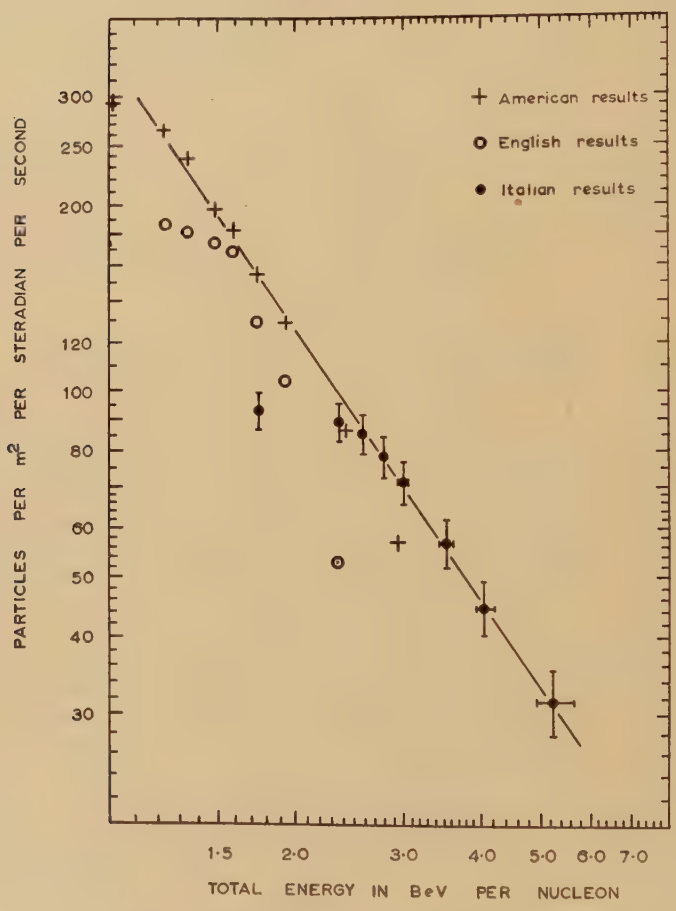

The integral α-particle energy spectrum from flights over Minneapolis, Southern England and Northern Italy. Those points shown as Italian results were obtained in this experiment. The errors shown on the energy correspond to $x=0{\cdot}6\pm0{\cdot}1$, while those on the flux represent the total numbers with energies greater than the appropriate value. Thus the flux errors shown are not independent. The American and English results, also included in the graph, are the data from Waddington (1956). The point obtained from a study of ' jets ' produced by α-particles with energy greater than 800 BeV per nucleon will lie on the continuation of the line shown for the energy spectrum.

where N ($>E$) is the number of particles with an energy greater than E, (m_0c^2+E) is thus the total energy in Bev per nucleon, and m and C are constants.

The values of m and C have been obtained analytically, by considering the relative numbers of particles with energies greater than 1·8 and 3·0 Bev per nucleon, and are $m=1{\cdot}50\pm0{\cdot}18$ and $C=370\ ^{+100}_{-90}$.

It can be seen from fig. 2 that if the spectrum obtained in this experiment is extended to higher fluxes and lower energies, the low energy results obtained in the American and English experiments lie closely on it. If the present spectrum had been severely distorted in slope this could hardly be true. We have therefore redetermined the values of m and C over an energy range of 0·4 to 3·0 Bev per nucleon, and find $m=1{\cdot}48\pm0{\cdot}12$, and $C=360\ ^{+50}_{-30}$. It may therefore be presumed that the present observations have given the true cosmic-ray spectrum.

If this assumption is correct it implies either that all the existing α-particle flux measurements made at geomagnetic latitudes of 30° and less are too high, or that the cut-off energies at these latitudes are much less than is usually assumed ; see for example fig. 6 (a) and (b) of Waddington (1956). That these flux values might be too high is supported by the, admittedly few, heavy primary fluxes observed at low latitudes ; in particular by the exceptionally low value observed by Danielson (1955) at 10° N in the Galapagos Isles.

(*b*) *From Alpha-Particle Produced ' Jets '*

Brisbout *et al.* (1956 b) in this laboratory have observed six high energy disintegrations initiated by α-particles. These particles are all estimated to have had energies greater than 800 Bev per nucleon. They were found from scans made for the cascades produced by the disintegrations and it is estimated that at such large initiating energies the detection efficiency was high. From the known volume of scanned emulsions we have estimated the total flux of α-particles with energies greater than 800 Bev per nucleon and find a value of $1{\cdot}7\ 10^{-2}$ α-particles/m²/ster/sec. Using this value, and the value found in the present experiment for the flux of α-particles with energies greater than the cut-off energy, we have estimated a new value for m of $1{\cdot}49\ ^{+0{\cdot}23}_{-0{\cdot}20}$. The errors on this value correspond to a two-fold fluctuation in *both* the flux and the estimated energy of the high energy α-particles.

(ii) The Cut-off Energy

The precise cut-off energy observed in this experiment may be derived from eqn. (6) by putting $N(>E)$ equal to the total primary α-particle

flux found in this experiment. A value of $1{\cdot}55 \pm 0{\cdot}06$ BEV per nucleon is found. It may be seen from fig. 2 that the cut-off value determined in this manner is not very sensitive to a distortion of the slope of the spectrum by a systematic effect on the energy determinations, provided that the low energy end of the energy range considered is not seriously affected. An example is provided by the English results shown, where there was obviously considerable distortion of the spectrum, but the cut-off energy determination was hardly affected.

Fig. 3

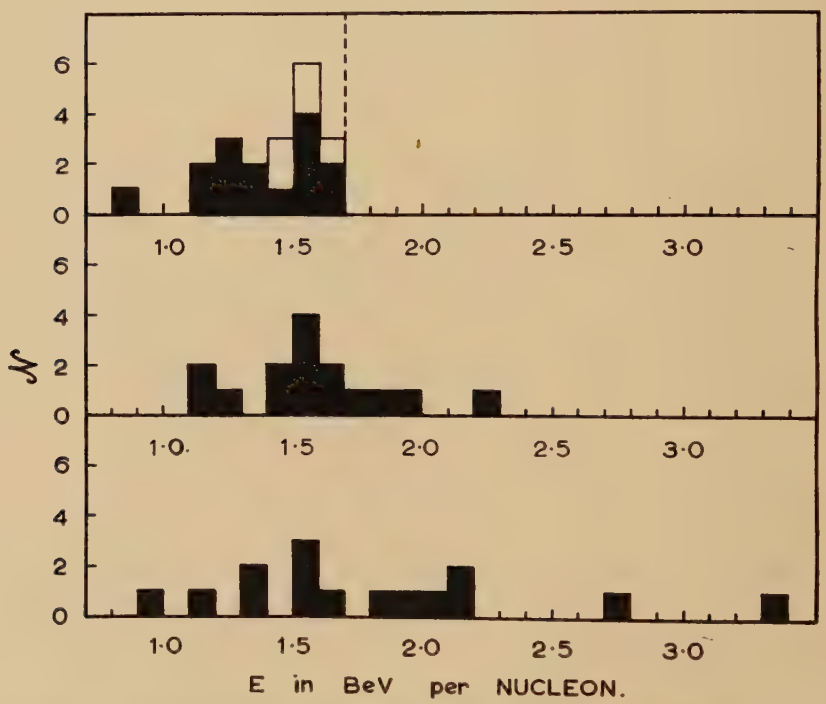

The effect of remeasurement on the low energy particles shown in fig. 1.

(i) The original distribution of those energies less than 1·7 BEV per nucleon. Those particles on which further measurements could not be made are shown unshaded.

(ii) The distribution of the energy values obtained when the extra measurements are included with the original ones.

(iii) The distribution of the energy values obtained from the extra measurements alone.

It may be noted that the flux value of α-particles at the above cut-off energy agrees closely with the flux values obtained over New Mexico, $\lambda = 41°$N, by Linsley (1955), Bohl (1955), Horwitz (1955), Webber (1956) and McDonald (1956). We therefore suggest that the true cut-off energy

over New Mexico is also about 1·55 Bev per nucleon, instead of the 1·8 Bev per nucleon previously assumed from geomagnetic theory.

The effect of the unavoidably large individual errors on the energy values is to spread out any sharp discontinuity that may be present in the energy distribution. As a result we have made further measurements on those particles with apparent energies less than the cut-off energy in order to see whether their true energies were actually greater than the quoted cut-off energy.

On those particles, with measured energies less than 1·7 Bev per nucleon, where there was appreciable additional path-length available for measurements of scattering, an average of an extra 12 independent cells were measured. Figure 3 shows the original energy distribution of those particles whose energy was remeasured in this manner, together with the energy distribution of the redetermined values obtained from all the measurements, and that obtained if the additional measurements are considered alone. It can be seen from these distributions that the result of such additional measurements is to shift the mean energy of the group to higher energy values, indicating that the true mean energy was actually higher than that measured by the original determinations. This behaviour cannot be attributed to the effects of distortion (§ 3 (*d*)), but must represent the effects of ordinary statistical fluctuations.

If a sharp cut-off energy of 1·55 Bev per nucleon is assumed, the expected spread introduced due to the individual mean errors of ~19% may be calculated. This distribution is shown on fig. 1, and can be seen to agree closely with that found experimentally. It appears therefore that the experimental data are consistent with a sharp cut-off energy, quite unlike that observed in emulsions flown at northerly latitudes, Fowler and Waddington (1956), and Ney (1955).

APPENDIX

The Detection Efficiency of Alpha-Particles in the Flux Determination

The reader is referred to Appendix I of Waddington (1956) for a detailed discussion of detection efficiencies in emulsion α-particle flux determinations.

Figure 4 shows the integral length distribution of all the tracks observed in the present flux determination. There does not appear to be any evidence for a missing of tracks of short length.

Figure 5 shows the observed grain-density distribution of the α-particles and the singly charged particles. It can be seen from this figure that there is no evidence that α-particles could have been missed due to an underestimate of their grain-densities by the scanner.

One overlapping scan of 5 cm was made in this experiment. All the eight tracks detected in one scan that should have been detected in the second one were detected.

Fig. 4

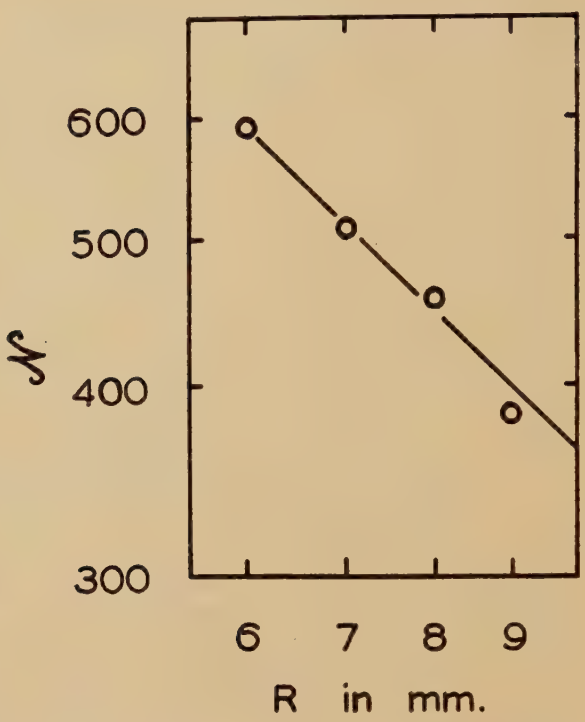

The integral length distribution of all those tracks found.

Fig. 5

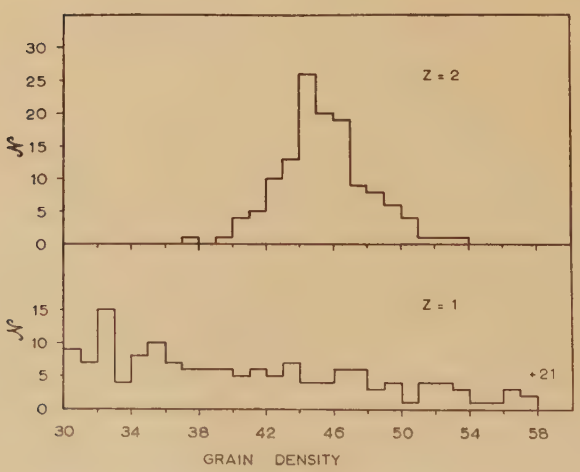

The grain-density distribution of the α-particles and the singly charged particles observed.

Figure 6 shows the distribution of the depth in the emulsions at which tracks were found for the α-particles and for the singly charged particles. There appears to be a slight indication of a missing of tracks near the glass, but it is only just statistically significant. The maximum correction

Fig. 6

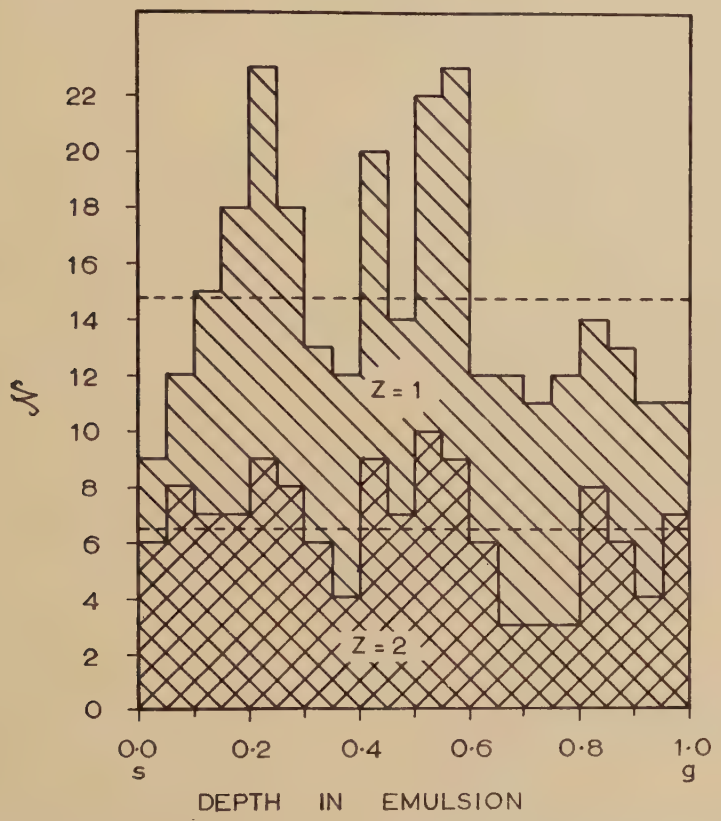

The distribution in depth in the emulsion at which each track observed was found.

that can reasonably be made for missed tracks will increase the final flux value by an amount less than the quoted statistical error. As a result we have neglected any possible influence of an inefficient detection of tracks.

Acknowledgments

We are grateful to Professor C. F. Powell for the hospitality of his laboratory, and to various members of the department, in particular to Dr. A. Engler, for helpful discussions. One of us, C. J. W., wishes to thank the Royal Society for the award of a Mackinnon Research Studentship.

References

Biswas, S., Peters, B., and Rama, 1955, *Proc. Ind. Acad.* A, **41**, 154.
Bohl, L., 1954, *Ph.D. Thesis*, University of Minnesota.
Brisbout, F. A., Dahanayake, C., Engler, A., Fowler, P. H., and Jones, P. E., 1956 a,—*Il Nuovo Cimento*, **3**, 1400.
Brisbout, F. A., Dahanayake, C., Engler, A., Fujimoto, Y., and Perkins, D. H., 1956 b, *Phil. Mag.* (in press).
Danielson, R. E., 1955, *M.Sc. Thesis*, University of Minnesota.
Fay, H., 1955, *Z. fur Naturforschung*, **10a**, 572.
Fowler, P. H., 1950, *Phil. Mag.*, **41**, 169.
Fowler, P. H., and Waddington, C. J., 1956 (to be published).
Horowitz, N., 1955, *Phys. Rev.*, **98**, 165.
Linsley, J., 1956, *Phys. Rev.*, **101**, 826.
Lohrmann, E., and Teucher, M., 1956, *Nuovo Cimento*, **1**, 59.
McDonald, F. R., 1956, private communication.
Ney, E. P., 1955, Mexico Conference.
Simpson, J. A., Fenton, K. B., Katzman, J., and Rose, D. C., 1955, Mexico Conference.
Singer, S. F., 1956, private communication.
Waddington, C. J., 1956, *Il Nuovo Cimento*, **3**, 930.
Webber, W. R., and McDonald, F. B., 1955, *Phys. Rev.*, **100**, 1460.
Webber, W. R., 1956, private communication.

LXV. *On the Theory of the Low-Temperature Internal Friction Peak Observed in Metals*

By Alfred Seeger †
Max-Planck-Institut für Metallforschung und Institut für theoretische und angewandte Physik der Technischen Hochschule Stuttgart

[Received February 24, 1956]

Abstract

Recent data by Niblett and Wilks on polycrystalline copper suggest that the low-temperature internal friction mechanism in metals first observed by Bordoni is determined by intrinsic properties of dislocations. This is contrary to an explanation by Mason according to which the activation energy of the process should depend on the impurity content of the material and the separation between dislocation nodes.

A mechanism proposed elsewhere seems to account for all the major features of the experimental results. The relaxation phenomenon is thought to be due to dislocations which are confined by the Peierls stress to certain crystallographic directions. Under the combined action of thermal fluctuations and the applied stress they may form pairs of kinks. Internal friction peaks are observed if the frequency of the applied alternating shear stress is equal to the frequency of the formation of these kink pairs. The Peierls stresses deduced from the experimental results are rather large, being of the order of one thousandth of the shear modulus.

§ 1. Introduction

In a recent paper, Niblett and Wilks (1956) report on an experimental investigation of the low-temperature relaxation peak in face-centred cubic metals first observed by Bordoni (1949, 1954). The salient features of their results on polycrystalline copper are as follows:

1. The internal friction versus temperature curve of copper shows *two low-temperature peaks* with different heights, corresponding to two relaxation processes. The *relaxation character* of the underlying processes is borne out by the observation that the internal friction does *not* show a marked dependence on the amplitude of the oscillating strain.

2. The *heights of these peaks* and therefore the strength of the corresponding relaxation processes depend on the plastic pre-strain to which the specimens have been subjected.

3. For a fixed frequency the *temperatures* at which the peaks occur are
(*a*) independent of the amount of pre-strain,
(*b*) independent of the concentration and the nature of the impurities present in the material.

† Communicated by the Author.

Prior to the low-temperature measurement of internal friction the pre-strained specimens were kept for some time at room temperature. The relaxation mechanism therefore cannot be due to the reorientation of divacancies or similar defects created by the plastic deformation, since these would anneal out rapidly at room temperature. The observation that the peak cannot be annealed out save by heating to 350°c suggests strongly, as Niblett and Wilks point out, that the internal friction is due to the motion of dislocation segments.

A tentative explanation of Bordoni's experimental results in terms of a dislocation mechanism has been proposed elsewhere (Seeger 1955 a). It now appears that it accounts rather well for the more detailed observations of Niblett and Wilks. In § 2 we shall present a qualitative discussion of the relaxation mechanism and its relation to the experiments. In § 3 we shall outline a quantitative theory and point out some particular features in the theoretical treatment which deserve to be investigated further.

§ 2. Qualitative Discussion of the Theory

The dependence on pre-strain and the annealing behaviour of the peaks suggest that they are due to dislocation mechanisms. Observation 3 (*b*) in § 1 shows that the activation energy of the process is not related

Fig. 1

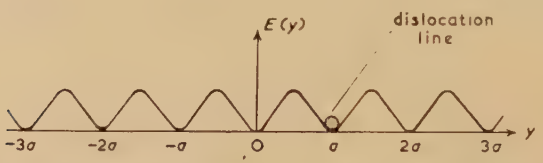

Section through the potential energy surface of a dislocation line lying perpendicular to the *y*-direction.

to the pinning of dislocation lines by impurities; observation 3 (*a*) shows that the density of the dislocation forest and the distance between dislocation nodes are not of importance either. We conclude that the mechanism is related to intrinsic properties of dislocations which are virtually unaffected by the presence of other dislocation lines or impurities.

Let us consider a dislocation line lying along a close-packed direction in a crystal (fig. 1). Its energy per unit length is a periodic function of its position y with respect to the crystal (Peierls 1940). The period a of the potential energy per unit length $E(y)$ is in general equal to or simply related to the dislocation strength b. In the state of lowest energy the dislocation line will be in one of the positions of minimum potential energy, corresponding to, say,

$$y_{\min} = \pm na \ (n = 0, 1, 2, \ldots\ldots). \quad \ldots\ldots \quad (1)$$

The minimum shear stress necessary in order to lift a straight dislocation line from one position of minimum potential energy to the next one is the Peierls stress τ_p^0. (The superscript 0 indicates that we are disregarding for the moment both thermal and quantum-mechanical fluctuations.)

As early as 1947 Shockley (see Mott and Nabarro 1948, Shockley 1952, Read 1953 a) pointed out that at moderately high temperatures a dislocation which on the average is parallel to a close-packed direction in the crystal contains a certain number of kinks as shown in fig. 2. Both the entropy and energy of the system are increased by kink formation. The energy of a kink W_k results from the increase of its potential energy when the dislocation crosses over from one valley of the $E(y)$-surface to the next one. The entropy of a kink is due to the increased ' randomness ' of a dislocation line containing a kink.

In thermal equilibrium the number of kinks per unit length of a dislocation line is proportional to $\exp(-W_k/kT)$. A small applied shear stress $\tau(\tau \ll \tau_p^0)$ acting in the glide system of the dislocation will cause the kinks to move sideways † and will at the same time change the statistical distribution of the kinks. The applied stress tends to move the dislocation line in, say, the $+y$ direction. The number of kinks corresponding to a displacement in this direction increases and the number of kinks corresponding to a displacement of the dislocation in the opposite direction decreases. The formation of the ' new ' pairs of kinks is thermally activated and may give rise to a relaxation phenomenon under the action of an alternating shear stress of frequency f. The internal friction due to this process shows a maximum if the applied frequency f coincides with the frequency ν of the formation of kink-pairs.

The calculation of ν as a function of the absolute temperature T is a rather formidable problem. Its main difficulties are connected with the fact that the standard derivation of the Arrhenius type formulae for jump frequencies of diffusional processes from the theory of absolute reaction rates (see e.g. Seitz 1951, Zener 1952) does *not* hold in the present case, since it applies only if the activated complex is of atomic dimensions. In the present problem, however, the length of the ' activated ' dislocation segment is of the order of 100 interatomic distances. H. Donth is investigating these aspects of the problem further by means of the general theory of stochastic processes.

---

† Due to the periodic structure of the crystal the sideways motion of a kink (in $\pm x$-direction) has to overcome potential barriers too. These potential barriers are very much lower than those opposing the dislocation movement in y-direction. If the applied stress is so small that thermal energy is essential for overcoming the potential barriers for sideways motion they may also give rise to internal friction phenomena. In metals the temperatures at which the corresponding relaxation peaks occur will be exceedingly low. There may be substances with particularly large Peierls stress τ_p^0 in which these peaks due to the sideways propagation of the kinks can be observed under suitable experimental conditions.

In this paper we are *assuming* that the frequency ν of the formation of pairs of kinks can be represented approximately by

$$\nu = \nu_0 \exp(-W/kT) \qquad . \quad . \quad . \quad . \quad . \quad (2)$$

where ν_0 is a temperature independent frequency and W is the ' activation energy ' of the process. This assumption seems to be justified by the experimental results so far available.

For the sake of both qualitative and quantitative discussions it is useful to introduce a close analogy between kinks and one-dimensional dislocations, which will be put on a mathematical basis in § 3. We interpret (fig. 2) $y(x)$ as the relative displacement of atoms facing each other on opposite sides of the glide-plane at the position x. The pair of kinks drawn in fig. 2 corresponds to a pair of dislocations of opposite sign. It is well known that the dislocations of such a pair attract each other. If the applied shear stress τ is zero, the dislocations will move towards and eventually annihilate each other. Under the action of a finite resolved shear stress τ in the glide system there exists a critical separation $d = d_{cr}(\tau)$, corresponding to unstable equilibrium. Only dislocation pairs with a separation d less than d_{cr} are able to annihilate, whereas pairs with a larger separation will separate further and thereby become virtually non-interacting with each other.

Fig. 2

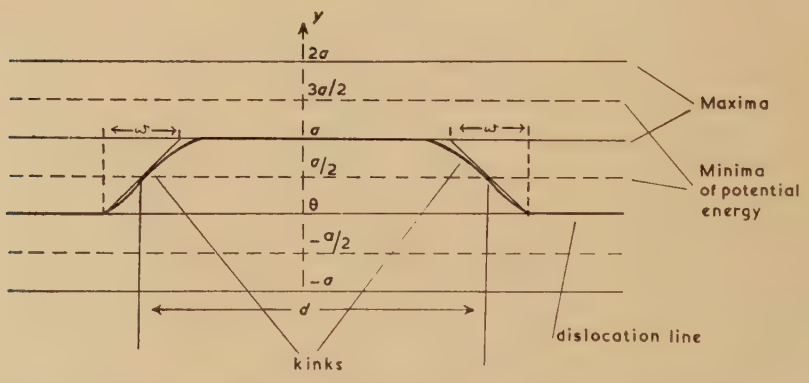

Kinks in a dislocation line lying on the average parallel to a close-packed direction in a crystal (x-direction). w is the width of the kinks. Maxima and minima of potential energy should be interchanged.

Exactly the same situation holds for kinks. There is a competition between the applied shear stress which exerts a force τb per unit length of the dislocation line and tends to increase the slipped area in the glide-plane on one hand, and the attractive force between the kinks on the other. The latter is due to the fact that the total length of the kinked dislocation diminishes if the kinks come together by sideways motion and eventually annihilate each other. The attractive force is particularly strong for small separations d of the kinks ; it is balanced by the applied

shear stress at the critical separation d_{cr}. The energy barrier connected with the critical separation d_{cr} is responsible for the activation energy W of the relaxation process. W depends on d_{cr} and therefore also on τ. As will be shown in § 3, this dependence is logarithmic only and probably hard to detect experimentally. Leaving aside this very slight amplitude dependence, the activation energy W is an *intrinsic* property of a dislocation line. (It does depend, however, on the character of the dislocation, i.e. the relative orientation of the Burgers vector and the direction of the dislocation line.)

Since the activation energy W is independent of the dislocation density and the impurity content of the material, thermally activated formation of pairs of kinks in dislocations is able to account for the main features of the relaxation phenomena as outlined in § 1. This is not true of the mechanism proposed by Mason (1955 a, b, c, 1956) which is therefore incapable of explaining the experimental data as has been pointed out on several occasions (Niblett and Wilks 1956, Seeger 1955 a, 1956). We therefore believe that the mechanism discussed in this paper is responsible for the ' Bordoni peak '.

The explanation why two relaxation peaks rather than one are observed in copper is thought to be as follows : According to the present theory the relaxation peak in f.c.c. metals is caused by the movement of dislocation lines with Burgers vector $\frac{1}{2}\langle 110\rangle$, lying in $\{111\}$ glide planes, along one of the close-packed directions. Since a $\{111\}$ plane contains several $\langle 110\rangle$ directions there are two distinct possibilities : the Burgers vector may either be parallel to or form an angle of $\pm 60°$ with the direction of the dislocation line. If we consider a metal such as copper with quite a considerable separation of complete dislocations into half-dislocations we expect in general the kink energies W_k to be different in these two cases. (This will be explained further in § 3.) It is therefore not surprising that in copper two peaks are observed, the activation energies of which differ by a factor of about two. There may be however f.c.c. metals in which both peaks coincide.

According to Niblett and Wilks the relaxation strength increases rapidly with pre-strain up to about 2% pre-strain. When the pre-strain is increased further the relaxation strength seems to pass through a slight maximum. This behaviour, which at first sight appears to be rather surprising, can be understood qualitatively as follows. Dislocation lines which on the average do not run approximately parallel to one of the densely packed directions of the crystals do *not* contribute to the internal friction mechanism discussed in this paper. They contain such a large number of kinks even at the absolute zero of temperature that the thermal activation of kinks is irrelevant. Since the energy per unit length of such a dislocation is not very much larger than that of a dislocation lying approximately along a close-packed direction, and since the geometrical probability that a dislocation line lies along a close-packed direction is small we expect only a small fraction of the total number of dislocations

to contribute to this internal friction mechanism. The *total number of dislocations* increases with increasing pre-strain. The *fraction of dislocations* lying along close-packed will in general decrease with increasing pre-strain. The reason for this is that the elastic interaction between the dislocations tending to force the dislocations into some other direction increases with increasing pre-strain, whereas the Peierls stress τ_p^0 which energetically favours those dislocations lying along close-packed directions remains constant. Since the number of dislocations contributing to the internal friction peak is determined by two opposing influences it is not surprising that it shows a maximum as a function of pre-strain. There may be special cases, however, in which the dislocation arrangement in the cold-worked state is such that the relaxation continues to increase with pre-strain.

§ 3. An Outline of the Quantitative Theory

In this section we shall first show how to calculate the activation energies W_k and W from a knowledge of the function $E(y)$ and how to relate them to the Peierls stress τ_p^0. As mentioned earlier we shall see that the kinks are related to dislocations in the one-dimensional (Dehlinger–Frenkel) dislocation model discussed by various authors (Dehlinger 1929 ; Frenkel and Kontorova 1938, 1939 ; Dehlinger and Kochendörfer 1940 ; Lennard-Jones 1940 ; Frank and van der Merwe 1949 a, b, 1950 a, b ; Kochendörfer and Seeger 1950 ; Seeger and Kochendörfer 1951 ; Seeger, Donth and Kochendörfer 1953 ; Seeger 1953, 1955 b). This correspondence between kinks and dislocations in the Dehlinger–Frenkel model is very useful in the discussion of the interaction between neighbouring kinks.

If we treat the dislocation line (lying nearly parallel to the x-direction) as a string with mass m per unit length we obtain the following partial differential equation for the shape $y(x, t)$ of the dislocation line (t=time) :

$$E(y)\frac{d^2y}{dx^2}=\frac{dE(y)}{dy}-b\tau y+m\frac{\partial^2 y}{\partial t^2}. \qquad . \ . \ . \ . \ (3)$$

Special cases of this equation have been discussed by various authors (e.g. Read 1953 b). $E(y)$ is a periodic function with period a, and can be represented by a Fourier series. For practical purposes we terminate this series and write (Seeger 1955 a)

$$E(y)=E_0-\alpha_1\cos\frac{2\pi y}{a}-\alpha_2\cos\frac{4\pi y}{a}. \qquad . \ . \ . \ (4)$$

E_0 is always very large compared with α_1 and α_2. On the left hand side of eqn. (3) we may therefore replace $E(y)$ by E_0. Time-dependent solutions of the resulting equation in the special case $\tau=0$, $\alpha_2=0$ have been discussed by Seeger, Donth and Kochendörfer (1953) and Seeger (1953). Although a complete treatment of the present problem should include the discussion of dynamic effects we shall confine ourselves mainly to time-independent solutions of eqn. (3).

The starting point of the mathematical treatment is the ordinary differential equation :

$$E_0 \frac{d^2y(x)}{dx^2} = \frac{2\pi\alpha_1}{a}\left(\sin\frac{2\pi y(x)}{a} + 2\gamma \sin\frac{4\pi y(x)}{a}\right) - b\tau \quad . \quad . \quad (5)$$

$$\gamma = \alpha_2/\alpha_1 \quad \tfrac{1}{4} > \gamma > -\tfrac{1}{4}. \quad . \quad . \quad . \quad . \quad . \quad . \quad . \quad . \quad (5\,a)$$

If we interpret $y(x)$ in the Dehlinger–Frenkel model † as the relative displacement of atoms facing each other on opposite sides of the glide plane the solutions of eqn. (5) represent dislocations or sequences of dislocations. The solution for a single kink ($\tau = 0$)is also the solution for a single dislocation in the one-dimensional dislocation model : The ' displacement ' $y(x)$ increases gradually from $y = n.a$ at $x = -\infty$ to $y = (n+1)a$ at $x = +\infty$. The analytic form is

$$y = \frac{a}{\pi}\tan^{-1}\left(\frac{(1+4\gamma)^{1/2}}{\sinh[2\pi x\{\alpha_1(1+4\gamma)/E_0\}^{1/2}/a]}\right), \quad . \quad . \quad . \quad . \quad (a)$$

which for $\gamma = 0$ reduces to‡

$$y = \frac{2a}{\pi} \cdot \tan^{-1}\exp\left\{\frac{2\pi x}{a}\left(\frac{\alpha_1}{E_0}\right)^{1/2}\right\} = \frac{a}{2} + \frac{a}{\pi}gd\left\{\frac{2\pi x}{a}\left(\frac{\alpha_1}{E_0}\right)^{1/2}\right\}. \quad (6\,b)$$

It will be noticed that the displacements connected with kinks or with one-dimensional dislocations die out exponentially, so that there is no long-range interaction between them.

The energy W_k of a kink can be found by inserting eqn. (6 *a*) into the expression

$$E_{\text{pot}} = \int_{-\infty}^{+\infty}\left\{\tfrac{1}{2}E_0\left(\frac{dy}{dx}\right)^2 + \alpha_1\left(1-\cos\frac{2\pi y}{a}\right) + \alpha_2\left(1-\cos\frac{4\pi y}{a}\right)\right\}dx \quad (7)$$

for the potential energy. We obtain

$$W_k(\gamma) = \frac{a}{2\pi}(E_0\alpha_1)^{1/2} \cdot f(\gamma) \quad . \quad . \quad . \quad . \quad . \quad . \quad . \quad (8)$$

$$f(\gamma) = 4(1+4\gamma)^{1/2} + \Gamma(\gamma) \quad . \quad . \quad . \quad . \quad . \quad . \quad (8\,a)$$

$$\Gamma(\gamma) = \begin{cases} \gamma^{-1/2}\tanh^{-1}\left(\dfrac{4\{\gamma(1+4\gamma)\}^{1/2}}{1+8\gamma}\right) & 0 < \gamma \leqq \tfrac{1}{4} \\ 4 & \gamma = 0 \\ (-\gamma)^{-1/2}\tan^{-1}\left(\dfrac{4\{-\gamma(1+4\gamma)\}^{1/2}}{1+8\gamma}\right) & -\tfrac{1}{4} \leqq \gamma < 0 \end{cases} \quad . \quad . \quad (8\,b)$$

† In the Dehlinger–Frenkel model α_1 and α_2 measure the interaction of adjacent lattice planes on opposite sides of the glide-plane. E_0 is proportional to the elastic interaction between neighbouring atoms and is of the same order of magnitude as α_1. The basic equation of the Dehlinger–Frenkel model is eqn. (3), if on its left-hand side $E\,(y)$ is rigorously replaced by E_0. The solutions of the kink model and of the Dehlinger–Frenkel model differ only in the numerical value of the scale-factor w/a (eqn. 11).

‡ For the function gdx see Jahnke–Emde (1933).

The Peierls stress τ_p^0 (which corresponds to the theoretical shear strength in the Dehlinger–Frenkel model) is

$$\tau_p^0(\gamma)=\frac{2\pi\alpha_1}{ab}.\sin\Psi.(1+4\gamma\cos\Psi) \quad . \quad . \quad . \quad . \quad (9)$$

$$\cos\Psi=\frac{-1+(1+128\,\gamma^2)^{1/2}}{16\gamma}. \quad . \quad . \quad . \quad . \quad . \quad . \quad . \quad (9\,a)$$

In the special case $\gamma=0$ we can express

$$W_k(0)=\frac{2a}{\pi}\left(\frac{2E_0ab\tau_p^0}{\pi}\right)^{1/2}\dagger \quad . \quad . \quad . \quad . \quad . \quad . \quad (10)$$

explicitly in terms of the Peierls stress

$$\tau_p^0=\tau_p^0(0)=2\pi\alpha_1/ab. \quad . \quad . \quad . \quad . \quad . \quad . \quad . \quad (10\,a)$$

Another important quantity is the width w of a kink as shown in fig. 2. It is independent of γ and given by

$$w=\tfrac{1}{2}a(E_0/\alpha_1)^{1/2}. \quad . \quad . \quad . \quad . \quad . \quad . \quad . \quad (11)$$

The minimum separation between two kinks in thermal equilibrium is of the order w. Therefore the linear concentration of kinks in thermal equilibrium is approximately given by

$$c=w^{-1}\exp(-W_k/kT). \quad . \quad . \quad . \quad . \quad . \quad . \quad (12)$$

From the analysis of the measurements on copper as given below we deduce $W_k=0{\cdot}04$ ev and $w=28\,a$. At $T=90°\text{K}$, the temperature of the peak in Bordoni's measurements, we obtain for the mean separation of kinks in thermal equilibrium

$$1/c=6200\,a, \quad . \quad . \quad . \quad . \quad . \quad . \quad . \quad . \quad (13)$$

which is large compared with d. It is to be noted, however, that if we adopt Mason's explanation, this gives $w=700a$. Mason derives $\tau_p^0=5{\cdot}2\times10^{-6}G$, where G=shear modulus. Using these values for the calculations of W_k and w, we find instead of eqn. (13)

$$1/c=240\,a\;e^{0{\cdot}31}=330\,a. \quad . \quad . \quad . \quad . \quad . \quad . \quad (13\,a)$$

In Mason's model therefore the mean separation of thermal kinks is small compared with the length of the dislocation loops and of the order of the kink width w. Therefore at the temperature of the internal friction maximum the dislocation cannot move as a rigid rod. Since this was an essential assumption in Mason's model, it is not self-consistent.

As pointed out earlier, the calculation of ν, and therefore of the temperature at which the peak occurs, presents a series of difficulties which are connected with the fact that the critical distance d_{cr} is larger than the length of coherency of the thermal fluctuations. Since at the moment a completely satisfactory treatment of the problem based on the theory of stochastic movements of dislocations is not yet available, we have to rely on physical intuition for approximate derivations of expressions for ν_0 and W.

---

† This is the correct expression which differs from the one given by Read (1953 b) by a factor of two.

We think that the position of maximum energy through which a dislocation segment has to pass when forming a pair of kinks is roughly as shown in fig. 3. The activation energy corresponding to this position is approximately †

$$W = W_k(\gamma) + 2\alpha_1 \cdot d_{cr}. \quad . \quad . \quad . \quad . \quad . \quad . \quad . \quad (14)$$

In order to obtain d_{cr} we have calculated the energy of interaction between two kinks of opposite sign (as shown in fig. 2) according to eqn. (7). In the position of unstable equilibrium the sum of the interaction energy and the work $\tau \cdot b \cdot a \cdot d$ done by the applied shear stress τ must be a maximum as a function of the distance d between the kinks. In the limit $\tau \ll \tau_p^0$ we obtain by this procedure for the critical separation

$$d_{cr} = \frac{w}{\pi}(1+4\gamma)^{-1/2} \log \frac{32\alpha_1}{\tau a b}. \quad . \quad . \quad . \quad . \quad . \quad (15)$$

Fig. 3

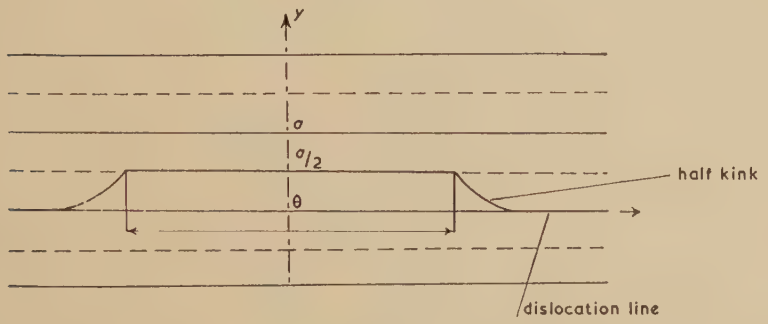

Intermediate stage in the formation of a pair of kinks of opposite sign as shown in fig. 2. This intermediate stage was used to calculate the activation energy of the thermal formation of such pairs. The length of the arrow is equal to the separation d_{cr} between two kinks of opposite sign as shown in fig. 2, corresponding to unstable equilibrium under the applied shear stress τ.

F. Pfaff (unpublished work) has checked by direct numerical integration of eqn. (5) that eqn. (15) gives good results for the whole range of parameters which is of interest in the present problem. Combining eqns. (14) and (15) we obtain

$$W = W_k(\gamma) + \frac{a}{\pi}\left(\frac{E_0\alpha_1}{1+4\gamma}\right)^{1/2} \log \frac{32\alpha_1}{\tau \cdot a \cdot b}, \quad . \quad . \quad . \quad (16)$$

which for $\gamma = 0$ reduces to

$$W = W_k(0) \cdot \{1 + \tfrac{1}{4} \log (16\tau_p^0/\pi\tau)\}. \quad . \quad . \quad . \quad . \quad (16\,a)$$

For most practical purposes eqn. (16 *a*) gives similar results as a formula derived elsewhere (Seeger 1955 a), which was based on a somewhat different assumption about the position of maximum energy.

† Equation (14) implies that the energies of two ' half-kinks ' as shown in fig. 3 add approximately to the energy W_k of one kink. A more accurate calculation will be published elsewhere.

The frequency ν_0 is taken (as in Mason's paper) to be equal to the frequency with which a rigid dislocation line oscillates in its potential well (fig. 1). From eqn. (3) we find

$$\nu_0 = \frac{v_t}{a}\left\{\frac{(1+4\gamma)\alpha_1}{E_0}\right\}^{1/2}, \quad \ldots\ldots\ldots \quad (17)$$

where v_t, the velocity of shear waves in the material, was introduced in order to eliminate the mass m of the dislocation line.

Since the dislocation displacements which we are considering are only of the same order as the dislocation strength the line energy of the dislocation will be rather small. In all the numerical calculations of this paper we have used

$$E_0 = \tfrac{1}{5} G \,.\, b^2. \quad \ldots\ldots\ldots \quad (18)$$

From internal friction measurements we can obtain data for W and ν_0. They suffice to evaluate τ_p^0 and γ (or any other pair of parameters determining $E(y)-E_0$). By combining the measurements of Niblett and Wilks and of Bordoni on copper we obtain for the main peak $W=0{\cdot}1$ ev. This corresponds to $\tau_p^0/G=4\times10^{-3}$ and to a γ-value of about zero or slightly negative. Evaluating the data available for lead (see Mason 1956) we get $\tau_p^0=5\times10^{-5}G$ and a γ-value only slightly larger than $-\frac{1}{4}$. This implies that the shape of the $E(y)$-curve is rather different in lead and copper.

The Peierls stresses obtained from experiment are considerably larger than is usually assumed in discussions of dislocation theory. However, a great portion of the dislocations in a crystal will not lie along close-packed directions and therefore will have an effective Peierls stress which is several orders of magnitude smaller than τ_p^0; thus even at very low temperatures crystals will deform at stresses far smaller than τ_p^0. Only if all dislocations involved in an experiment (e.g. the stress induced movement of a low-angle grain boundary) lie along a crystallographic direction can we observe the Peierls stress in static experiments (Seeger 1954).

We have already pointed out that although we have used eqn. (2) in our discussion we cannot expect to describe the phenomenon completely by a single relaxation process.† It is therefore necessary to observe a certain amount of care in evaluating the experimental data and also to investigate the mechanism over as large a frequency range as possible. This is particularly true since there are three other features which could give rise to a temperature dependent internal friction not describable by a constant activation energy :

(1) Since some of the measurements (e.g. those on lead) are performed at rather low temperatures quantum mechanical effects may come in. These would oppose the localization of a straight dislocation line in a definite valley of its $E(y)$-surface and therefore tend to decrease τ_p^0.

† This could be investigated further by measuring simultaneously internal friction *and* elastic modulus.

(2) If γ is negative and not very different from $-\frac{1}{4}$ the bottoms of the $E(y)$ valleys are rather shallow. The thermal fluctuations in the position of the dislocation may then be so large that the dislocation will oscillate non-harmonically. If this is the case, ν_0 is no longer a constant but depends on temperature.

(3) In most face-centred cubic metals dislocations lying in {111} glide-planes are extended ones. They consist of two parallel partial dislocations which are connected by a stacking fault. Each of the partial dislocations moves in an $E(y)$-surface of its own. For the purpose of the present discussion we may consider them to be rigidly connected with each other at a separation that depends on the character of the dislocation line. The $E(y)$ function of the complete dislocation is again a function of the type of eqn. (4), the parameters of which depend on the separation of the partials. We therefore expect parallel dislocations with different Burgers vectors to have different values of τ_p^0. Rather small changes of the stacking-fault energy with temperature may cause changes in the stacking-fault width of the order $\frac{1}{2}a$ and thereby influence very strongly the parameters α_1 and α_2 of the complete dislocations. Such a temperature variation would lead to a wrong activation energy if evaluated in too narrow a frequency range.

The preceding discussion warns us against taking the numerical results of this paper too literally. The qualitative implications and the orders of magnitude are, however, believed to be correct.

Acknowledgments

The author is indebted to Dr. J. Wilks and Mr. D. H. Niblett for stimulating discussions of their results and for communicating their data prior to publication. Discussions with Dipl. Phys. E. Kröner and cand. phys. F. Pfaff are also gratefully acknowledged. The latter greatly helped with the computational work necessary for analysing the experimental data.

References

Bömmel, H. E., 1954, *Phys. Rev.*, **96**, 220.

Bordoni, P. G., 1949, *Ricerca sci.*, **19**, 851 ; 1954, *J. Acoust. Soc. Amer.*, **26**, 495.

Dehlinger, U., 1929, *Ann. Phys.*, **2**, 749.

Dehlinger, U., and Kochendörfer, A., 1940, *Z. Phys.*, **116**, 576.

Frank, F. C., and van der Merwe, J. H., 1949 a, *Proc. Roy. Soc.* A, **198**, 205 ; 1949 b, *Ibid.*, **198**, 217 ; 1950 a, *Ibid.*, **200**, 125 ; 1950 b, *Ibid.*, **201**, 261.

Frenkel, J., and Kontorova, T., 1938, *Phys. Z. Sowjet.*, **13**, 1 ; 1939, *J. Phys.*, U.S.S.R., **1**, 137.

Jahnke, E., and Emde, F., 1933 ; *Funktionentafeln*, 2nd ed. (Leipzig : Teubner), p. 58.

Kochendörfer, A., and Seeger, A., 1950, *Z. Physik*, **127**, 533.

Lennard-Jones, J. E., 1940, *Proc. Phys. Soc.*, **52**, 38.

Mason, W. P., 1955 a, *Phys. Rev.*, **97,** 557 ; 1955 b, *J. Acoust. Soc. Amer.*, **27,** 643 ; 1955 c, *Bell. Syst. Techn. J.*, **34,** 903 ; 1956, *Proceedings of the Colloquium on Flow and Deformation of Solids*, Madrid 1955 (Springer).

Mott, N. F., and Nabarro, F. R. N., 1948, Report of a Conference on the Strength of Solids. (London : The Physical Society.), p. 1.

Niblett, D. H., and Wilks, J., 1955. *Proceedings of the International Conference on Low Temperature Physics*, Paris 1955, p. 484 ; 1956, *Phil. Mag.*, **1,** 415.

Peierls, R., 1940, *Proc. Phys. Soc.*, **52,** 34.

Read, W. T., 1953, *Dislocations in Crystals*, McGraw-Hill. (*a*) p. 46, (*b*) p. 53, *et seq.*

Seeger, A., 1953, *Z. Naturforsch g.*, **8***a*, 246 ; 1954, *Ibid.*, **9***a*, 758 ; 1955, *Theorie der Gitterfehlstellen in Encyclopedia of Physics* (Springer), (*a*) sect. 72 ; (*b*) sect. 67 ; 1956, *Proceedings of the Colloquium on Flow and Deformation of Solids*, Madrid 1955 (Springer), p. 322.

Seeger, A., Donth, H., and Kochendörfer, A., 1953, *Z. Physik*, **134,** 173.

Seeger, A., and Kochendörfer, A., 1951, *Z. Physik*, **130,** 321.

Seitz, F., 1951, *Phase Transformations in Solids* (Wiley & Sons), p. 77.

Shockley, W., 1952, *Trans. Amer. Inst. Min. Met. Engrs.*, **194,** 829.

Zener, C., 1952, *Imperfections in Nearly Perfect Crystals* (Wiley & Sons), p. 289.

LXVI. *The Elasticity and Antiferromagnetism of* Cr_2O_3†

By R. Street
Department of Physics, The University, Sheffield,
and B. Lewis
Research Laboratories of The General Electric Company, Wembley

[Received February 15, 1956]

Abstract

Measurements have been made of Young's modulus of pressed bars of Cr_2O_3 as a function of temperature. Near the Néel temperature an anomalous variation of modulus is observed. The character of this anomaly is however completely different from the anomalies previously observed for NiO and CoO. It is suggested that the difference is a domain phenomenon: the structure of NiO and CoO, but not of Cr_2O_3, allows the existence of antiferromagnetic domains.

§ 1. The Influence of Domain Structure on Elasticity

Measurements of the temperature variation of the Young's modulus of CoO and NiO have been made by Street and Lewis (1951) and the observations on CoO confirmed by Fine (1952, 1953). In the region of the Néel temperatures of the compounds the values of Young's modulus increase rapidly with increasing temperature and the moduli are approximately step functions of temperature. The ratios of the values measured at temperatures above and below the Néel temperatures are 2·3 and 1·6 for CoO and NiO respectively. A rather similar variation of modulus is observed for some ferromagnetic substances, e.g. the modulus versus temperature curve for unmagnetized nickel shows a maximum and a minimum with a ratio maximum : minimum of 1·6 (Siegel and Quimby 1936).

A number of workers have shown by x-ray techniques that linear distortion of the crystal lattices of antiferromagnetics occurs on cooling through the Néel temperature. Thus NiO and CoO have face-centred cubic structures above their Néel temperatures; Tombs and Rooksby (1950) found that linear deformations along [111] and [100] directions, respectively, occur on cooling through the Néel temperature. Thus at lower temperatures NiO becomes rhombohedral and CoO becomes tetragonal. For these substances the lattice deformation is large when compared to the magnetostrictive strain of a ferromagnetic, e.g. for CoO

†Communicated by Professor W. Sucksmith, F.R.S.

the strain due to antiferromagnetism ranges from 10^{-3} to 10^{-2}, increasing with decreasing temperature.

Shull, Strauser and Wollan (1951) have examined NiO and CoO by neutron diffraction techniques and have proposed a structure in which the spins of the Ni^{++} and Co^{++} ions are arranged in four antiparallel pairs of sublattices. They interpret the neutron diffraction spectra as showing that the spins are aligned along [100] axes in both NiO and CoO, and that the configuration of ionic spins is such as to give a [111] magnetic symmetry which Shull considers to be the axis of lattice deformation in NiO. Recently Li (1955) has re-examined the question and has proposed that it is the axis along which the spins are aligned, rather than the configuration into which the spins are coupled, which determines the character of the lattice deformation. On Li's hypothesis, the spin directions in NiO and CoO are along [111] and [100] respectively. It is possible for these compounds, and others of the same general type, to have an antiferromagnetic domain structure, each domain being characterized by its particular axis of lattice deformation. The division of an antiferromagnetic crystal into domains may result in relatively large scale lattice distortion and this may underlie the observation made by Roth (reported by Li, loc. cit.) that single crystals of NiO are always badly twinned.

The observed temperature variation of the Young's modulus of CoO and NiO may be visualized in terms of a domain mechanism. At temperatures below the Néel temperature the application of, for example, an external compressive stress will result in a preferential growth of those domains which are deformed so that the shorter dimension lies near to the axis of compression.† Thus there is a component of strain, ϵ_m, of antiferromagnetic origin, in addition to the ordinary elastic strain component, ϵ_e. Under an external stress, z, $1/E_m=(\epsilon_e+\epsilon_m)/z$, where ϵ_m is Young's modulus measured in the antiferromagnetic region. Above the Néel temperature, in the paramagnetic region $\epsilon_m=0$ and the value of Young's modulus, E_p is given by $1/E_p=\epsilon_e/z$. Hence $E_p>E_m$, the magnitude of the difference being given by

$$\Delta\frac{1}{E}=\frac{1}{E_m}-\frac{1}{E_p}=\frac{\epsilon_m}{Z}.$$

On the domain hypothesis the necessary conditions for the existence of large temperature variations of Young's modulus are (*a*) the lattice must undergo linear deformation on cooling through the Néel temperature and (*b*) the deformation must occur along a crystallographic direction

† For CoO, whether the structure is that proposed by Shull et al. or by Li, and for NiO with Li's proposed structure, the change of the axis of deformation to a crystallographically equivalent one will be accompanied by a corresponding change in spin direction. For NiO, with Shull's proposed structure, a change in the direction of the deformation axis from say [111] to [$\bar{1}$11] must be accompanied by a reversal of the spins of the ions on two of the four pairs of sublattices.

having a multiplicity greater than unity. Both these conditions are satisfied for MnO, FeO, CoO, NiO, MnS and MnSe (table 1, Li, loc. cit.) and large modulus anomalies are to be expected for these materials. In the case of Cr_2O_3, which has a rhombohedral structure above and below the Néel temperature, the axis of deformation and the direction of the spins are along the crystallographically unique [111] direction (Brockhouse 1953, Greenwald 1951, 1956). Thus if the domain hypothesis of the temperature variation of Young's modulus is valid, Cr_2O_3 should not exhibit the type of modulus change observed for NiO and CoO.

§ 2. Specimens and Method

Bar specimens of Cr_2O_3 of approximate dimensions 25 mm × 4 mm × 2 mm were prepared by compressing finely ground powder in a die and firing the resultant compact in air in the temperature range 1000°c to 1500°c. In no case was shrinkage observed but the fired bars were mechanically strong indicating that recrystallization across particle boundaries had occurred. By successive firing and grinding and by using pressures up to 50 tons/in.^{2}, specimens were obtained having densities up to 3·7 gm/cm^3. The ideal density calculated from x-ray data is 5·21 gm/cm^3. X-ray powder photographs of the specimens showed that they contained a single homogeneous rhombohedral phase with lattice parameters in agreement with the accepted values for Cr_2O_3.

Measurements of Young's modulus and the coefficient of internal friction ($1/Q$) were made at various temperatures using a dynamic method similar to that described by Zacharias (1933). A quartz crystal bar of natural frequency 100 kc/s was used as the generator of longitudinal oscillations.

After Young's modulus measurements had been made, the temperature variation of the magnetic susceptibility of the material was determined using samples cut from the bars.

§ 3. Results and Discussion

Typical results of the temperature variation of Young's modulus are shown in fig. 1. The specimen used had a density of 3·69 gm/cm^3. The results show a general steady decrease of modulus with increasing temperature, except within the range 25°c to 95°c. The departure of the observed modulus values from a smooth curve is shown in fig. 2. Figure 3 shows the temperature variation of the reciprocal of the magnetic susceptibility of the specimen used to obtain the results plotted in fig. 1.

It is immediately obvious that there is no similarity between fig. 1 and the 'stepped' modulus versus temperature curves obtained with CoO and NiO. Furthermore both CoO and NiO show a marked increase of internal friction below the Néel temperature. This behaviour may again be attributed to domain action in these materials, e.g. any resistance to the free movement of the boundary walls between antiferromagnetic domains

will cause the strain ϵ_m to be out of phase with the applied stress z. In contracts to the behaviour of NiO and CoO, the coefficient of internal friction of the Cr_2O_3 specimens was $(5\pm0{\cdot}5)\times10^{-3}$ over the entire range of temperature.

Fig. 1

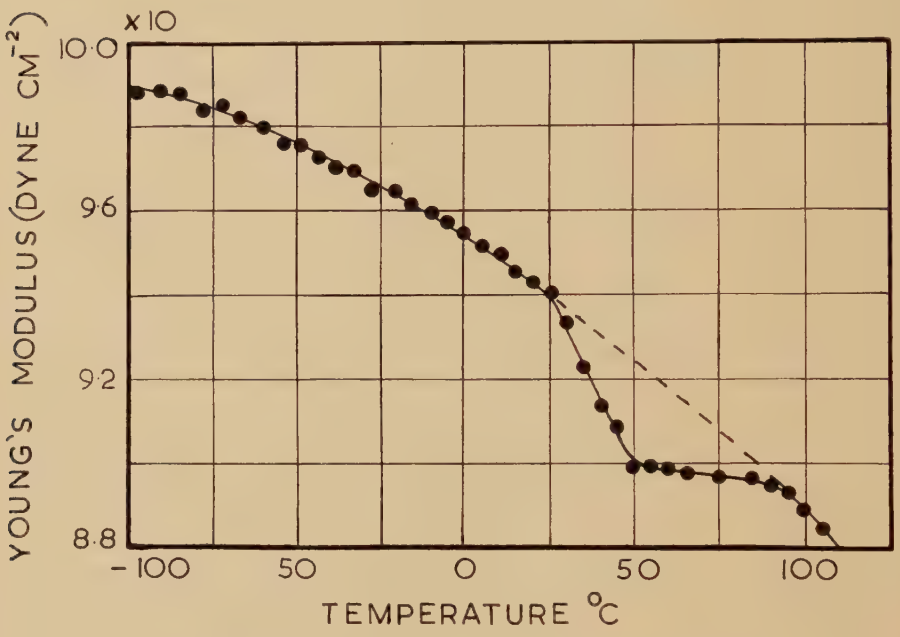

The temperature variation of Young's modulus of Cr_2O_3.
– – – – Smoothed curve drawn through points above and below Néel temperature.

The experimental results presented above thus confirm the predictions of § 1, that domain phenomena should not be exhibited by Cr_2O_3. The differences in the observed behaviour of Cr_2O_3 on one hand and of NiO and CoO on the other, are strong evidence that antiferromagnetic domain structures exist in NiO, CoO and similar compounds.

From fig. 3 it will be seen that the Néel temperature, usually taken as the temperature of minimum inverse susceptibility, cannot be determined with accuracy. However, within the limits of experimental error the maximum Young's modulus deviation given in fig. 2, occurs at the Néel temperature. It is considered that the observed change of modulus near the Néel temperature is caused by a modification of the binding energy versus ionic distance curve produced by the disappearance of magnetic ordering forces at the Néel temperature. An analogous situation occurs in some ferromagnetic materials, notably the alloy of 42% nickel in iron. Engler (1938) found that there is an anomalous change of Young's modulus

at the Curie temperature even when all domain effects were eliminated by the application of a strong magnetic field. Döring (1938) has shown that the anomaly is related to the volume expansion which occurs at the Curie temperature. Antiferromagnetic materials also show volume expansion at their Néel temperatures and measurements by Jeffrey and Viloteau (1948) show that this is particularly large for Cr_2O_3.

Fig. 2

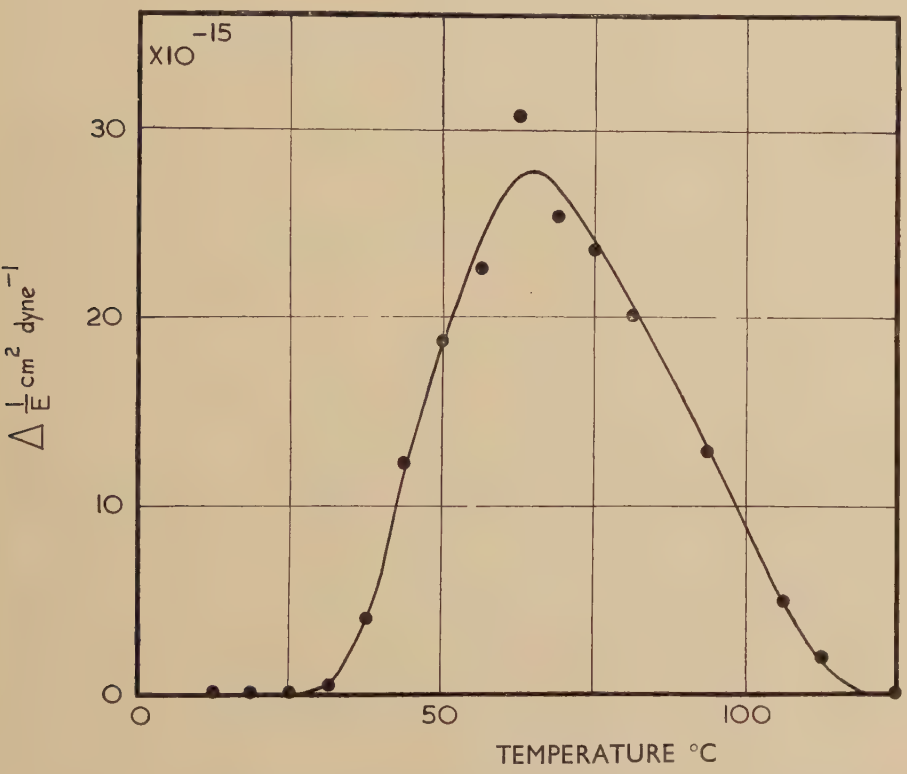

The deviation of the measured values of Young's modulus as a function of temperature

$$\Delta\frac{1}{E}=\frac{1}{E_0}-\frac{1}{E_p}=(E_p-E_0)/E_pE_0$$

where E_0=observed value of modulus,
E_p=value of modulus taken from smooth curve of fig. 1.

Finally it may be noted that there are other antiferromagnetics in which the spins are aligned along crystallographically unique directions e.g. α-Fe_2O_3 below −20°c and CrSb. As for Cr_2O_3, so with these compounds, no large stepped variation of Young's modulus or temperature dependence of internal friction should be observed.

Fig. 3

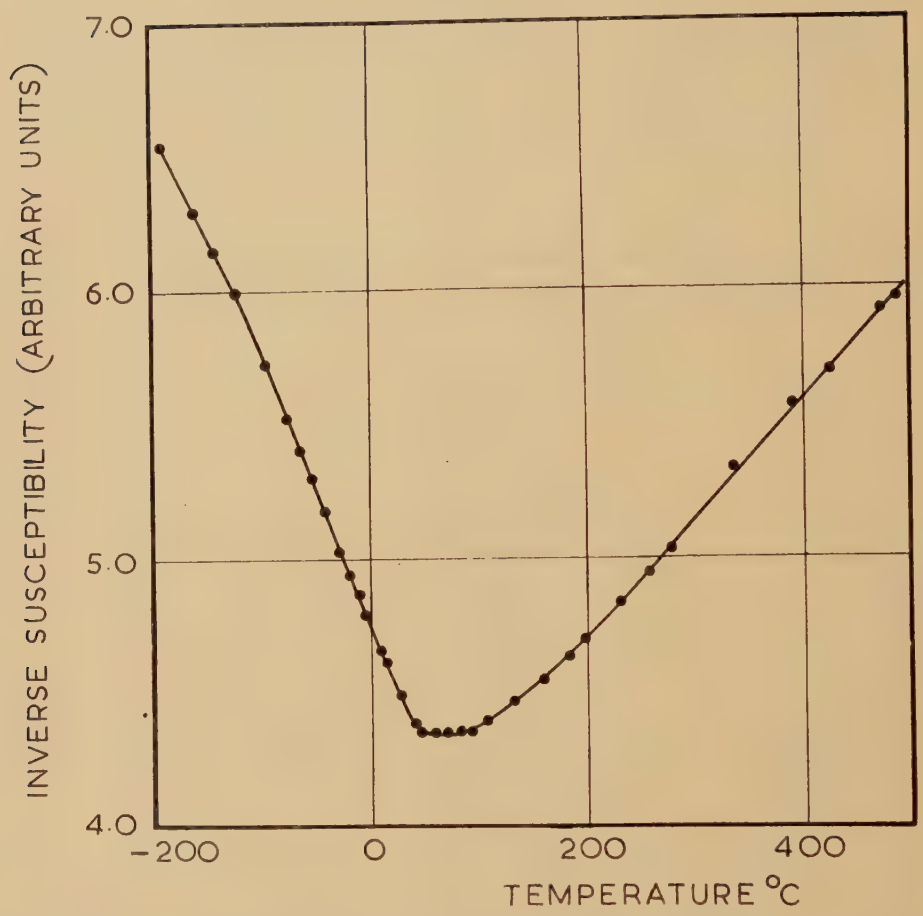

The temperature variation of the inverse magnetic susceptibility of Cr_2O_3 specimen used to obtain results plotted in fig. 1.

Acknowledgment

The magnetic susceptibility measurements were made by Mr. I. W. Dunmur and his help is gratefully acknowledged.

References

Brockhouse, B. N., 1953, *J. Chem. Phys.*, **21**, 961.
Döring, W., 1938, *Ann. Phys., Leipzig*, **32**, 465.
Engler, O., 1938, *Ann. Phys., Leipzig*, **31**, 145.
Fine, M. E., 1952, *Phys. Rev.*, **87**, 1143 ; 1953, *Rev. Mod. Phys.*, **25**, 158.
Greenwald, S., 1951, *Nature, Lond.*, **168**, 379 ; 1956, *Ibid.* (to be published).
Jeffrey, J., and Viloteau, J., 1948, *C.R. Acad. Sci.*, **226**, 1701.
Li, Y-Y., 1955, *Phys. Rev.*, **100**, 627.
Shull, C. G., Strauser, W. A., and Wollan, E. O., 1951, *Phys. Rev.*, **83**, 333.
Siegel, S., and Quimby, S. L., 1936, *Phys. Rev.*, **49**, 663.
Street, R. and Lewis, B., 1951, *Nature, Lond.*, **168**, 1036.
Tombs, N. C., and Rooksby, H.P., 1950, *Nature, Lond.*, **165**, 442.
Zacharias, J., 1933, *Phys. Rev.*, **44**, 116.

LXVII. *The Solar Daily Variation of the Cosmic Ray Intensity*

By H. Elliot and P. Rothwell
Imperial College of Science and Technology, London †

[Received February 2, 1956]

Abstract

Some recent measurements of the solar daily variation for cosmic rays incident from the east and west directions at 45° to the vertical in London are described. The results do not agree with those to be expected if the variation was due to a non-isotropic flux of primary particles entering the earth's magnetic field. This result is discussed in relation to other evidence and it is concluded that the daily variation is probably due to a modulation of the primary cosmic ray intensity in the earth's magnetic field.

§ 1. Introduction

It is generally believed that the solar daily variation of the cosmic ray intensity is due to a variation of the primary radiation incident on the earth's atmosphere, this intensity variation being produced in some way which is at present not understood. Observations to date have been made at sea level using ionization chambers, counter telescopes and neutron monitors. Counter telescopes have the advantage that they make it possible to measure the variation for different directions of incidence at the earth's surface whereas ionization chambers and neutron monitors accept radiation within a solid angle which is limited only by atmospheric absorption. Since counter telescopes record primarily either the μ-meson flux or the combined μ-meson and electron components, the intensity observed at sea level is dependent on atmospheric temperature and pressure. In relating the intensity changes observed at sea level to changes in the primary intensity, it is therefore necessary to correct for these meteorological variables. In investigations of the solar daily variation it is possible to make an adequate correction for the variation in barometric pressure, but in order to correct for temperature it is necessary to know the daily variation in temperature throughout the atmosphere. At present the daily variation in atmospheric temperature is uncertain because of the limitations, in particular the susceptibility to radiation errors, of the instruments used for routine measurements.

In the absence of accurate information about the daily variation in atmospheric temperature, attempts have been made to separate the part of the cosmic ray variation due to atmospheric temperature from that

† Communicated by Professor P. M. S. Blackett, F.R.S.

due to variations of the primary intensity by using directional telescopes. These telescopes have been so arranged that they record radiation arriving from quite different parts of the sky but respond in an identical manner to variations in intensity due to atmospheric temperature and pressure changes (Dolbear and Elliot 1951, Malmfors 1949). Measurements of this kind together with observations on the nucleonic component, which is not temperature sensitive, have established beyond doubt that the daily variation is largely due to a variation in primary intensity incident on the atmosphere. This variation has been generally attributed to an anisotropic primary intensity entering the earth's magnetic field.

In order to determine the true direction of anisotropy from the observed daily variation, it is necessary to know the deflection experienced by the primary particles in passing through the earth's magnetic field. The trajectories of cosmic ray particles in the earth's field have been investigated by Brunberg and Dattner (1953) by means of scale model experiments. Using the data on the trajectories obtained in this way, Brunberg and Dattner (1954) have shown that it is possible to account for the daily variation observed with counter telescopes pointing in the north and south directions at $\sim 30^\circ$ to the vertical if it is assumed that the mean energy of the primary radiation responsible for the variation lies in the region 2 to 4×10^{10} ev. With this assumption, an anisotropy of the primary radiation with a direction lying near the plane of the ecliptic would produce a daily variation of nearly the same amplitude for the north and south directions but with a phase difference of about two hours as was indeed observed in 1948 and 1949 (Malmfors, Elliot and Dolbear *loc. cit.*).

Brunberg and Dattner's data on trajectories show that at latitude 50° primary particles of energy 3×10^{10} ev, which have initial directions nearly parallel to the earth's magnetic axis, are deflected in the earth's field so as to arrive from the west at 45° to the vertical. Those with the same energy but with initial directions in the geomagnetic equatorial plane, arrive from the east at 45° to the vertical. Consequently, if we point a counter telescope in the east direction at 45° to the vertical, it should record the daily variation due to anisotropy of the primaries plus any variation of atmospheric origin since, as the earth rotates, this telescope will scan a strip round the celestial sphere. A telescope pointing at 45° to the west, however, collects radiation from very nearly the same direction throughout the day and should therefore show only the atmospheric part of the variation.

Observations have been made over a period of one year in London using two counter telescopes arranged in this way and the results are described below.

§ 2. Experimental Arrangement

Each counter telescope consisted of three trays of counters 60 cm by 60 cm in coincidence, the extreme trays being separated by 140 cm. The

Fig. 1

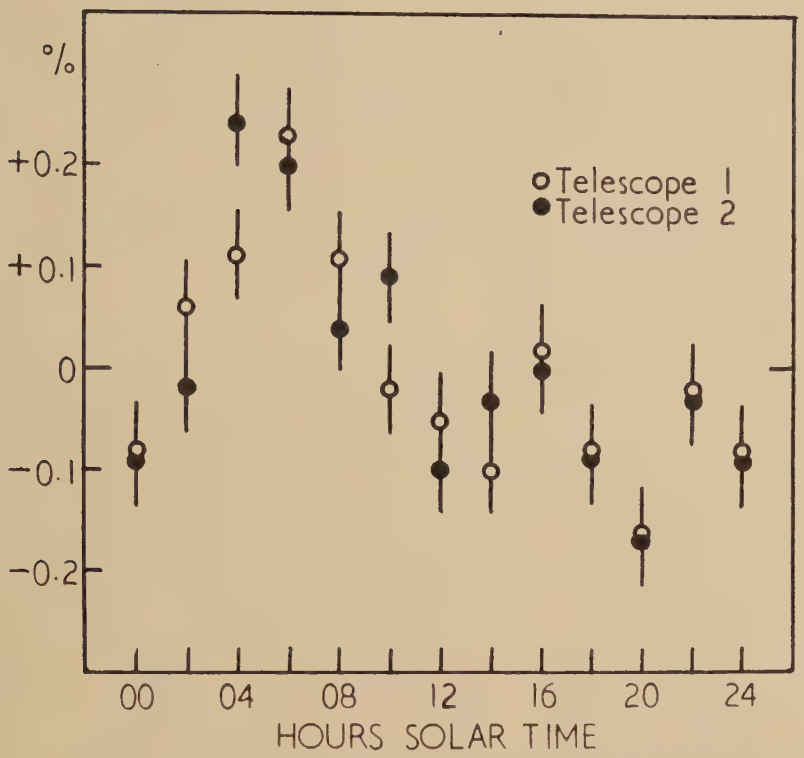

Bi-hourly departures from the mean for the two telescopes averaged over the period of the measurements.

Fig. 2

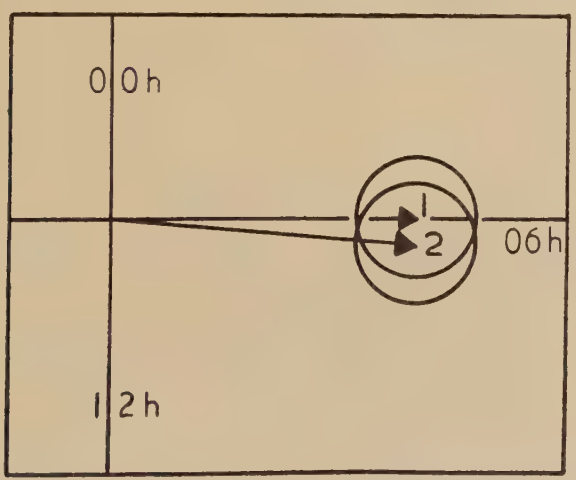

Data from fig. 1, plotted on a harmonic dial showing the absence of any systematic difference between the two telescopes.

trays were mounted in metal frameworks so that the axes of the telescopes pointed east and west at 45° to the vertical. No absorber was used and the counting rate of each counter set was ~15 000 per hour. The apparatus was in operation from May 1954 to April 1955 and during this period the two telescopes were interchanged from time to time in order to

Fig. 3

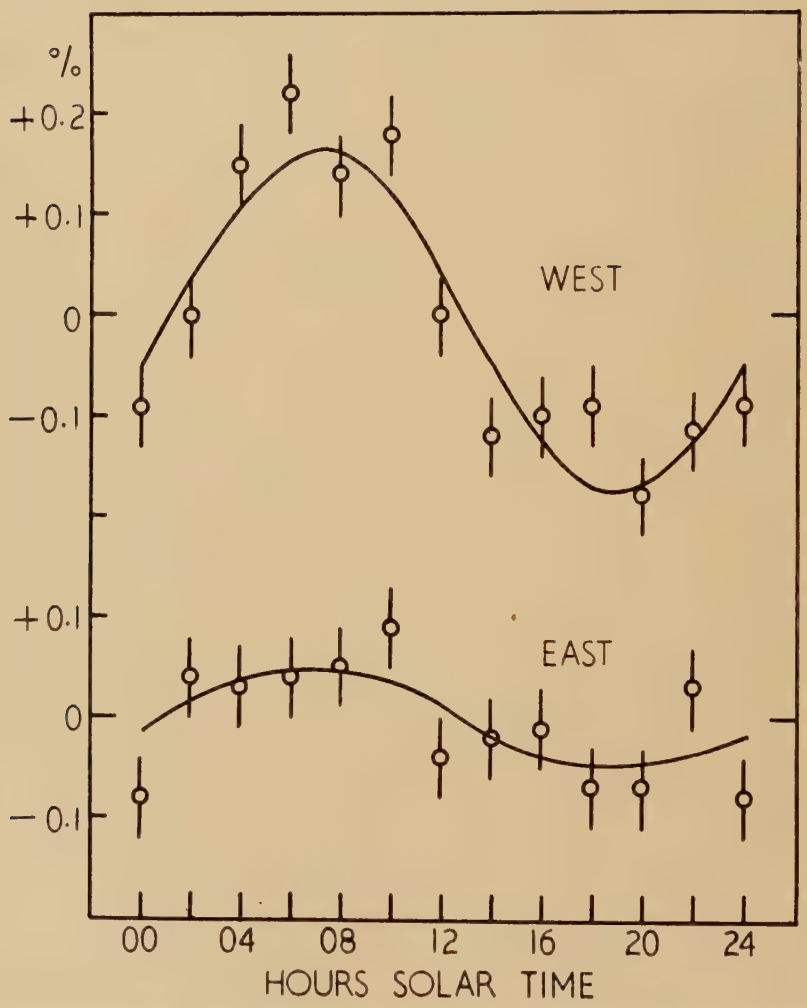

The mean solar daily variations for the east and west directions after correction for barometric pressure. May 1954 to April 1955 inclusive.

eliminate any systematic instrumental difference which might have influenced the daily variation measured by the two telescopes.

As a check on the performance of the equipment, the daily variation data have been added together for each of the two telescopes over the

period during which the observations were made. Each telescope having spent the same length of time looking east and west, any instrumental difference would be revealed as a difference between the average daily variation measured by the two counter sets. Figure 1 shows the bi-hourly departures from the mean for each of the two telescopes. It can be seen that there is no obvious systematic difference and this is confirmed by fig. 2 in which the first harmonics for the two sets of data are plotted on a harmonic dial. The harmonic coefficients agree to within the statistical error and we therefore conclude that any systematic difference due to instrumental defects is so small that it can be neglected.

§ 3. The Daily Variation for the East and West Directions

Figure 3 shows the mean daily variation for the east and west directions for the period April 1954 to April 1955. The data have been corrected for the variation in barometric pressure using a coefficient of 2·7% per cm Hg. This coefficient was deduced from the day to day changes in the rates of the two telescopes due to variations in pressure. The daily

Fig. 4

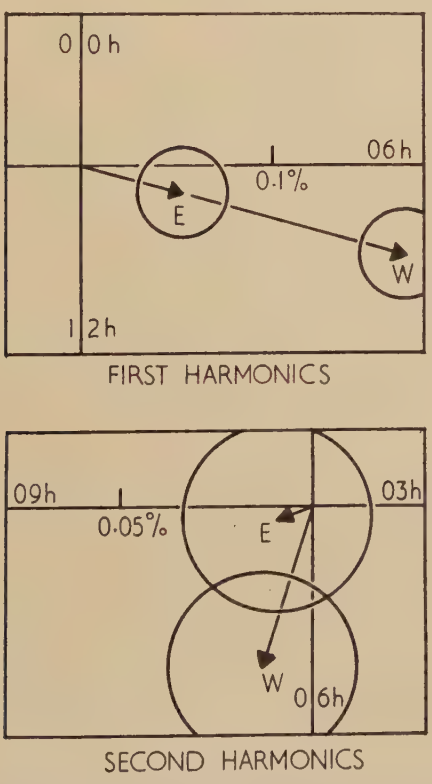

Harmonic dials showing the mean 24 hour and 12 hour waves for the east and west directions after correction for barometric pressure.

variation in barometric pressure in these latitudes is small and the correction does not greatly change the appearance of the curves. Figure 4 shows the first and second harmonics of these curves plotted on harmonic dials which show that the amplitude of the 12-hour waves are not statistically significant. The amplitude of the 24-hour wave in the west direction is seen to be about three times as great as that for the east direction.

§ 4. Discussion

It is extremely difficult to reconcile this result with the view that the daily variation is produced by an anisotropy of the primary radiation existing at large distances from the earth since, as pointed out in § 1, such an anisotropy would lead to a larger variation in the east direction than in the west. The basic assumptions involved in this argument are

(*a*) that the average energy of the primaries responsible for the variation is in the range 2×10^{10} ev to 4×10^{10} ev, as deduced by Brunberg and Dattner (1954) from the observed variation in the north and south directions in 1948, and

(*b*) that the direction of greatest anisotropy lies in or near the plane of the ecliptic.

The measurements in the north and south directions were made during 1948 and it is possible that the mean energy of the primary radiation responsible for the daily variation has changed since that time. It is certainly true that the amplitude of the variation has decreased and that the phase has also changed (Thambyahpillai and Elliot 1953, Sarabhai and Kane 1953). This could be interpreted as a decrease in average energy of the primaries producing the variation, and if one supposes that the energy has decreased to a value of $1{\cdot}5\times10^{10}$ ev or less, the trajectories for primaries incident on the earth from either east or west have initial directions which lie in or near the equatorial plane. Under these circumstances both telescopes would be exploring the same strip of sky and should therefore show the same daily variation. It does not seem possible, however, even on this basis, to account for a larger variation from the west than from the east unless one supposes the mean energy to have decreased to a value well below 10^{10} ev when such particles are unable to reach the earth from an easterly direction because of the earth's shadow cone. It then becomes impossible to account for the existence of a daily variation in the equatorial region since the primaries responsible would be unable to reach the earth's equator from any direction.

Turning now to assumption (*b*), it is possible to envisage some direction of anisotropy which, lying at an angle of 70° or 80° to the plane of the ecliptic, might produce a larger variation on the west pointing telescope than the east. This again leads to difficulty, however, in accounting for the existence of an appreciable daily variation at the equator since the amplitude of the observed variation would be smallest at the equator

and increase with increasing latitude. In fact the reverse applies (Elliot 1952).

In summarizing, we may conclude that it is extremely difficult to envisage a state of affairs which enables us to account for the observed variation in the east and west directions in terms of an anisotropy which exists at such a distance from the earth that the asymptotic directions of the primary particles are relevant.

Apart from these results for the E/W directions, there are other characteristics of the variation which are equally difficult to understand on this interpretation and these will now be briefly discussed under (*a*) and (*b*).

(*a*) It is known from comparison of the latitude variations (Fonger 1953) that the nucleonic component at sea level arises from primaries of lower average energy than those which produce the bulk of the μ-mesons and electrons at sea level. Because of this difference in primary energy, the deflection in azimuth of the primaries which produce the nucleonic component must be greater than that for the primaries of the ionizing component. The sense of this deflection is such that a given direction of anisotropy would produce a daily variation in the nucleon flux with an earlier phase than that for the ionizing component. Simultaneous measurements of the daily variation for the ionizing component and for the nucleonic component were made in Manchester during the period June 1952 to May 1954. During the two periods June 1952 to May 1953 and June 1953 to May 1954, the times of maximum for the nucleon variations were 1330^{h} and 1300^{h} rsepectively, compared with 1040^{h} and 0840^{h} for the ionizing component. During both these periods the phase of the daily variation for the ionizing component was in advance of that for the nucleons which is the contrary of what would be expected from consideration of the primary energies involved.

(*b*) During the period of the present measurements in the east and west directions, simultaneous measurements in the vertical direction in London revealed some remarkable changes in phase of the daily variation for vertical particles (Possener and Van Heerden 1956). During the period June to November 1954 the time of maximum intensity was 0300^{h} whereas from December 1954 to March 1955 it was 1000^{h}. No comparable change in phase was observed in either the east or west directions, and if this phase change represented a genuine change in direction of the anisotropy at this time, it is hardly conceivable that it should not, at the same time, have appeared in the east/west data.

The discussion above leads us to conclude that the interpretation of the cosmic ray daily variation as the result of a non-isotropic primary flux entering the earth's magnetic field may well be incorrect. Directional telescope measurements, however, show that the amplitude and phase of the daily variation depend on the direction of observation, so the variation cannot originate in the atmosphere. If these two statements are to be reconciled, it seems that the intensity modulation, which we observe as a solar daily variation, must take place in the earth's magnetic field.

§ 5. Conclusion

The results of measurements in the east and west directions, together with other known characteristics of the daily variation, lead to the conclusion that the daily variation is not due to an anisotropic primary flux entering the earth's magnetic field but is most probably produced by modulation of the primary intensity within the region occupied by the field.

References

Malmfors, K. G., 1949, *Tellus*, **1**, 2.
Elliot, H., and Dolbear, D. W. N., 1951, *J.A.T.P.*, **1**, 205.
Brunberg, E. A., and Dattner, A., 1953, *Tellus*, **5**, Nos. 2 and 3 ; 1954, *Ibid.*, 6, No. 1.
Thambyahpillai, T., and Elliott, H., 1953, *Nature, Lond.*, **171**, 918.
Sarabhai, V., and Kane, R. P., 1953, *Phys. Rev.*, **90**, 204.
Elliot, H., 1953, *Progress in Cosmic Ray Physics* (North Holland Publishing Company), p. 468.
Fonger, W. H., 1953, *Phys. Rev.*, **91**, 351.
Possener, M. N. A., and Van Heerden, I. J., 1956, *Phil. Mag.*, **1**, 253.

LXVIII. *Direct Observations of the Arrangement and Motion of Dislocations in Aluminium*

By P. B. Hirsch, R. W. Horne and M. J. Whelan
Crystallographic Laboratory and Electron Microscopy Group,
Cavendish Laboratory, Cambridge†

[Received June 25, 1956]

Abstract

Electron optical experiments on Al foils have revealed individual dislocations in the interior of the metal. The arrangement and movement of individual dislocations have been observed. Most of the dislocations occur in the boundaries of a substructure, the diameter of the subrains being of the order of 1 μ or more. Tilt-boundaries, networks and dislocation nodes have been resolved. The results apply to aluminium recovered at 350°c after heavy deformation by beating ; the dislocation density is $10^{10}/cm^2$.

The dislocations can be seen to move along traces of (111) slip planes ; the motion of the dislocations can be either rapid or slow and jerky. Cross-slip by the screw dislocation mechanism has been observed frequently.

§ 1. Introduction

Recent experiments (Hedges and Mitchell 1953, Amelinckx 1956) have revealed the dislocation structures inside optically transparent crystals of AgBr and NaCl. For metals, however, it has so far been possible to demonstrate the presence and arrangement of dislocations only at the surface, for example by the use of etching and preferential precipitation techniques (Lacombe and Beaujard 1948, Wilsdorf and Kuhlmann-Wilsdorf 1955). Most of the information about dislocation arrangements in the interior of a cold-worked metal has been derived from x-ray diffraction experiments (see for example Hirsch 1956). The present paper gives a preliminary account of electron–optical experiments on Al foils, which have revealed the arrangement and motion of individual dislocations in the interior of the metal.

In previous electron microscope studies of electrolytically thinned specimens of Al foils the substructure was observed, but no evidence was advanced to suggest that individual dislocation lines could be seen (Heidenreich 1949). In these new experiments beaten Al foils were examined, after suitable annealing and etching treatments, by electron

† Communicated by the Authors.

microscopy and electron diffraction, in a high resolution electron microscope. The results suggest that individual dislocation lines are revealed in the interior of the metal on account of the strain field associated with them, and no ' decoration ' is therefore required. The arrangement of the dislocation lines in the sub-boundaries and within the subgrains can be studied directly, and the motion of individual dislocations followed. Many complex effects have been observed, and it is not possible at present to account for more than a few of these in detail. A number of interesting points have however already emerged, and it has therefore been considered worthwhile to publish this preliminary account.

§ 2. Experimental Technique

Specimens of high purity (99·99+%) and commercially pure (99·8%) aluminium were beaten by Messrs. George M. Whiley Ltd., to a thickness of 0·5 μ. The foils were annealed *in vacuo* at 350°C, and subsequently etched in dilute hydrofluoric acid.

The specimens were examined in the Siemens and Halske ' Elmiskop ' electron microscope operating at 80 kv. The foils were found to be transparent to electrons over large areas. High resolution electron micrographs in bright and dark field, and diffraction patterns from preselected areas were taken. The instrumental magnification was $\times 40\,000$ for all the plates, except for fig. 1, which was taken at $\times 8000$. The instrument was accurately corrected for astigmatism, using suitable test objects, prior to examining the specimens, and under these conditions the resolution attained was probably of the order of 10 to 20 Å.

§ 3. Evidence for the Visibility of Dislocation Lines

Figures 1–15 show some typical micrographs obtained. Experiments designed to elucidate the nature of the contrast mechanism have shown that the contrast is due to differences in intensities of Bragg reflections, and that the observed effects are complicated owing to certain interference effects. Details of these experiments will be described in a later paper. The following facts, however, leave little doubt that individual dislocation lines are being observed :

(*a*) The specimens contain a substructure of subgrain diameter about 1 μ or more (fig. 1). The misorientations across the boundaries have been determined from diffraction experiments and are found to be about 1° or 2°. These low-angle boundaries presumably consist of arrays or networks of dislocations.

(*b*) The boundaries of the substructure consist (under higher magnification) of black lines or dots (figs. 2–9). The spacings of the dislocations in the boundaries expected from angles of rotation measured in two cases across particular boundaries agreed within a factor of 1·5 with the observed spacings. In view of the difficulties involved in

counting the individual irregularly spaced dislocations, and owing to the uncertainty in knowing the type of boundary involved, this agreement is considered satisfactory.

(*c*) The average distance between the lines or dots is about 100 Å, corresponding to average angular misorientations of about $1\frac{1}{2}°$. This is in excellent agreement with the order of magnitude of the rotation determined from many diffraction patterns, from areas covering several subgrain boundaries.

(*d*) On tilting the illumination or the specimen through small angles, the lines are seen to remain fixed in position, although the contrast changes. Experiments such as these and dark field experiments show that the visibility of the lines is due to Bragg contrast, and that they represent a definite property of the specimen.

(*e*) It is already possible in some cases to explain the detailed geometry of the lines and dots in terms of dislocations. Some examples will be given below.

(*f*) When working with large condenser apertures at high beam currents, the lines are observed to move ; in areas with a [001] direction normal to the foil, the movement occurs along straight lines parallel to the traces of (111) slip planes (figs. 10–13). The behaviour of these moving lines is identical with that expected of dislocation lines.

These observations leave little doubt that the lines represent single dislocation lines of unit Burgers vector. There are, however, some complicating features. Some of the dislocation lines have a ' spotty ' appearance (figs. 5, 9) ; this effect may be understood in terms of an interference mechanism which will be discussed in a later paper. Some of the micrographs show a fringe structure at the boundaries which is due to the same cause. ' Ghost ' images, similar to the dislocations, but displaced from them, are due to Bragg reflections which are included in the image (fig. 5) but which have suffered spherical aberration in the objective lens. In addition to all these effects ' extinction ' contours are also observed (Heidenreich 1949). These are mainly due to misorientations caused by buckling of the foil, although thickness contours may also occur. On tilting the illumination or the specimen through angles of the order of 1° or 2° the extinction contours move, whereas the dislocation lines remain fixed.

§ 4. Arrangement of Dislocations

Figure 1 shows the substructure in Al at low magnification. The average subgrain size is about 1 μ, the average angular misorientation about $1\frac{1}{2}°$. The dislocation density measured from other photographs is of the order of $10^{10}/\text{cm}^2$. All these figures are in excellent agreement with the results deduced from x-ray data (Hirsch 1952, Gay, Hirsch and

Kelly 1953). The photographs leave no doubt at all that most of the dislocations are in the sub-boundaries, and relatively few within the subgrains.

The broad bands running across the subgrains are extinction contours (A). The difference in contrast from one grain to the next is due to differences in the intensities of Bragg reflexions caused by small changes in orientation.

Figure 2 shows dislocations spaced uniformly along a boundary. Generally the boundaries appear to be less regular. The boundary planes in this region are all nearly normal to the foil.

Figure 3 shows an area in which most of the boundaries are not normal to the plane of the foil. Some of the boundaries appear to consist of parallel dislocation lines (A), so that they must be pure tilt boundaries, others (B) appear to contain cross-grids of dislocations. The micrograph shows the three-dimensional nature of the substructure ; in particular the junction of the boundaries can be observed quite clearly. In some cases nodes where three dislocation lines meet at a junction can be recognized (C). (For a discussion of networks and boundaries in face-centred cubic crystals reference should be made to Frank (1955), Ball and Hirsch (1955) and Amelinckx (1956).)

Figure 4 shows a square cross-grid of dislocations (A) representing probably a twist boundary on (100). Other networks can be seen at B ; dislocation nodes can be recognized clearly in boundary junctions at C. A few isolated dislocations occur within the grain at D.

Figure 5 shows a dislocation node inside a subgrain (A). The dislocations appear to consist of a number of spots. This appearance is probably due to an interference effect at dislocations with a screw component, which will be discussed in a later paper. At B two dislocations appear to cross in characteristic manner (Read 1954). A cross-grid can be seen at C. At D a boundary appears to terminate in the middle of a subgrain. The strain around this region is apparent from the curvature in the extinction contour. Single dislocation lines can be seen at E and F; at E the dislocations are considered to be more nearly parallel to the foil than at F ; the spots at E are thought to be due to the interference effect mentioned above. At F, on the other hand, each pair of spots corresponds to one dislocation steeply inclined to the foil ; this follows from the experiments on the motion of dislocations (see § 5). The two spots on each dislocation pair are thought to be due to the increased distortion on the top and bottom surfaces due to the oxide layer which must be present. More precisely, in the transition region between metal and oxide the lattice begins to deviate appreciably from the perfect face-centred cubic arrangement, and the dislocation may be considered very ' joggy ' in this region. These jogs are thought to be responsible for the additional distortion. This area shows some typical extinction contours at G.

Figure 6 shows hexagonal networks of dislocations (A, B). These are the only clear hexagonal networks observed so far. Many of the

boundaries (e.g. C) however appear to consist of more or less distorted hexagonal networks, but the clarity of the networks is spoiled by interference effects. At D the nodes of the dislocations at the boundary junction can again be clearly recognized.

Figure 7 shows square cross-grids of dislocations of large mesh size (A, B). From a diffraction pattern taken from B it was shown that the dislocations in B are parallel to [110] directions and that the normal to the foil is almost [001]. This network, therefore, is likely to be a twist boundary on (001).

Figure 8 shows an irregular network, the dislocations of which are bowed out, presumably owing to some local strain.

In some areas the arrangement of the dislocations is quite complex. Figure 9 shows such a case ; many complex networks can be seen (A). This photograph shows interesting interference effects at boundaries (B) and single dislocations (C).

§ 5. Movement of Dislocations

When working at high beam currents and with large condenser apertures, the dislocations are observed to move. Two types of motion are observed, either rapid or slow and jerky.

First there is a movement of the extinction contours. Subsequently the dislocation lines often bow out and in many cases move. The bowing-out effect is presumably direct confirmation of the mechanism suggested for the decrease in elastic modulus due to dislocations (Mott 1952). The movement of the extinction contours shows that the foil buckles ; the dislocations therefore move presumably under the strain ; their movement may be aided by heat. The temperature rise in the specimen is not known at present.

Figures 10 (*a*), (*b*), (*c*) is a sequence showing the break-up of a sub-boundary. Dislocations leave the boundary and move in straight lines parallel to the direction marked with an arrow. The interval between the exposures is about 15sec. The moving dislocations leave behind them bands, which have been found by selected area diffraction experiments to be parallel to the traces of (111) slip planes. Thus, the appearance of slip traces at right angles suggests immediately that this area has the usual (100) orientation. The width of the band is governed by the length of the dislocation (e.g. A or B). The bands appear either as white on black, or black on white background ; both types are observed in fig. 10. The edges of the band are always more intense than the middle. After a time interval of the order of several seconds the contrast disappears. It is possible to account for the results tentatively in the following way. The dislocation lines may be ' joggy ', and non-conservative motion of these jogs results in the formation of vacancies and interstitials. Alternatively impurity atoms might be left behind after the dislocation has passed. These point defects cause a reduction in intensity of the Bragg reflexion (equivalent to a temperature factor) and an increase in

the background intensity. The bands on the micrograph appear white or black according to whether the intensity scattered outside the objective aperture is greater or smaller than in the surrounding regions. The intense edges of the bands are then due to the larger numbers of point defects generated in the surface layer. After the passage of the dislocation, the point defects are concentrated near a (111) plane. The vanishing of the slip plane contrast is explained by the diffusion of the defects away from the slip plane.

In the course of the sequence 10 (*a*), (*b*), (*c*) the sub-boundary is being depleted of dislocations. The disappearance of the contrast of the bands can be clearly seen.

If the suggested explanation of the bands is correct, the edges of the bands correspond to the top and bottom of the foil. Since the orientation of the foil is known, the thickness of the foil can be claculated from the width of the bands. The thickness varies from about 500 Å to 1000 Å.

Figures 11 (*a*), (*b*), (*c*), (*d*) shows slip in another area ; the plane of the foil is apparently not quite parallel to (100). Complicated cross-slip can be observed. The disappearance of the contrast is again noticeable.

Figure 12 shows a fine example of cross-slip. It is quite clear here that a single dislocation has transferred from one slip plane to another. This represents direct proof of the Mott–Frank screw dislocation mechanism of cross-slip (Mott 1951). The plane of the foil is again approximately parallel to (100) ; it should be noted that several of the boundaries in this region are parallel to (100) and (110), suggesting that they contain only one or two sets of dislocations which differ in their Burgers vector or slip plane (Ball and Hirsch 1955).

Cross-slip has been observed very frequently ; fig. 13 shows another example ; here the dislocation started at A and eventually penetrated the boundary at B. An interesting feature about this photograph is the fact that the original line splits into two branches at C, CD and CE. The precise process here is uncertain, but it may involve the splitting of a single dislocation into two. Another slip line is seen at FG.

Figure 14 show a sequence in an area where the dislocations moved slowly. This type of movement may perhaps correspond to creep. In addition to sub-boundaries, isolated dislocations can be seen within the subgrains. The single dislocations are typically more intense at the ends. Comparing 14 (*a*) and (*b*) it is clear that a number of dislocations have moved, for example at A, B and C. The boundary at D has disappeared ; dislocation E has moved to dislocation F which, judging from its contrast, lies in another slip plane. This suggests that E is held up by F because of the difficulty of cutting through a dislocation. However, fig. 14 (*c*) shows that E has moved on to G where it is again stopped. It is also clear that many other dislocations have moved ; in particular H has moved along the path HIJ. This path is quite irregular and indicates that the dislocation may move by a very intimate cross-slip mechanism and possibly by climb. Other dislocations also

appear to have moved by similarly irregular paths. Motion of this type tends to be jerky when observed in the microscope.

Figure 15 shows another sequence in which dislocations are moving in very jerky and irregular paths. It appears that the dislocations are attempting to form a boundary at A. Many of the dislocations appear to be bowed at the centre. This indicates clearly that the ends of the dislocations can be moved only with difficulty. Long dislocation loops are seen to move in region B.

Many observations of moving dislocations have been made in the microscope, and many complex effects have been seen. Although the growth of dislocation loops has been observed, so far it has not been possible to locate the dislocation sources. It is clear, however, that sometimes dislocations come out of boundaries, and sometimes they originate in complex regions such as those of fig. 9. On the whole, regions with very well formed polygons are most stable. Many of the dislocations are stopped at the boundaries, others appear to pass through them. The movement of parts of boundaries as a whole has also been observed.

§ 6. Conclusions

The experiments show that individual dislocations can be seen in aluminium foil, and that their arrangement and movement can be studied. While the results reported in this paper are only preliminary, some conclusions can already be drawn. Most of the dislocations are arranged in sub-boundaries; relatively few occur inside the grains. Nevertheless, isolated dislocations are observed in many cases. Pure tilt boundaries, square and hexagonal networks have been observed. Many of the boundaries appear to consist of networks, but the nature of these is confused at present owing to possible interference effects. Dislocation nodes at boundary junctions and inside grains can be observed quite clearly. Many features of the dislocation arrangement are similar to those observed in AgBr (Hedges and Mitchell 1953) and NaCl (Amelinckx 1956), although in this case the dislocations are spaced at distances of only 100 Å, compared with the corresponding distance of $1\,\mu$ in the inorganic crystals. It appears now that the theoretical predictions about the geometry of networks (Frank 1955) and of sub-boundaries (Ball and Hirsch 1955) apply for Al as well as for AgBr and NaCl. It follows that the dislocation arrangement in a heavily deformed and recovered metal is similar to that in the well-annealed inorganic crystals; the only difference is one in the scale of the arrangement. Combined diffraction and microscopy experiments are now in progress to study the details of the dislocation arrangements.

Ciné films have been prepared showing the movement of the dislocations, and it is hoped that a detailed study will reveal some of the important features of the motion, and in particular, the nature of dislocation sources and obstacles. So far the experiments have shown

the bowing out of dislocations, the spreading of dislocation loops and the movement of dislocations along (111) slip planes. The Mott–Frank mechanism of cross-slip has been observed in many cases. The experiments suggest that the dislocations are ' imperfect ' (probably very ' joggy ') near the surface, and it appears that the oxide film acts as an obstacle.

It is proposed to extend these observations to other metals.

Acknowledgments

Our thanks are due to Professor N. F. Mott, F.R.S., Dr. W. H. Taylor, and Dr. V. E. Cosslett, for their interest, encouragement and helpful discussions. The micrographs were taken on a Siemens and Halske Elmiskop I electron microscope, purchased through a generous benefaction from the Nuffield Foundation. We are also grateful to Messrs George Whiley and Co. for supplying the beaten foils.

Acknowledgments for grants are due to the Ministry of Supply (P. B. H.), to the Agricultural Research Council (R. W. H.), and to the Department of Scientific and Industrial Research (M. J. W.).

References

Amelinckx, S., 1956, *Phil. Mag.*, **1,** 269.
Ball, C. J., and Hirsch, P. B., 1955, *Phil. Mag.*, **46,** 1343.
Frank, F. C., 1955, *Report of the Conference on Defects in Crystalline Solids* (London : Physical Society), p. 159.
Gay, P., Hirsch, P. B., and Kelly, A., 1953, *Acta Met.*, **1,** 315.
Hedges, J. M., and Mitchell, J. W., 1953, *Phil. Mag.*, **44,** 223.
Heidenreich, R. D., 1949, *J. Appl. Phys.*, **20,** 993.
Hirsch, P. B., 1952, *Acta Cryst.*, **5,** 172 ; 1956, *Progress in Metal Physics*, Vol. 6 (Permagon Press), in the press.
Lacombe, P., and Beaujard, L., 1948, *Revue de Metallurgie*, **45,** 317.
Mott, N. F., 1951, *Proc. Phys. Soc.* B, **64,** 729 ; 1952, *Phil. Mag.*, **43,** 1151.
Read, W. T., 1954, *Dislocations in Crystals* (McGraw-Hill).
Wilsdorf, H., and Kuhlmann-Wilsdorf, D., 1955, *Report of the Conference on Defects in Crystalline Solids* (London : Physical Society), p. 175.

LXIX. CORRESPONDENCE

Wave Motions on a Free Oil Surface

By J. R. D. Francis
Imperial College, London †

[Received January 5, 1956]

In 1954 I published an account of some experiments where air was blown over lubricating oil in a wind tunnel (Francis 1954). At a certain critical windspeed tiny ripples were seen on the surface, and some of them rapidly grew and accelerated down-wind. The appearance of the phenomenon and the windspeed at which it occurred corresponded closely with the instability of surface waves forecasted by Kelvin and Helmholtz (quoted by Lamb 1932) but which does not appear on a water surface such as the sea. The experiments were done on one oil only, Shell S2883, and its viscosity μ (2·2 poise) was such that the other type of instability (Jeffreys 1925) should have occurred at a windspeed only just higher than the critical windspeed actually found. There may therefore be a possibility that the phenomenon was fortuitous and was not really due to the Kelvin–Helmholtz instability. However, some additional experiments with still more viscous fluids seem to confirm the earlier results.

Lubricating oil of density $\rho=0{\cdot}875$ g/cm^{-3}, and $\mu=25{\cdot}2$ poise (S3003 oil kindly supplied by the Shell Petroleum Company Ltd.), and Lyle's Golden Syrup, $\rho=1{\cdot}47$ g/cm^{-3} and $\mu=850$ poise (kindly supplied by Messrs. Tate & Lyle Ltd.) were the fluids used. The tests were carried out in the same wind tunnel and in the same way as in the previous experiments. Both of the more viscous fluids showed the same phenomenon of the ripples as was observed before, though the critical windspeeds were somewhat different. The table shows the observed windspeed at 10 cm above the surface, when the phenomenon was just occurring, together with the extrapolated value for the windspeed at about the level of the crests of the ripples. The extrapolation has been done by assuming that the slope of the logarithmic velocity profile is given by the stress of the wind on the fluid. In the case of the oil the stress was measured directly (see later) ; and in the case of the syrup it was assumed that the stress coefficient was the same as that for unrippled oil. It was observed on both the 25 poise oil and on the syrup that the ripples just before they became unstable seemed to be a little higher than those on the oil of 2·2 poise viscosity, but no measurement could be made. When a ripple had become unstable and was going off downwind, its velocity and height were both much less than those appearing on the 2·2 poise oil. Clearly, viscosity had a large effect on both the speed and height of waves at this

† Communicated by the Author.

stage, though it had little, if any, effect upon the critical windspeed needed for them just to become unstable. Bearing in mind the uncertainty of the extrapolation of the windspeed to the height of the ripple crests, the agreement between the observed critical windspeeds and those calculated

Critical windspeeds for wave motions to appear on fluids of different viscosities

Experiments with water and S2883 oil described in Francis (1954)

Fluid	Water	S2883 Oil	S3003 Oil	Lyle's Golden Syrup
ρ gm cm^{-3}	1·0	0·875	0·875	1·47
μ in poise at room temperature	0·018	2·2	25·2	850†
Surface tension in dynes cm^{-1}	73	34	34	60
Windspeed (cm sec^{-1}) for Kelvin–Helmholtz instability				
Calculated	660	516	516	700
Observed at 10 cm height	not observed	984	1030	1220
Extrapolated to 0·05 cm	not observed	500 to 560	560	660
Calculated windspeed for Jeffreys' instability in cm sec^{-1}	110	570	1290	3940

† Note that this value may be rather too high for the surface layers—see below.

by the Kelvin–Helmholtz theory is fairly good : also the observed wavelength and speed of the ripples (estimated as 1·5 cm and 1 cm sec^{-1} respectively) are again approximately those predicted by the theory. It would therefore appear that the phenomenon observed is at least closely allied to the Kelvin–Helmholtz instability, even though the theory assumed perfect fluids with no gradient of velocity which was of course present in the air above the oils or syrup.

The Shear Stress of the Wind on a Viscous Oil

While the S3003 oil (μ=25·2 poise) was in the windtunnel the opportunity was taken of determining the shear stress of the wind on its surface. The slope of the oil surface was measured and converted to the shear stress coefficient C' as was described in the earlier paper. The graph

shows the values of C found from the mean slope from one end of the tunnel to the other. For comparison, the values found previously for S2883 oil and for water are also given. It will be seen that at windspeeds above the critical windspeed, C increases though at a lower rate than it did for the S2883 oil. Possibly the higher viscosity causes a slower growth of the small ripples on the surface which seem to be the active ones in forming aerodynamic roughnesses. Thus for a given windspeed a more viscous fluid has a smaller aerodynamic roughness. The fan on the wind tunnel was not sufficiently powerful to produce large, breaking waves such as were observed on the S2883 oil.

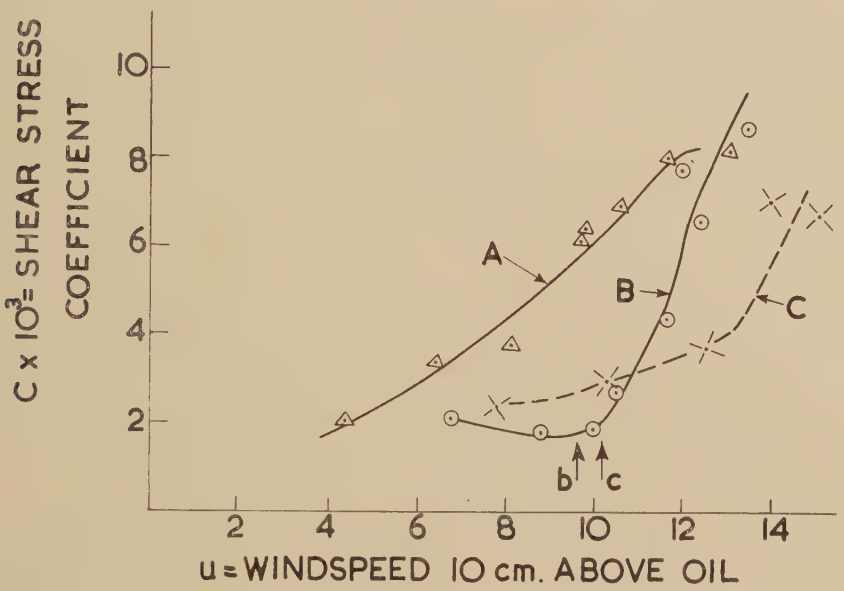

Variation of shear stress coefficient $C=\tau/\rho u^2$ with windspeed measured 10 cm above surface of oil. Waves produced by fan at leeward end of wind tunnel. Curve A refers to water, B to S2883 oil (Francis 1954), the stress being measured over the whole 4·7 m length of the wind tunnel. Curve C refers to the more viscous S3003 oil. Arrow *b* shows the critical windspeed for ripples just to form on S2883 oil; arrow *c* shows that on S3003 oil.

It was found impossible to measure the stress on the syrup surface in the same simple way as was done for the oil. Syrup, being hygroscopic, takes up water from the moist atmosphere of the hydraulics laboratory in which the wind tunnel is situated. The top layers are thus diluted and become rather less viscous. The drag of air therefore sets up a circulation in the diluted layer about 1 cm deep which slides relative to the undiluted, more viscous layer below. The depth of the layer cannot be accurately determined and as this is an important measurement in calculating the stress, it makes unreliable any values of stress found from the slope of the syrup surface. The lower viscosity of the surface layer will reduce

slightly the value of the Jeffreys' critical windspeed in the final column of the table, but the dilution of the syrup was not enough to reduce this critical windspeed to below the Kelvin–Helmholtz windspeed.

Acknowledgments

The experimental work described here was done in the Civil Engineering Laboratories of Imperial College, London ; and I am indebted to Mr. H. Charnock for the suggestion to use the syrup in these experiments.

References

Francis, J. R. D., 1954, *Phil. Mag.*, **45,** 695.
Jeffreys, H., 1925, *Proc. Roy. Soc.* A, **107,** 189.
Lamb, H., 1932, *Hydrodynamics*, 6th Edn. (Cambridge: University Press).

LXX. REVIEWS OF BOOKS

Science and Applications of Photography. (London : The Royal Photographic Society.) [Pp. 664+xvii.] Price 63*s*.

This volume of 664 pages gives a detailed account of the organization and of the proceedings of the International Conference which was held in London in September, 1953, on the occasion of the Centenary of the Royal Photographic Society. It has been edited by the Secretary of the Conference and it deserves careful examination by anyone charged with the responsibility of organizing a broadly based international conference and of preparing a permanent record of the proceedings.

It would not have been possible to include full versions of the 161 papers read during the conference in a volume of reasonable size and it is indeed to be doubted whether this would have been desirable at the present time when the publication of a considerable fraction of the papers read at international conferences is often duplicated through their appearance in the national journals of the countries of their authors. Apart from the Presidential Addresses in the five sections and three of the public lectures, which are of general interest, the 150 papers which appear in the volume are in the form of abstracts of not more than 2000 words. That a remarkably clear and adequate account of the proceedings has been presented in this way is due in large measure to the outstanding editorial work of Dr. R. S. Schultze who brought to the task many years of experience as the Research Librarian of Kodak, Ltd. Deeply concerned with the problems for scientific workers and librarians arising from the ever increasing volume of publications, he has made good use of the opportunity provided by this conference to demonstrate the advantages of abridged publication. The full versions of all the papers which have not appeared elsewhere are available from the library of the Royal Photographic Society to those especially interested in them.

The volume will serve as an invaluable guide to fields of current interest in the science and applications of photography and, from the point of view of the non-specialist reader with a wide general interest in the subject, there is no doubt that much has been gained by the abridgement of the papers. There are few involved in any aspects of photographic processes and of photographic methods of recording and reproducing information who will not find stimulating material within its pages. J. W. M.

Théorie Générale de L'Equation de Mathieu et de quelques autres équations differentielles de la mécanique. By Robert Campbell. (Masson et Cie, Paris.) In French [Pp. xvi+271.] Price : Paper 2,400*fr*. Cloth 2,900*fr*.

Mathieu's equation is a special case of a more general class of linear differential equations with periodic coefficients. A significant achievement of the author of this book is that he has shown how well known methods of solving Mathieu's equations may be extended to some of the more general equations, particularly the related equations associated with the names Whittaker and Lamé.

The book is divided into three parts. The first part deals with periodic solutions of Mathieu's equations and the related equations. Part two is very short and deals with Mathieu functions of the second kind, and with the analogous second solutions to the related equations. Part three discusses the more general theory of this group of equations when there may be no periodic solutions.

The book is clearly written. It gives many examples of the occurrence of these differential equations in physical problems, and should be of interest to physicists and engineers as well as to mathematicians. K.G.B.

Meteor Astronomy. By A. C. B. Lovell. The International Series of Monographs on Physics. (Oxford : Clarendon Press, 1954.) [Pp. xiv+463.] Price 60*s*.

The last comprehensive book on meteors, that of Olivier, was published 28 years ago. Since then the subject, like most others in science, has been developed tremendously by the introduction of new techniques. These include the two-camera measurements at Harvard with the more recent employment of the Super Schmidt cameras whose focal ratio of 0·85 enables results to be gathered much more rapidly ; and the application of radar methods to the determination of meteor velocities and radiants.

Much of the radio work has been carried out at the Jodrell Bank Experimental Station under the direction of Professor Lovell and he is thus perhaps uniquely qualified to write this book, which reviews with lucidity and completeness our present knowledge of meteor astronomy.

The author starts with a historical account of the observational methods used at visual and radio wavelengths, and continues with chapters on the equations of meteoric motion, the diurnal and seasonal distribution of sporadic meteors, and the number and mass distribution of sporadic meteors. He devotes more than one hundred pages to the very interesting topic of the velocity of sporadic meteors. Its importance lies in the question of the origin of such meteors, for if they possess heliocentric velocities greater than 42 km sec^{-1}, their orbits are hyperbolic and they come from outside the solar system. A fierce controversy has been raging for many years on this point, some workers claiming velocities as high as 200 km sec^{-1} while others, using a similar number of observations, found few or none with hyperbolic velocities. In at least one case an observation has been claimed as confirmatory evidence by both parties. It seems now, however, that the matter has been settled by the radio measurements which show that not more than $\frac{1}{2}\%$ of meteors have velocities greater than hyperbolic and the exceptions, if any, are probably due to planetary perturbations rather than an external origin.

The major meteor streams are described in detail, including the day-time streams discovered by the radio-echo technique, and there are final chapters on the dispersive effects in meteor streams and the cosmological relationships of meteors.

There are a large number of figures, tables and references to add further clarity and usefulness to the book. Professor Lovell points out that neither meteorites nor meteor physics are considered but he hopes to write a complementary volume on meteor physics at some future date. J. R. S.

An Introduction to Linear Algebra. By L. Mirsky. (Oxford : Clarendon Press. London : Cumberlege.) [Pp. 444.] Price 35*s*.

This is a rather satisfactory book, covering approximately the ground normally covered in an undergraduate course on Linear Algebra. After a somewhat formidable chapter on determinants, vector spaces (most of which are here called linear manifolds) are introduced and the study of matrices is in general related to the study of vector spaces and their mappings. The reader will not find in this book any treatment of compound matrices nor of dual vector spaces nor of the classical canonical form for a class of similar matrices ; there are however some agreeable sections on inequalities and on groups of linear transformations. The book is pleasantly written and printed, and is perhaps the most suitable book on the subject now available for undergraduates.

S.W.

Principles and Problems in Energetics By J. N. Brønsted. Translated by R. P. Bell. (New York : Interscience Publishers, 1955) [Pp. vii + 119.] Price $3.50.

In this monograph, first published in Danish in 1946, Professor Brønsted attempts to present the relations of thermodynamics in a new and more satisfactory form. The first and second laws are replaced by two new equivalent energy principles, and it is pleasing to find that no appeal is made to either reversible heat engines or Caratheodory. Heat is introduced and defined solely on the basis of the irreversible production of entropy. Professor Brønsted claims that his treatment removes many of the difficulties inherent in the ordinary presentations of thermodynamics, but the examples he gives of such difficulties come mainly from obviously inadequate textbooks. His treatment also offers a new starting point for the discussion of irreversible processes, but as the author was in Denmark all through the war and died in 1947 this aspect is not discussed in relation to other recent work. The book gives a lively and fresh approach to an old established branch of physics and as such may be warmly recommended to anyone interested in the teaching of thermodynamics. However if, we accept Professor Brønsted's approach we find that his definitions lead to such sentences as " the conversion of heat to work is impossible under any circumstances ". At present energetics hardly seems to offer such advantages as will persuade people to accept such a drastic rewriting of well known principles. J.W.

Champs de Vecteurs et de Tenseurs. By E. Bauer. (Paris : Masson et Cie.) [Pp. 204.] Price 2,200*fr.*

All theoretical physicists will appreciate this sraightforward account of vectors, tensors and electromagnetism. Practical problems are not considered but the basic theory is presented as a whole, ready to apply to hydrodynamics, elasticity, relativity, electricity etc. Numerous historical notes, and references to more sophisticated ideas, enliven the text. The style is seductively simple, and a safe course is steered between physical intuition and mathematical rigour. Recommended, alpha plus, for third-year undergraduates and their elders.

J.M.Z.

Electromagnetically Enriched Isotopes and Mass Spectroscopy. Edited by M. L. Smith. (London : Butterworths Scientific Publications, 1956.) [Pp. vx+272.] Price 45*s.*

This book contains a full account of the thirty papers given at an International Conference on Electromagnetically Enriched Isotopes held at Harwell in September 1955. Many aspects of the design, construction and operation of separators both large and small are dealt with in detail, as well as numerous applications in nuclear and solid state physics, spectroscopy and qualnttative analysis K.S.

Thermodynamics and Statistical Mechanics. By Arnold Sommerfeld. (New York : Academic Press.) [Pp. 400.] Price $7.

This is a translation, by J. Kestin, of volume V of Sommerfeld's ' Lectures on Theoretical Physics ', completed by F. Bopp and J. Meixner after the author's death. The treatment is simply and robustly written, sensible, concise, and illuminated by witty asides towards applied science and history. It contains what every theoretical physicist ought to (but, alas, in this country seldom does) know on these subjects, and would form an admirable basis for a general " graduate course " to research students. J.M.Z.

Nuclear Magnetic Resonances. By E. R. Andrew. (Cambridge : University Press, 1955.) [Pp. xi+265.] Price 35*s*.

In the last few years the nuclear magnetic resonance technique has been developed from a method of measuring nuclear g factors with high precision into a research tool with applications in many fields of science. It has been used by chemists, for example, to follow nuclear reactions and determine molecular structures, by biologists to determine the water content in samples, and by metallurgists to investigate the structure of alloys. The technique has also found application in the rubber, plastics and oil industries, in the measurement and stabilisation of magnetic fields and in isotope estraction. This book is a well balanced review of the subject, suitable for both the newcomer and the research worker in the field. The experimental procedures are adequately described and the applications and limitations of the various techniques are indicated. The essentials of the theory are developed in the text or moved to the appendix, which also includes tables of the nuclei and molecules which have been investigated by radiofrequency resonance techniques. An ample bibliography is included and the book can be warmly recommended as a reference book to all who are interested in the theory and application of nuclear magnetic resonance. K.F.S.

Methods of Mathematical Physics. By Sir Harold Jeffreys and Bertha Swirles (Lady Jeffreys). (Cambridge University Press.) [Pp. ix+714.] Price 84*s*.

The third edition of the book by Sir Harold and Lady Jeffreys contains no major alternations, though the proofs of some of the theorems have been modified and some mistakes corrected.

BOOK NOTICES

Techniques Generales du Laboratoire de Physique. Edited by J. Surugue. (Paris : Centre National de la Recherche Scientifique.) [Pp. 671.] Price 2,400*fr*.

Vector Analysis. By Homer E. Newell, Jr. (McGraw–Hill.) [Pp. xi+216.] Price 41*s*. 6*d*.

Advanced Calculus. By Louis Brand. London : Chapman and Hall.) [Pp. xii+574.] Price 68*s*.

Physics of Fully Ionized Gases. By Lyman Spitzer, Jr. (London : Interscience Publishers Ltd.) [Pp. ix+105.] Price $1.75, paper-backed ; $3.50, hard-cover.

International Atomic Policy. By Admiral Elis Biörklund, translated by A. Read. (London : George Allen and Unwin Ltd.) [Pp. 148.] Price 15*s*.

Risk and Gambling. By John Cohen and Mark Hansel. (London : Longmans, Green and Co. Ltd.) [Pp. x+153.] Price 14*s*.

[*The Editors do not hold themselves responsible for the views expressed by their correspondents.*]

(*a*) (*b*)

(*a*) A primary alpha particle of ~ 10000 BEV/nucleon interacts with a nucleus in the emulsion and produces a closely collimated shower of 41 particles and one evaporation particle.

(*b*) The central core at a distance of 500μ from the origin. It will be seen that the core is still not clearly resolved.

A neutral particle, probably a heavy meson or neutron, emitted from the disintegration shown in Pl. 21, produces a secondary interaction. The tracks appearing on the side are due to charged particles emitted from the original star and the accompanying electromagnetic cascade. It can be easily seen that the direction of the neutral primary can be inferred within very close limits.

Fig. 1

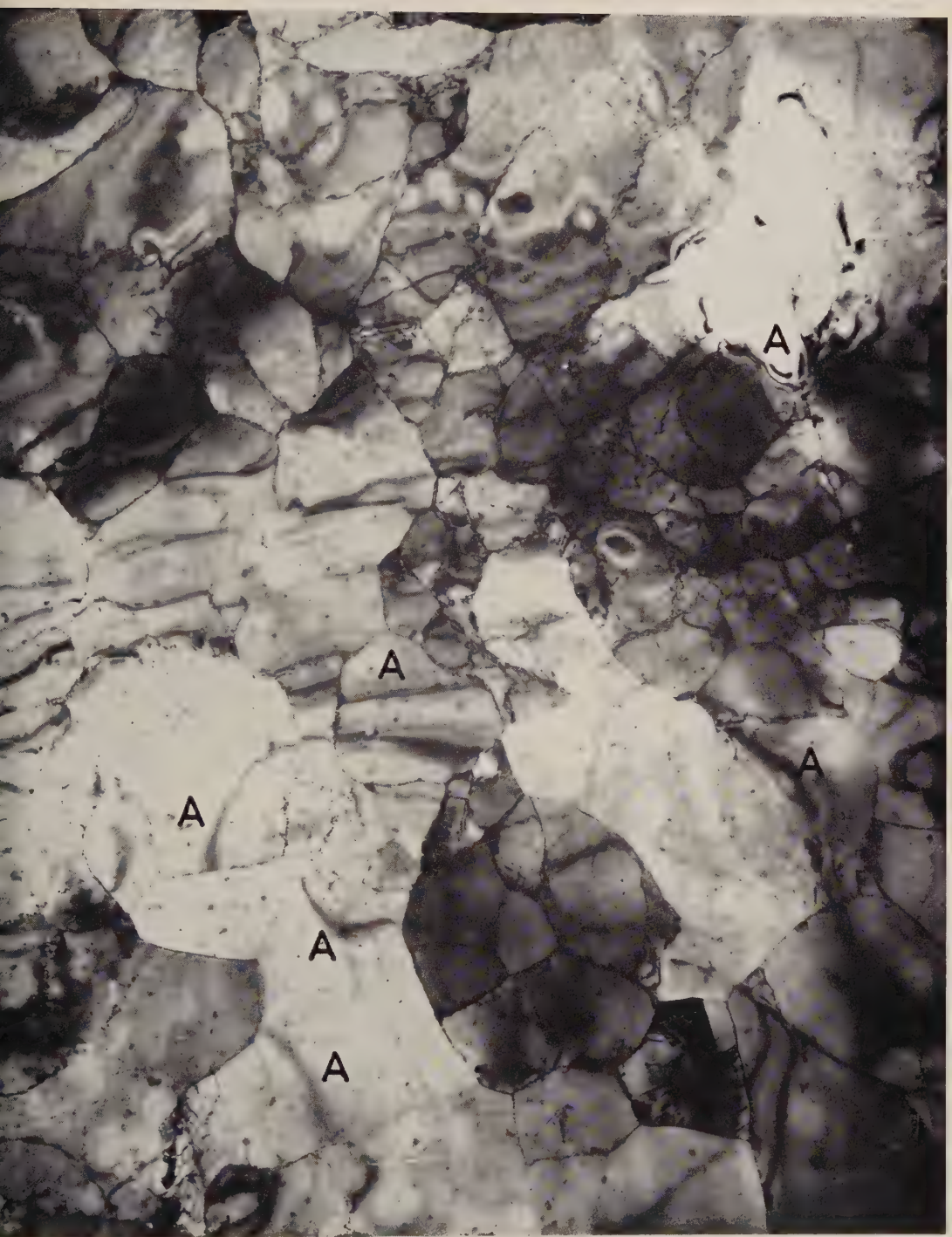

Substructure in Al annealed at 350°c after beating at room temperature. The average subgrain size is about 1 μ, the average angular misorientation about $1\frac{1}{2}^\circ$. The dislocation density is about 10^{10} per cm^2. Extinction contours are shown at A.

Fig. 2

1000 A

Mag. ×100 000

A sub-boundary consisting of uniformly spaced dislocations. The average spacing of the dislocations is about 175 Å.

Fig. 5

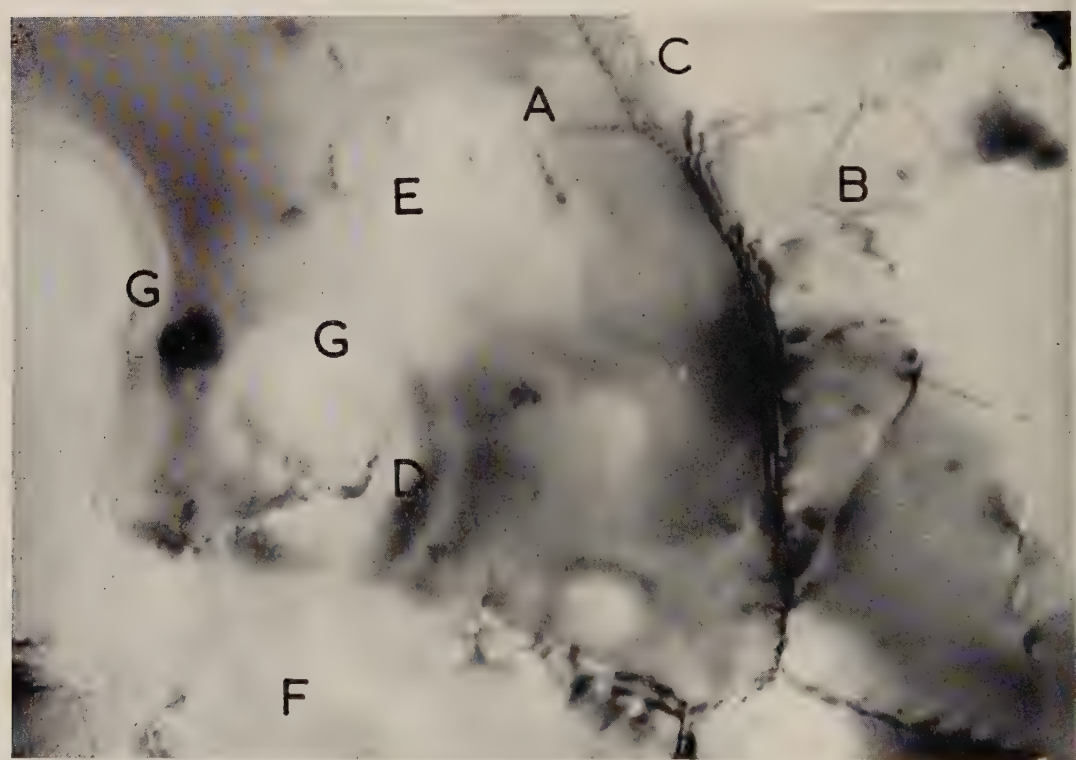

1000 A

Mag. ×100 000

A :—Dislocation node ; the 'spotted' appearance of the dislocation lines is probably due to an interference effect. B :—Crossing of two dislocations. C :—Cross-grid of dislocations. D :—Termination of boundary. E, F :—Single dislocation lines. G :—Extinction contours.

Fig. 3

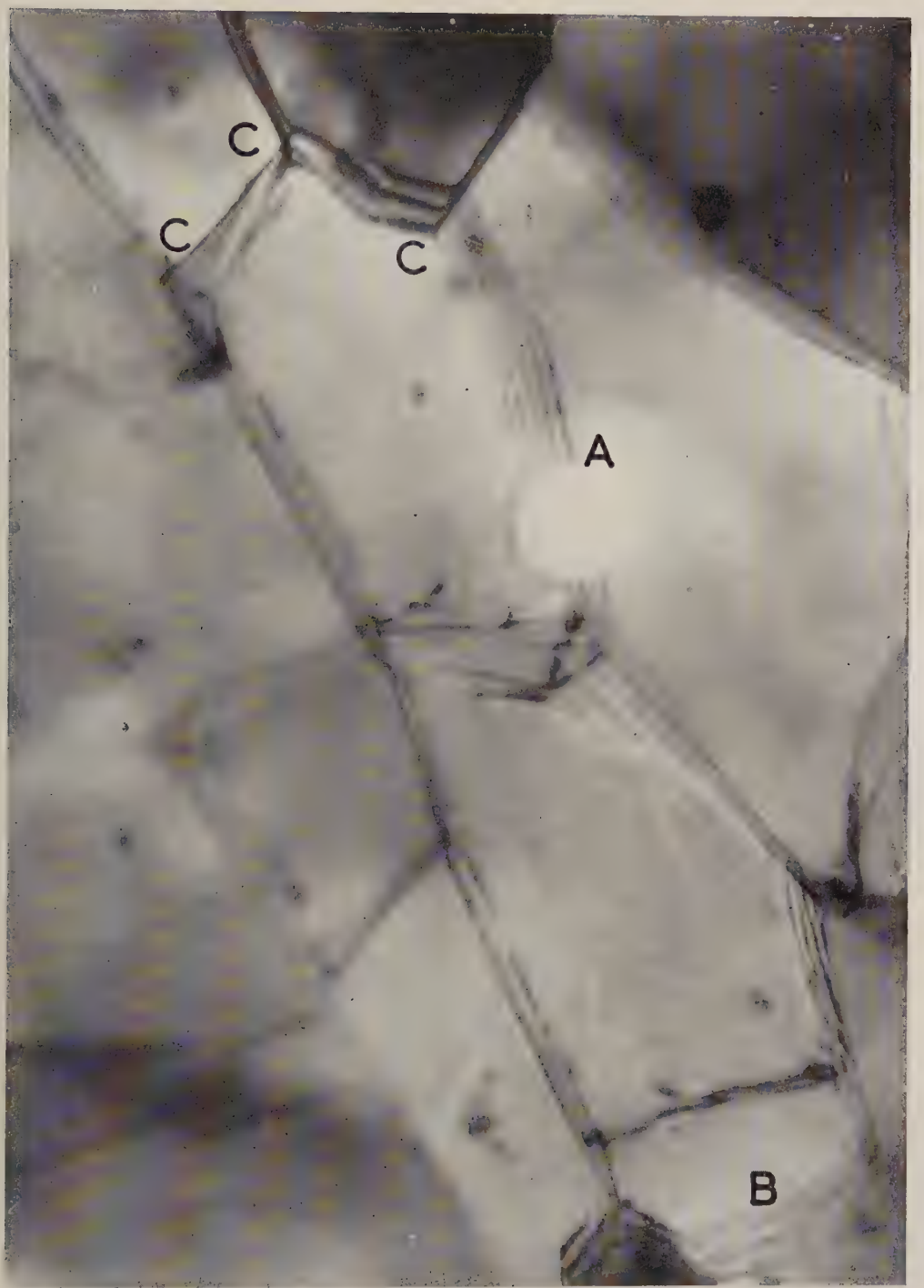

1000 A

Mag. ×100 000

Boundaries whose planes are not normal to the plane of the foil. A :—Pure tilt boundary. B :—Cross-grid of dislocations. C :—Dislocation nodes.

Fig. 4

1000 A

Mag. ×100 000

Boundaries containing dislocation networks. A :—Square cross-grid. B :—Other networks
C :—Dislocation nodes. D :—Isolated dislocations.

Fig. 6

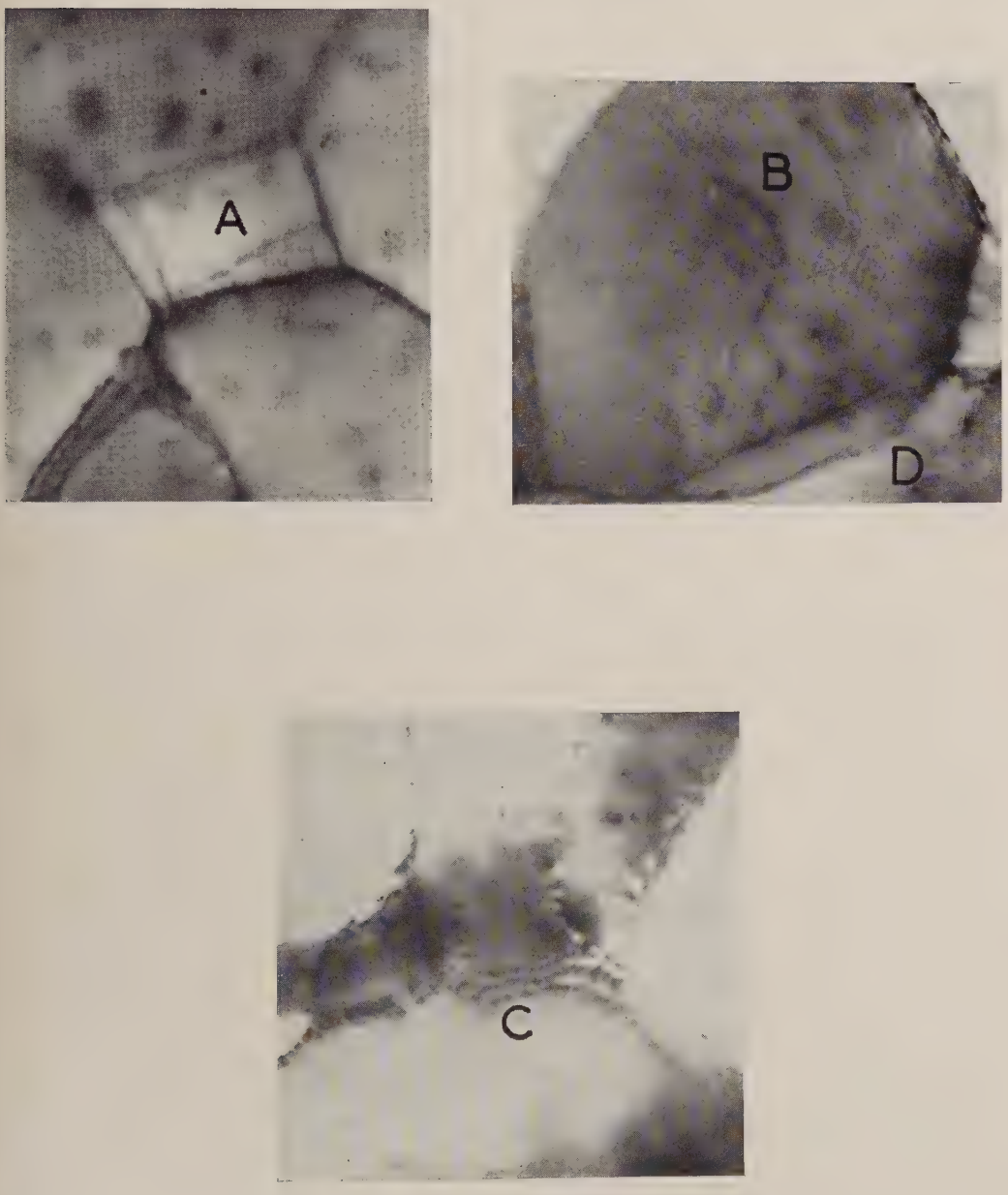

1000 A

Mag. $\times 100\,000$

A, B :—Hexagonal networks of dislocations. C :—Indistinct network.
D :—Dislocation nodes.

Fig. 7

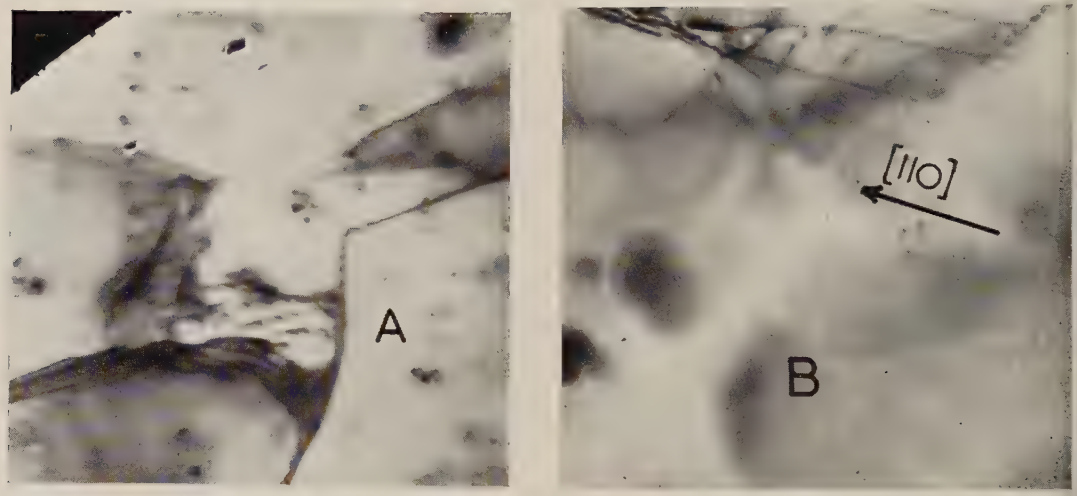

1000 A

Mag. $\times 100\,000$

A, B :—Square cross-grids of dislocations. The dislocations in B are approximately parallel to [110] directions.

Fig. 8

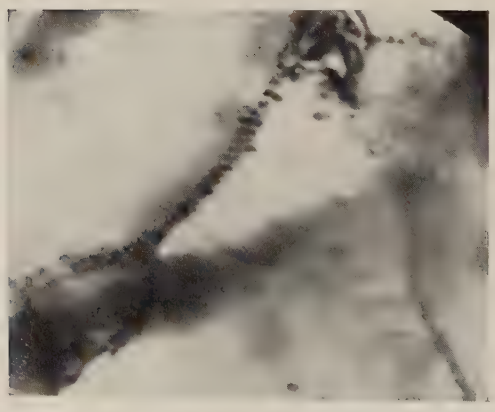

1000 A

Mag. $\times 100\,000$

Irregular network consisting of bowed-out dislocations.

Fig. 9

1000 A

Mag. $\times 100\,000$

Complex arrangement of dislocations. A :—Irregular network. B :—Interference effect at a boundary. C :—Interference effect at single dislocations.

Fig. 10

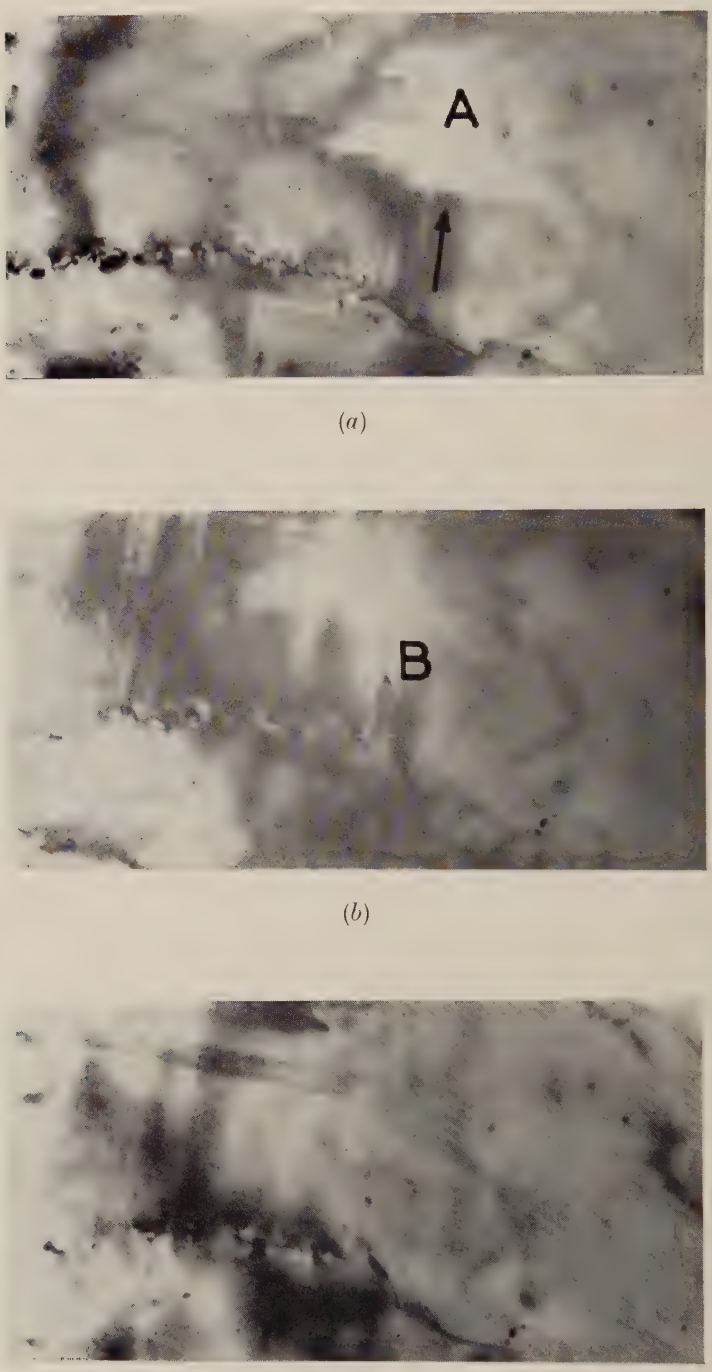

Sequence showing slip and break-up of a sub-boundary. The length of the dislocations (A, B) determines the width of the bands. The bands are parallel to traces of (111) planes, and their contrast disappears after a few seconds.

Fig. 11

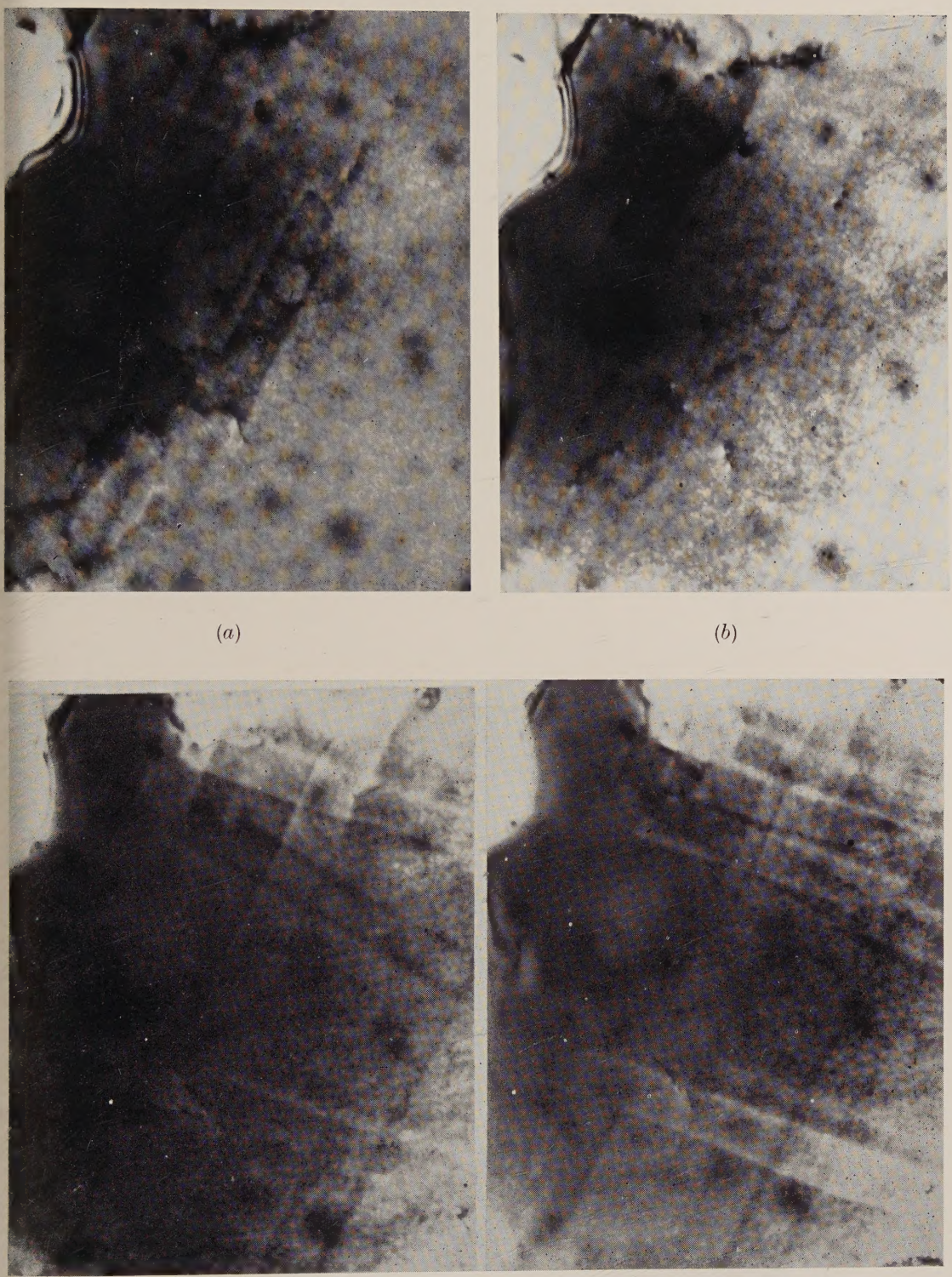

(a) (b)

(c) (d)

1000 A Mag. ×60 000

Sequence showing slip. The disappearance of the contrast in the bands can be followed in the sequence.

Fig. 12

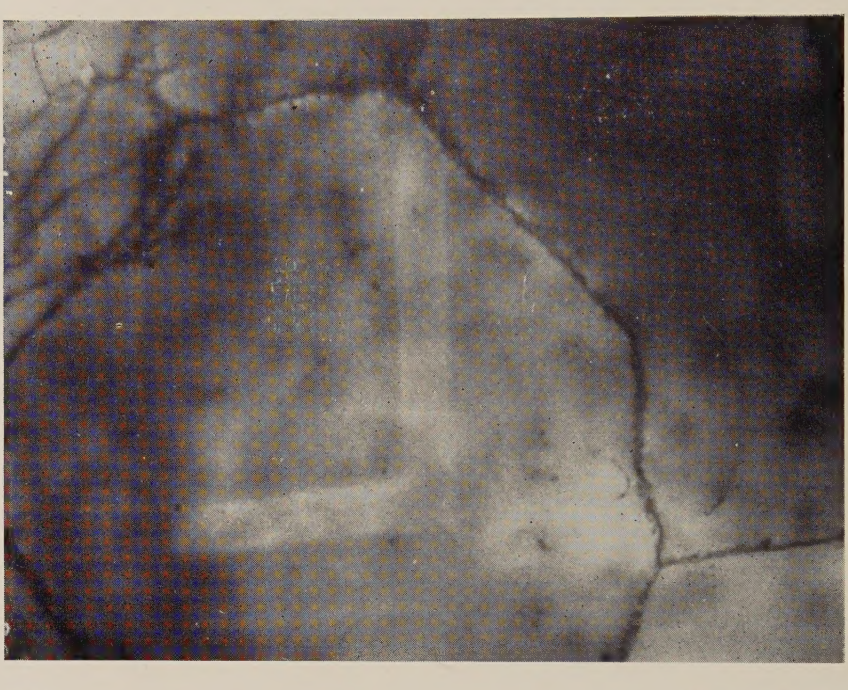

1000 A

Mag. ×60 000

Cross-slip by the screw dislocation mechanism.

Fig. 13

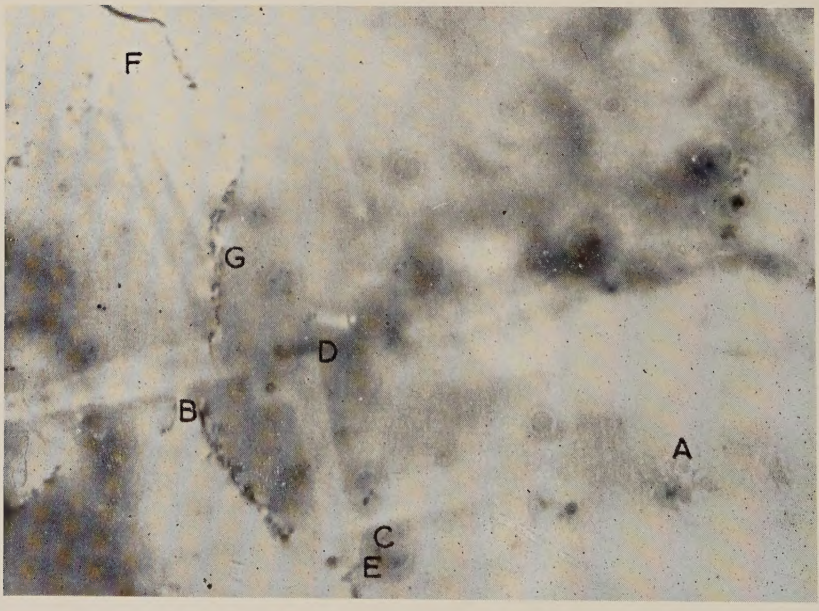

1000 A

Mag. ×60 000

Cross-slip ; the dislocation started at A and penetrated the boundary at B. Note that the original band splits into two branches at C, CD and CE. Another slip line is seen at FG.

Fig. 14

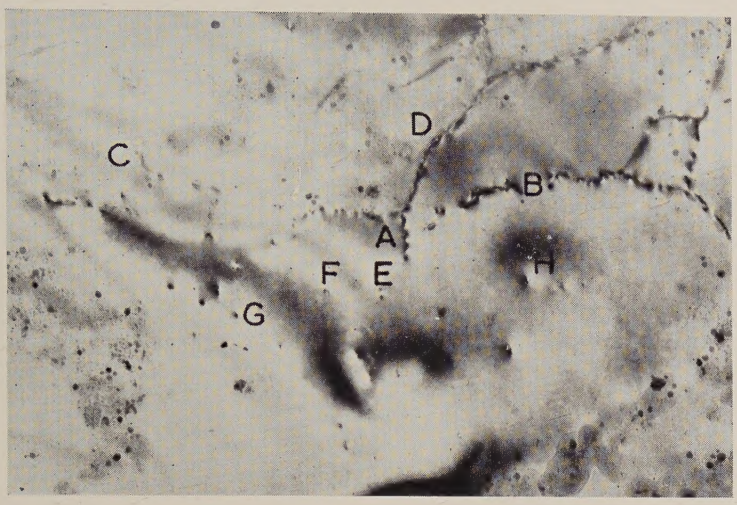

(a)

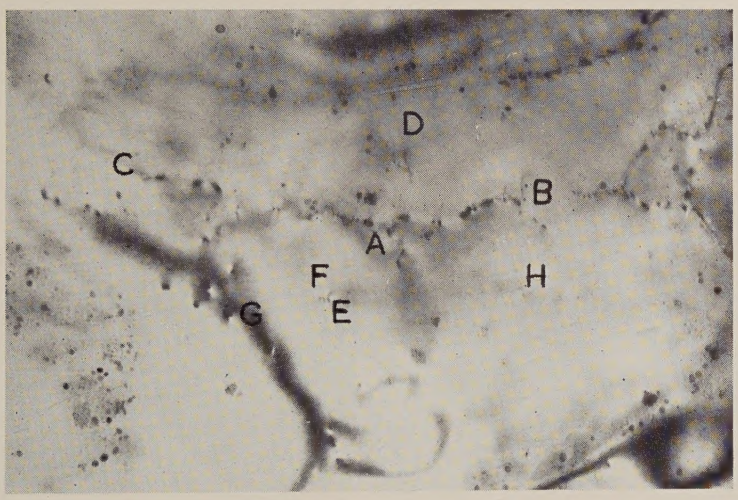

(b)

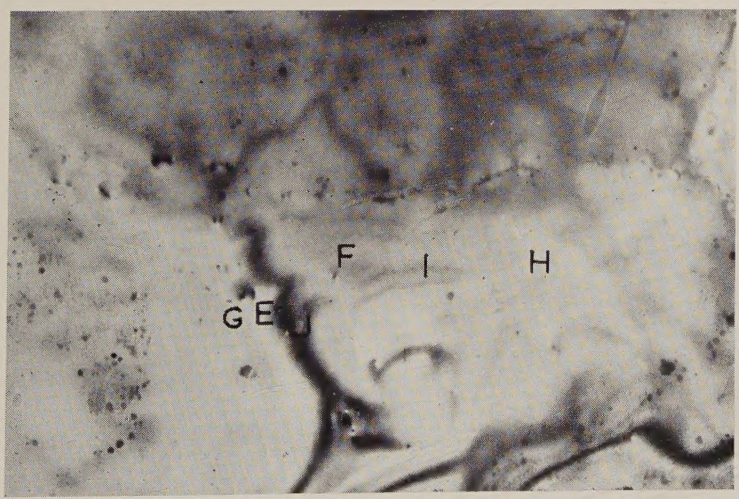

(c)

1000 A

Mag. ×60 000

Sequence showing slowly-moving dislocations. Refer to text for detailed description.

Fig. 15

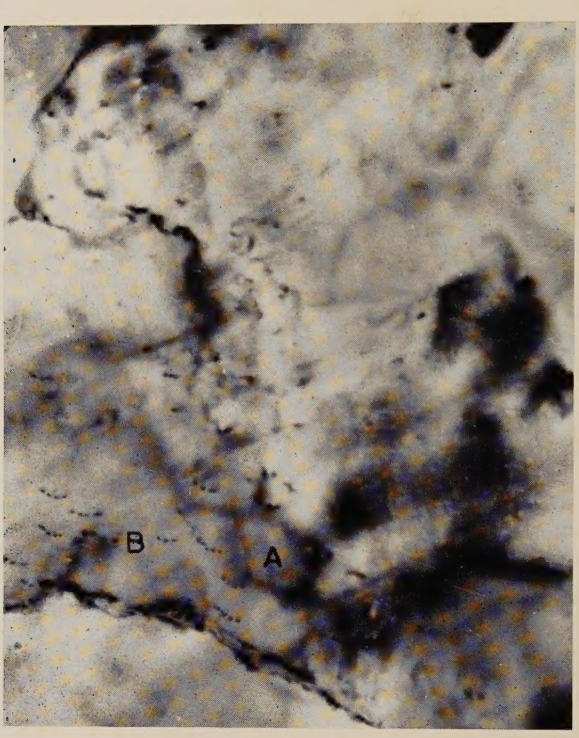

(*a*)

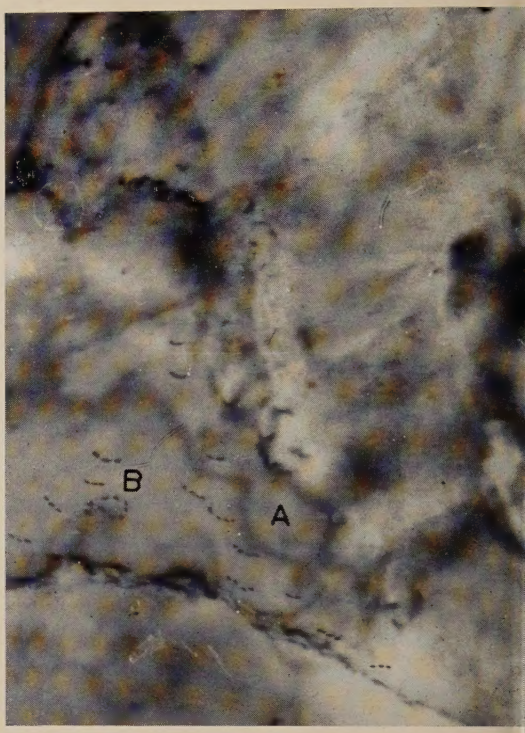

(*b*)

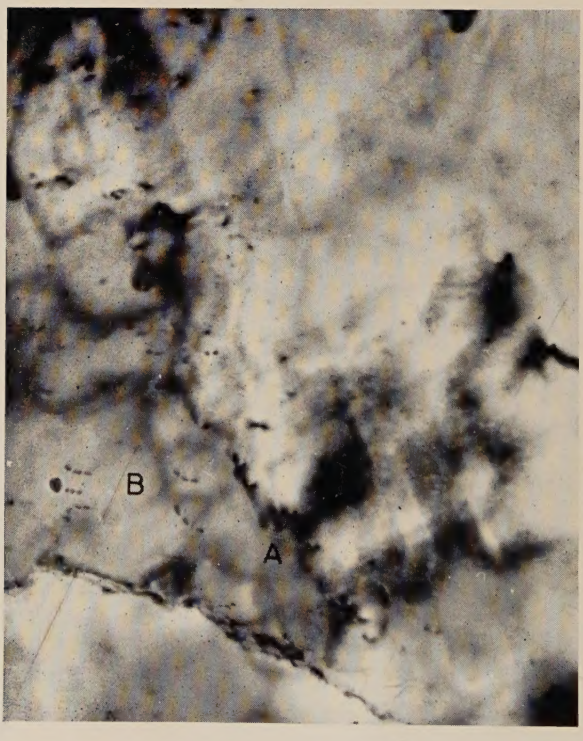

(*c*)

(*d*)

1000 A

Mag. ×6

Sequence showing slowly-moving dislocations. Some of the dislocations move along irregular paths. At A the dislocations may be attempting to form a boundary. B :—dislocation loops.